DROP-ON-DEMAND INKJET DROP FORMATION OF DILUTE POLYMER SOLUTIONS

A Dissertation
Presented to
The Academic Faculty

by

Xuejia Yan

In Partial Fulfillment
of the Requirements for the Degree
Doctor of Philosophy in the
School of Material Science and Engineering

Georgia Institute of Technology
DECEMBER 2010

DROP-ON-DEMAND INKJET DROP FORMATION OF DILUTE POLYMER SOLUTIONS

Approved by:

Dr. Wallace W. Carr, Advisor
School of Material Science and Engineering
Georgia Institute of Technology

Dr. Sven H. Behrens
School of Chemical and Biomolecular Engineering
Georgia Institute of Technology

Dr. David G Bucknall
School of Material Science and Engineering
Georgia Institute of Technology

Dr. Hongming Dong
School of Material Science and Engineering
Georgia Institute of Technology

Dr. Donggang Yao
School of Material Science and Engineering
Georgia Institute of Technology

Date Approved: [July 22, 2010]

To the past years

ACKNOWLEDGEMENTS

My most sincere thanks go to my advisor, Dr. Wallace W. Carr. During my four years of Ph.D study at Georgia Tech, Dr. Carr has been nothing but thoughtful, responsible, available, resourceful, supportive, and entertaining. He has been offering not only his great contributions to my research but also the outstanding mentorship that he has provided me and many other fortunate students.

I would like to thank Dr. Hongming Dong in my research group for his generous instructions and significant efforts to my dissertation. I am also thankful for my committee members, Dr. David Bucknall, Dr. Donggang Yao and Dr. Sven Behrens for their alternative ideas, which undoubtedly augmented this work, and their time flexibility.

I would like to thank my parents Mr. Jie Yan and Mrs. Xiulan Xu for their unconditional supports. Special thanks to my girlfriend Hui Lin, I will never make this without her by my side. Thanks to all my friends for being part of my life these years.

TABLE OF CONTENTS

Page

LIST OF TABLES

Page

LIST OF FIGURES

Page

SUMMARY

The research discussed in this dissertation was conducted to obtain a fundamental understanding of drop formation of inkjet printing with inks containing polymer. Solutions containing a water soluble polymer, poly ethylene oxide (PEO), with different molecular weights and polydispersities were used as inks. A flash photographic technique was used to visualize the whole process of DOD drop formation of dilute polymer solutions. The effects of driving signal, frequency and liquid properties on drop speed, drop size, breakup time and the formation of satellites were studied in detail.

The addition of PEO increases the shear viscosity at all molecular weights, but the change is small for dilute solutions. However, the addition of a small amount of PEO can have a significant effect on the DOD drop formation process, increasing breakup time, decreasing primary drop speed and decreasing the number of satellites in some cases. The effects depend on both molecular weight and concentration. At lower molecular weights (14k and 35k g/mol), the effect of PEO over the dilute solution regime was small when the drop formation process for the dilute solution was compared with that of a Newtonian liquid having similar shear viscosity, and the effect of PEO was small even at concentrations large enough that the solution does not fall in the dilute regime.

As molecular weight is increased, the effects of PEO on DOD drop formation increase significantly, and the effects of concentration become important. These effects are explained by the fluid elasticity which increases with increasing in molecular weight and concentration. When the liquid jets out of the nozzle, the polymer chains are stretched, and thus depart from their ideal coiled state. As a result, an elastic stress

develops in the liquid column and resists capillarity-driven pinch off from the nozzle and is responsible for the decrease in drop speed and longer breakup time.

DOD drop formation data were shown to correlate closely with effective relaxation time, λ_{eff}, proposed by Tirtaatmadja [1] based on Rouse-Zimm theory. When driving voltage amplitude is 44.2 V, two important parameters (breakup time and primary drop speed) in DOD drop formation for solutions containing monodispersed PEO and aqueous solutions containing mixtures of monodispersed PEO were closely predicted by correlation equations involving λ_{eff}. A mixture rule was developed to calculate the relaxation time for mixtures of monodispersed PEO. However, for polydispersed PEO, λ_{eff} was based on viscous molecular weight since the molecular weight distributions of the polydispersed PEO were unknown. When breakup time was plotted versus λ_{eff} for 1000k g/mol PEO, the data did not lie on the same line as the 100k and 300k g/mol PEO. This is believed to be due to the molecular weight distributions of the polydispersed PEO. When more than one species are present, viscous average molecular weight does not adequately account for the long chain species making up the polymer sample.

DOD drop formation dynamics is highly affected by the actuating waveform, including the driving voltage, waveform shape, and frequency. The effects of parameters (jetting frequency, voltage amplitude and the shape of waveform) characterizing the signal were investigated. The open time and first drop problem [2] were also studied.

Research in this dissertation gives a better understanding of DOD drop formation of polymer solutions, which may lead to improvement of inkjet printing quality for a variety of industry inks and polymer micro scale deposition and patterning in large areas.

CHAPTER 1

INTRODUCTION

Patterning of polymers in a small scale is of great importance in many areas of modern science and technology, with the applications ranging from the production of integrated circuits, information storage devices, and display units to the fabrication of micro-electromechanical systems (MEMS), miniaturized sensors, microfluidic devices, biochips, photonic bandgap crystals, micro-optical components, and diffractive optical elements [3]. Depending on the requirements of applications, various patterning methodologies, such as writing [4], self-assembly [5] and replication [6], are used. Inkjet printing is a type of writing. Compared to other methods of patterning, inkjet printing has many advantages such as the high flexibility in deposition area, materials and substrates. Inkjet printing has become one of the ideal choices in many cases of polymer patterning. Although inkjet printing technology has been successfully used in a variety of polymer patterning applications [7], the fundamental dynamics of inkjet drop formation of dilute polymer solutions is still not yet fully understood, which sparks the research in this thesis.

The objective of this research is to obtain a better understanding for DOD drop formation of polymer solutions. Based on the flash-photography technique, an experimental setup was developed, which enable visualize the micron-scale motions involved in inkjet deposition with temporal resolution of 500 ns and spatial resolution of 0.81 μm/pixel. The effects of the driving waveform, jetting frequency and the composition of the polymer solutions on the dynamics of DOD drop formation were analyzed in detail. The effects on important printing parameters such as drop speed, drop size, breakup time and the formation of satellites were investigated. By

quantifying the effects, predictive equations involving molecular weight, concentration and solvent viscosity were obtained which can be used to predict the jetting behavior of DOD drop formation of dilute polymer solutions. Additional tests were used to verify the predictive equations.

The remainder of this thesis is organized in seven chapters. Chapter 2 presents background and literature review of drop formation processes for dripping, continuous and DOD modes of operation for various inks. Chapter 3 discusses the theoretical background of dilute polymer solutions. Chapter 4 introduces the experimental setup and materials. The next three chapters are devoted to the experimental results and discussion: Chapter 5, DOD drop formation of polydispersed PEO solutions; Chapter 6, DOD drop formation of monodispersed PEO solutions; and Chapter 7, the effects of waveform and jetting frequency on DOD drop formation of dilute PEO solutions. Finally, the conclusions of the present work are summarized and some recommendations for future investigations are given in Chapter 8.

CHAPTER 2

BACKGROUND AND LITERATURE REVIEW

In 1873, Joseph Plateau found experimentally that a vertically falling stream of water will break up into drops if its length is greater than about 3.15 times its diameter. Later, Lord Rayleigh showed theoretically that a vertically falling column of non-viscous liquid with a circular cross-section should break up into drops [8]. Since then, generations of researchers have conducted studies to better understand the drop generation process. A variety of applications related to drops have greatly changed people's lives [7, 9-14].

2.1 Introduction to Drop-on-Demand (DOD) Inkjet Printing

Three common modes of producing single drops are dripping, continuous jetting and drop-on-demand (DOD) jetting. Dripping occurs when liquid is forced out of a capillary at low flow rates. When the gravitational force acting on the liquid exceeds the capillary force holding the liquid to the surface, pinchoff occurs and a drop is formed. In the dripping mode, the rate of drop formation is low since it takes a relatively long time for pinchoff to occur. As flow rate is increased through the capillary, transition from dripping to continuous jetting occurs [2, 15-16]. The jet will break up due to Raleigh instability [17]; however, drop size will vary significantly. By introducing a cyclic disturbance, a continuous stream of uniform drops can be generated. The continuous jetting mode, which has been successfully used in inkjet printing, has the advantage of high drop formation rate, but produces drops continuously whether or not they are needed. Consequently, complicated control and

recycling systems are required. For the drop-on-demand (DOD) mode, drops are produced only when they needed. A DOD inkjet printer ejects out a tiny amount of liquid by applying a short pressure wave to liquid filling a channel. Under the appropriate conditions, the blob of fluid exiting the nozzle evolves into a single drop [2].

DOD inkjet printing is an ideal method to deposit micron-size liquid on a substrate in many applications because it is compatible with various materials and easily controlled by tuning the driving electrical signal [2]. In addition, DOD inkjet printing is a non-contacting process which means less contamination. It also has high flexibility in materials and substrates, as well as in deposit area, size and shape.

Functional materials, especially polymers are more preferably processed from solution. Based on the advantages that mentioned before in depositing liquids, DOD inkjet printing has become a particularly attractive technique, especially for the controlled solution deposition of polymer patterns and delivery of small quantities of functional materials [18].

DOD inkjet printing technology has been applied in many fields from physics [19-20], electronics [11, 14, 21-30] to chemistry [31-32], tissue engineering [33-34] and biology [35-37].

Bharathan and Yang [38] first reported using DOD inkjet printing technology to produce a polymer light emitting device (PLED), an emitting logo, in which an aqueous solution of semiconducting poly(3,4-ethylenedioxythiophene) (PEDOT) was utilized as ink. Since then, the manufacture of multicolor PLED displays has become one of the most important applications of inkjet printing. Kamiruka and Duineveld both reported on the inkjet fabrication of a true full color 80 ppi active and passive

matrix displays, using the PI-barrier technique for pixel definition [7]. Much effort has been put into resolution improvement and ink composition.

Similarly, DOD inkjet printing is also used for the manufacturing of polymer electronics, which are potentially useful when cost rather than speed is essential. Syrringhaus [14] first reported a high resolution inkjet printing of all polymer transistor circuits.

Hoth et al. [9, 39] also showed that DOD inkjet printing technology can be used for the fabrication of organic photovoltaics which can reach a 3% power conversion efficiency [39].

2.2 Drop Development, Formation and Breakup of Newtonian Fluids in DOD Inkjet Printing

Although DOD inkjet printing has been widely used in many areas since it was introduced in 1970s, a better understanding of the fundamentals is still needed. Drop formation via the dripping mode is slow and can easily be visualized. On the other hand, the entire process of inkjet drop formation lasts only about a hundred micro second, which makes it difficult to observe and record with normal high speed imaging.

Almost all of the published inkjet printing research on drop formation that is for Newtonian liquids. By using an ultrafast digital image system, Chen and Basaran [40] were able to record the DOD Drop formation process continuously, and based on the images. The effects of ink properties on the liquid thread length ejected from the nozzle were discussed[41][42].

Dong et al.[2, 16, 43-44] developed an imaging system with an interframe time of 1 μs and a spatial resolution of 0.81 μm/pixel to visualize a series of Newtonian fluids with viscosity ranging from 1.0 to 5.0 cP and surface tension

ranging from 35 to 73 mN/m jetting from the nozzle orifice with a diameter of 53 μm. Each step of the DOD drop formation has been experimentally studied and the first breakup time was found related to liquid properties as well as the signal waveform[16]. Numerical simulations of DOD dynamics have been developed based on one-dimensional models [45-46]. Yidirim and Basaran [47-48] were able to predict numerically the transitions from symmetric flow for a low-viscosity Newtonian fluid to asymmetric inertial viscous flow. Two dimensional axisymmetric Navier-Stokes equations have also been used to simulate the process. Xu and Basaran [49] was able to simulate the formation of liquid drops of incompressible Newtonian fluids from a simple capillary tube by imposing a transient flow rate upstream of the nozzle exit.

2.3 Drop Development, Formation and Breakup of Non-Newtonian Fluids in Jetting Processes

Previous work in the field of drop formation is mainly for Newtonian fluids. Over the last few years, interest in jetting of polymer solutions has received attention. In some cases, the formation and subsequent break up of drops from a nozzle are significantly affected by the addition of polymers to the inkjet ink.

Hoyt and Taylor [50] observed that a pure water stream continuously jetting out of a nozzle generated a number of satellite droplets, while there were no satellite droplets near the stream with polymer additive. They assumed it is the resistance of the polymer molecules to elongation which was responsible for liquid stabilization.

For the drop formation process, the addition of polymer gives elasticity to the liquid, which may greatly affect the process. The degree to which elasticity is important is closely associated with the polymer relaxation time. Attempts have been made to obtain relaxation time both theoretically [51-54] and experimentally [1, 55].

Tirtaatmadja, McKinley and Cooper-White [1] investigated the dynamics of drop formation and pinch-off in the dripping mode for a series of low viscosity elastic fluids possessing similar shear viscosities, but differing substantially in elastic properties. A one-dimensional nonlinear elastic dumbbell model was able to capture the basic features of their experimental observations. The model along with experimental measurements was used to obtain relaxation times of polyethylene oxide solutions of varying concentrations and molecular weights. The effective relaxation times were up to an order of magnitude higher than those from Zimm theory. An equation for calculating effective relaxation time was obtained by using experimental data to modify relaxation time estimated from Rouse-Zimm theory.

Christanti and Walker [1, 55-56] investigated the influence of polymer (PEO) on jet stream break up for continuous jetting. They found that both the polymer molecular weight and polymer concentration affect the breakup dynamics, and showed that solutions with higher extensional viscosity and relaxation time are more effective at retarding break up. For dilute solutions, the measured relaxation times are on the same scale as the calculated values from Zimm model. The drop formation process of dilute polymer solutions for continuous jetting mode is determined by the fluid relaxation time and the disturbance growth rate.

The addition of small amount of polymer was shown to have a significant effect on DOD drop formation [57], suppressing the satellite drop and affecting primary drop speed in some cases. Xu et al. [58] investigated the influence of polymer concentration on DOD inkjet printing for concentrations from dilute through the overlap regimes. They found that the physical behavior of the fluids in drop formation is due to the dominance of viscoelastic effect within the timescale of the process, in preventing ligament break up at the pinch point compared with a Newtonian fluid of

similar viscosity. Measured relaxation times were much longer than those calculated using the relationship reported by Tirtaatmadja et al. [1].

Vadillo et al. [59] developed a high speed filament stretch and breakup device for viscoelastic fluids with shear viscosities as low as 10 mPa·s. The filament breakup of polymer solutions was investigated and three regimes including the end pinching Newtonian drop formation, viscoelastic filament thinning and intermediate Rayleigh filament breakup were identified. The breakup behaviors were also compared to a scenario of DOD inkjet breakup; however, detail information on DOD drop formation of polymer solution is still needed.

Besides dilute polymer solutions, other non-Newtonian fluids such as fluids with colloidal particles are also widely investigated in the inkjet printing process. A review of this area can be found in Xi Wang's thesis [60].

2.3 Objective of Present Work

As a method of polymer patterning, inkjet printing has advantages compared to other techniques. Inkjet printing is a non-contact direct-deposition process, which means less contamination. There are wide ranges of materials and substrates available, and the deposition area, size and shape can be varied on demand. Therefore, inkjet printing has become an ideal choice in many cases for polymer patterning.

The basic requirement for inkjet printing is to generate a drop. Although DOD inkjet printing has many advantages compared with dripping mode and continuous jetting mode, the previous research has not cover much on DOD drop formation because it is extremely difficult to investigate under micron scale especially for polymer solutions. Many processes including the time evolution of liquid thread shape and velocity, breakup of liquid thread, satellite formation, and combination of

satellites and primary drop have not yet been investigated for DOD drop formation of polymer solutions.

The objective of this dissertation is to apply flash photography to visualize the DOD drop formation process of dilute polymer solutions so that a fundamental understanding of the dynamics of DOD drop formation of dilute polymer solutions could be developed based on experimental results. To achieve the objective, the effects of the driving waveform, jetting frequency and the composition of the polymer solutions on the dynamics of DOD drop formation were analyzed. The effects on important printing parameters such as drop speed, drop size, breakup time and the formation of satellites were studied. By quantifying the effects, predictive equations involving molecular weight, concentration and solvent viscosity were obtained which can be used to predict the jetting behavior of DOD drop formation of dilute polymer solutions. Additional tests were used to verify the predictive equations. The research in this thesis gives a better understanding of drop formation and of inkjet printing of dilute polymer solutions.

CHAPTER 3

THEORETICAL BACKGROUND OF DILUTE POLYMER SOLUTIONS

In this chapter, basic relationships for characterizing the PEO solutions and methods used to study the drop formation process are presented. Also important parameters in drop formation are discussed.

3.1 Relaxation Time Theory

3.1.1 Critical Concentration and Intrinsic Viscosity

The critical overlap concentration, c*, is defined as the concentration at which the polymer coils start to overlap with each other. Below c*, the solution is considered to be in the dilute regime and the viscoelastic properties of the solution are governed by the behavior of a single polymer molecule. The classification of Flory for flexible polymer solutions was used to calculate c* of the polymer solutions:

$$c^* = 1/[\eta] \qquad [3.1]$$

where $[\eta]$ is intrinsic viscosity with units of cm^3/g.

For the polymer solutions, $[\eta]$ was calculated using the Mark-Houwink-Sakurada (MHS) equation:

$$[\eta] = 0.072 M_w^{\alpha} \qquad [3.2]$$

where M_w is weight average molecular weight with units of g/mol. The MHS exponent (α) was assumed to be 0.65, which was recommended by Tirtaatmadja [1] for PEO solutions.

3.1.2 Relaxation Time Theory

During the DOD inkjet process, the polymer molecules experience elongation which orients the polymer chains and strain hardens the solution, which opposes pinchoff due to capillarity. The rate at which Brownian motion disorients the chains, which is characterized by relaxation time, is important in determining if the liquid ejected will pinch off from the nozzle and form a drop. In this study, relaxation time is estimated using a parameter referred to as effective relaxation time which is obtained by modifying the relaxation time,λ_z, from Zimm's model [1].

In Zimm's model, a polymer chain is represented by a chain of beads connected by ideal springs. The chain consists of N identical segments joining N+1 identical beads with complete flexibility at each bead. Each segment, which is similar to a submolecule, has a Gaussian probability function. According to Zimm's model, if a chain is suspended in a viscous liquid, each bead j encounters three different forces: mechanical force, Brownian force, and the hydrodynamic drag force.

In dilute solutions, hydrodynamic interactions between the segments in the polymer chain are strong. These hydrodynamic interactions also are strong between the segments and the solvent within the pervaded volume of the segment. The Zimm model, which deals with the polymer dynamics in a dilute solution, effectively treats the pervaded volume of the chain as a solid object moving through the surrounding solvent [61].

A relationship for relaxation time in terms of intrinsic viscosity and other parameters can be obtained from either Rouse's or Zimm's models, as described by Rubinstein [61]. Intrinsic viscosity is defined as:

$$[\eta] = \lim_{c \to 0} \frac{\eta - \eta_s}{\eta_s c}$$

where η is shear viscosity of the solutions, η_s is shear viscosity of the solvent and c is weight concentration.

The value of the stress relaxation modulus, G(τ), at the relaxation time τ is of the order of kT per chain:

$$G(\tau) \approx kT \frac{\phi}{Nb^3}$$

where N is the number of Kuhn monomer, k is Boltzmann constant, T is temperature, ϕ is volume fraction of polymer and b is the length of a Kuhn monomer.

The polymer contribution to the viscosity is proportional to G(τ) τ:

$$\eta - \eta_s \approx kT \frac{\phi}{Nb^3} \tau$$

The typical experimental concentration used in defining intrinsic viscosity is the polymer mass per unit volume of solution,

$$c = \phi M_0 / (b^3 N_A)$$

where M_0 is the molar mass of a Kuhn monomer and N_A is Avogadro's number. Thus:

$$[\eta] \approx \frac{kTN_A}{\eta_s M_0 N} \tau$$

Substituting λ_z for τ, using $M_w = NM_0$ and rearranging gives

$$\lambda_z \propto \frac{[\eta] M_w \eta_s}{N_A k_B T}$$

For a polymer chain in a good solvent, Tirtaatmadja gives the following relationship for the longest relaxation time (λ_z) in the Zimm theory:

$$\lambda_z \cong \frac{1}{\zeta(3\nu)} \frac{[\eta] M_w \eta_s}{N_A k_B T} \qquad [3.3]$$

Using this equation together with the values of intrinsic viscosity, the longest Zimm relaxation time can be calculated from the polymer molecular weight and solvent viscosity (noting that the intrinsic viscosity is assumed to be a function only of

the weight average molecular weight for dilute solutions). The relaxation times for the dilute aqueous solutions used in this study span the range $2.58\times10^{-6}\,s \le \lambda_z \le 1.15\times10^{-4}\,s$. Although these values are small, they are on the same time scale as that for emergence of liquid from the nozzle to first breakup when liquid pinches off from nozzle.

3.2 Viscosity and Surface Tension Effects

Ohnesorge number, a dimensionless number, comparing the ratio of viscous and surface tension effects, was calculated using the following relationship:

$$Oh = \frac{\eta_0}{\sqrt{\rho\sigma R_0}} \qquad [3.4]$$

The values of Oh for the experiments range from 0.025 to 0.153 (see Table 2 and 3 in Chapter 4).

According to Chandrasekhar's formula [17], the dimensionless growth rate (ω/ω_0) of the disturbance along the liquid thread as a function of the dimensionless wave number can be written as follows:

$$\omega/\omega_0 = \left\{\left[\frac{1}{2}x^2\left(1-x^2\right)+\frac{9}{4}Oh^2x^4\right]^{1/2} - \frac{3}{2}Ohx^2\right\} \qquad [3.5]$$

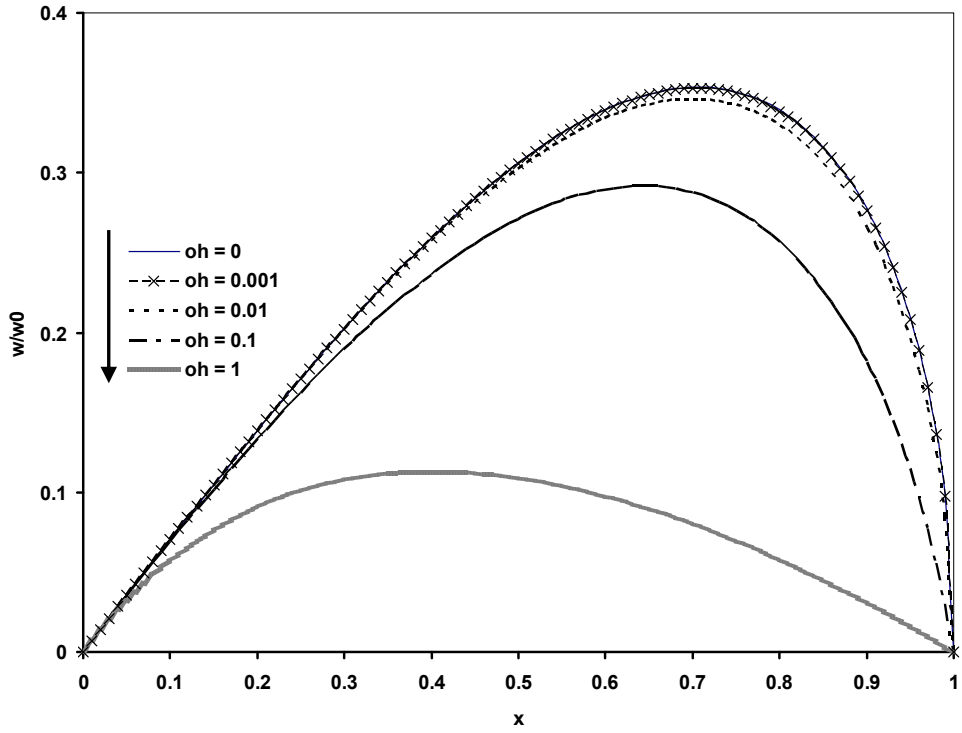

Figure 1 Dimensionless growth rate ω/ω_0 plotted as a function of dimensionless wave number x based on Chandrasekhar's formula.

In Figure 1, Equation 3.5 is used to plot the dimensionless growth rate, ω/ω_0, as a function of dimensionless wave number x. The figure shows that for values of Oh < 0.01, the curves of disturbance growth rate versus x are almost identical to that for Oh = 0. Thus for Oh < 0.01, the fluid can be treated as inviscid when considering disturbance growth rate. However, for Oh > 0.01, the curves are different for various values of Oh, and the fluid cannot be considered inviscid. In most of the millimeter-scale drop formation processes, the values of Oh for PEO aqueous solutions Oh<0.01, and thus the viscous effects are negligible, and the drop formation process can be considered as inviscid elastic flow [1, 62]. On the other hand, the DOD inkjet drop formation process is on the micron scale, and Oh is large enough that viscosity may have a small influence the disturbance growth rate, and the ink viscosity affects the DOD drop formation process. By using Newtonian aqueous solutions with shear

viscosities similar to those used in this dissertation, Dong et al. [16] showed that breakup time (t_b) depended only on capillary time, $t_{ca} = \sqrt{\rho R_0^3 / \sigma}$ and dimensionless growth rate:

$$t_b = C t_{ca} / (\omega / \omega_0) \text{ where C is constant.}$$

Thus, when the elasticity of the polymer solution is neglected, the characteristic time scale for break up, t_b, can be scaled by the capillary time [16-17, 62].

When elasticity of the liquid cannot be neglect, the relaxation time, λ, of the polymer solution becomes important. The ratio of the two time scales is a dimensionless number called the Deborah number (De) [63]:

$$De \equiv \frac{\lambda}{t_{ca}} = \frac{\lambda}{\sqrt{\rho R_0^3 / \sigma}} \qquad [3.7]$$

When De is small, elasticity is not important and can be neglected. For larger values of De, elasticity becomes important. At a critical value of De, elastic effects can prevent DOD drop formation.

Chapter 4

EXPERIMENTAL

In this chapter, the experimental setup and the materials used in the thesis are discussed. Some key parameters of the imaging system and the inkjet printhead are also discussed.

4.1 Visualization System

The method used for visualizing on the DOD drop formation is based on flash photography [2] and utilizes the setup shown schematically in figure 2 which was developed by Dong [2]. The camera, laser system and print head are fastened on an optical table to minimize vibration. By synchronizing the pulsed laser, CCD camera with the inkjet print head, sharp image of drop formation can be obtained.

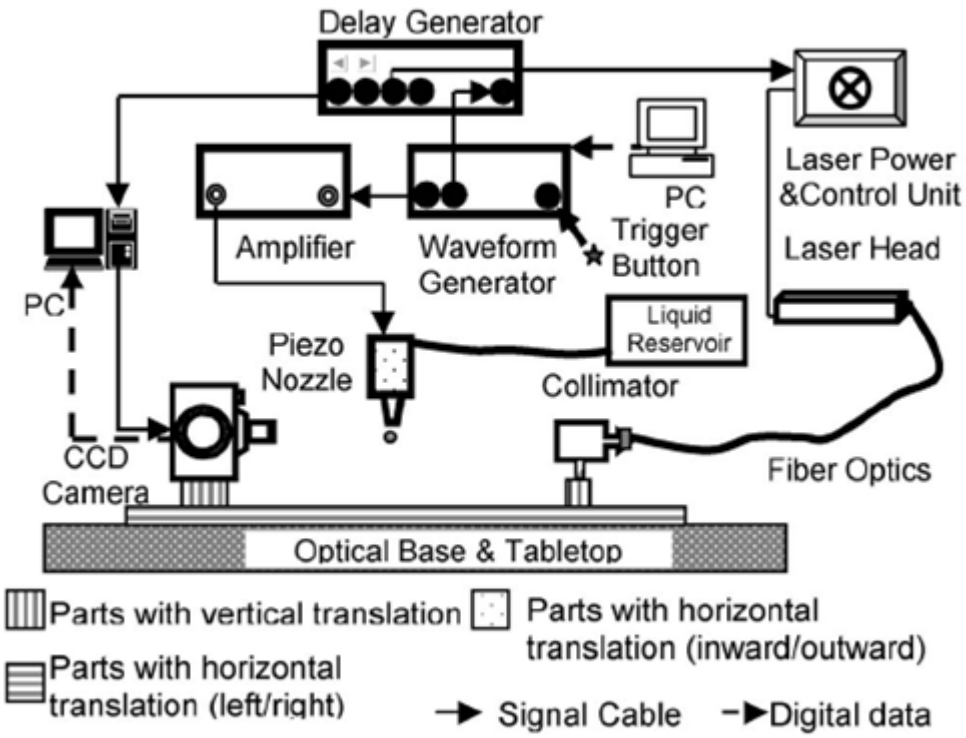

Figure 2 Experimental setup [2]

To achieve synchronization, a trigger signal generated from Agilent 33220A is sent to a waveform generator (Tegam 2414B), the waveform generator then sends a driving pulse to the amplifier (Trek Model PZD 350) and a TTL signal, which is in sync with the driving pulse, to a delay generator (BNC 500). After amplification, the driving pulse is applied to the piezo transducer in the printhead (Trident) to eject liquid. The amplitude and shape of the driving pulse can be programmed according to the requirements of the printhead and liquid being ejected. Upon receiving the TTL trigger signal, the delay generator sends out two signals: a 5- volt TTL signal to the CCD camera (SensiCam), and a burst of TTL signals with a preprogrammed number of cycles to the laser systems. The delay time and width of TTL signals are parameters that are set before the experiment begins. By adjusting delay times for the camera and laser, the drop generation by the printhead, shutter operation of the camera and laser flash are synchronized. Hence, one image can be obtained. Through

changing the delay times of the camera and laser, images with different delay time from drop ejection are captured. These images are combined to obtain a sequence of images of drop formation and/or impaction.

There are 640x480 pixels on the CCD sensor used in this study with the dimension of 6.3 mm by 4.8 mm. Using a group of microscope objectives with a working distance of about 25.4 mm, the spatial resolution of image is up to 0.81 mm/pixel with this system; the resolution could, in principle, be increased by use of a higher resolution CCD (operating at low frame rate). However, for the visible light with the wavelength of about 550 nm as used in present experiments, the resolution of a compound microscope lenses is about 250 nanometers according to the Rayleigh criterion. The camera system can be triggered via an external, edge active TTL signal. The CCD camera has a maximum frame rate of 30 frames per second and a storage capability of 727 images. The image data are read from the camera and transferred via PCI-Bus to the PC memory once the storage memory is full.

As the visualization window is 518.4X388.8 μm, and sometimes the images are larger than the visualization window. An optical base which can move vertically is attached to the printhead so that the images can be taken at different vertical positions at the same delay time. The images taken at the same delay time can be processed and integrated into one image, by this way, the images that are larger than the visualization window can be obtained.

The Trident printhead is based on a push mode design (Trident User's Manual, 1997). When a voltage is applied to the transducer, the transducer contracts, enlarging the ink chamber and causes ink to fill it. When the voltage is rapidly released from the transducer, the transducer resumes its original length, which creates a sudden pressure pulse on the liquid in the ink chamber. A sufficient and well-shaped pressure pulse

causes liquid to be ejected from the nozzle (D = 53 μm and L = 75 μm) at the end of the chamber, and a drop is generated.

4.2 Laser System Adjustment to Reduce Speckle

The Cu vapor laser used in previous inkjet research at Georgia Tech failed and was too expensive to be replaced. A solid-state laser (Quantronix Osprey Air-cooled, Diode-Pumped CW/Q-switched Laser Systems) was purchased for the visualization system. The solid-state laser has several advantages over the Cu vapor laser including cost, precise time delay control, small size, etc. However, the laser is highly coherent both temporally and spatially, which cause a major problem with speckle.

A speckle pattern is a random intensity pattern produced by the mutual interference of a set of wavefronts. This phenomenon has been investigated by scientists since the time of Newton; however, speckle did not come into prominence until the invention of the laser. In a conventional laser microscope, the image quality is strongly degraded by speckle coming from unwanted interference of scattered light. Speckle is a direct consequence of the interaction of a rough surface with a laser beam possessing a high degree of spatial and temporal coherence. Our laser (Quantronix Osprey Air-cooled, Diode-Pumped CW/Q-switched Laser Systems) has a wavelength of 532 nm, pulse width of 22 ns, maximum power of 8 W (at current = 40 A), and frequency in the range of 1 – 53.2 kHz. The laser beam ($1/e^2$) diameter coming out of the laser head is 0.5 mm with a divergence angle of 0.09 degrees. According to the manufacturer, the laser light is highly coherent which leads to speckle.

The speckle pattern can be eliminated in many cases with moving optical elements, multiple beam illumination, redundancy, coded diffusers, or adjustment of illumination and viewing apertures. However, most of them are not suitable for our microsecond exposure photographs [64]. We modified our system to reduce beam

coherence so that speckle was reduced to an acceptable level, see Figure 3. After the highly coherent laser beam exits the laser head, it is expanded 10 times its original diameter using a BeamX® laser beam expander, and then the expanded beam travels through an optical fiber bundle, which contains 50 optical fibers of varying lengths. The length difference between any two fibers is at least 1 cm which is longer than the coherence length of the laser. When the beam exits the optical fiber bundle, it passes through a diffuser and is then refocused by a collimator to get a concentrated laser beam with reduced coherence. In Figure 4, drops photograph with and without the speckle reducer are compared.

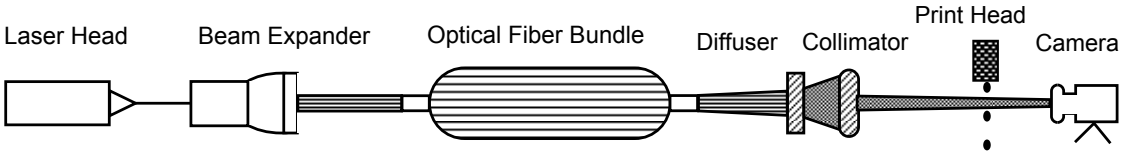

Figure 3 Experimental setup of the speckle reducer

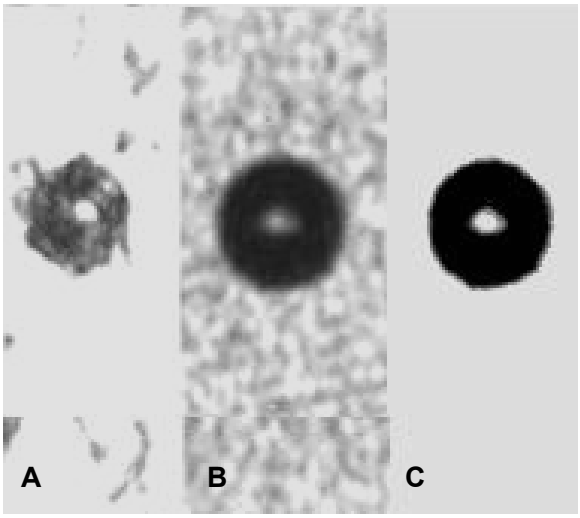

Figure 4 (A) Picture illuminated by highly coherent laser beam; (B) Picture illuminated by laser after passing through the speckle reducer; and (C) Photograph in B after processing.

4.3 Waveform of the Driving Signal

A double peak waveform, suggested by the Trident printhead user's manual and shown in Figure 5, was used for all tests except one tests discussed in Chapter 7. For most of the test, the voltage amplitude, V, was either 29.6 or 44.2 volts. The times shown in Figure 5 were used in all of the tests except those discussed in Chapter 7. During the rising time (T_1), the piezo transducer expands which causes liquid to fill the nozzle chamber. A slow rising time is used to prevent air from being sucked into the channel through the nozzle orifice. During the falling time (T_2), the reduction of voltage causes the transducer to retract to its original length, increasing the pressure on the liquid in the chamber. As a result, liquid is ejected from the nozzle orifice. After the voltage falls to zero, it is held there for a short time (T_3). Then a smaller pulse is applied to the transducer. The shape is similar to the initial pulse, but the voltage maximum amplitude is smaller, and corresponding the rising time (T_4) is shorter. After reaching the voltage reaches its maximum, it falls over a falling time (T_5) in a fashion similar to that of the initial pulse. The smaller pulse is used to promote separation of liquid from the nozzle orifice by producing a negative pressure in the nozzle. The falling pressure decelerates the liquid causing it to break from the nozzle orifice.

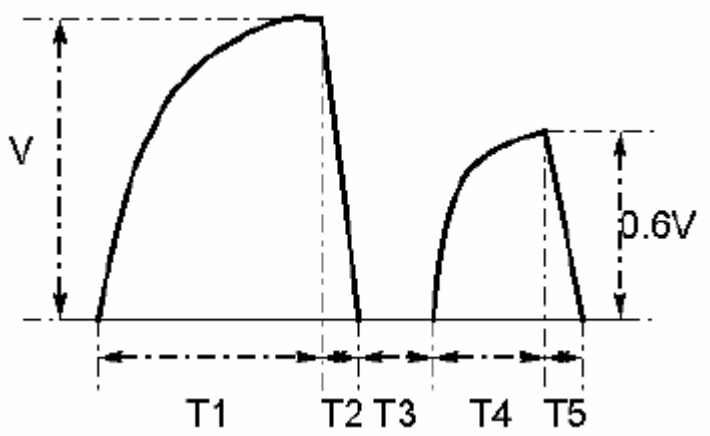

Figure 5 Double Peak waveforms rising time T_1=10.6 μs, falling time T_2=2.6 μs, dead time T_3=5.3 μs, rising time T_4 of minor peak=4.4 μs, falling time T_5 of minor peak=3.0 μs.

4.4 Materials

The inks used for the experiments were dilute polymeric solutions with the solvent being mixtures of distilled water and glycerin. The polymer primarily used was poly (ethylene oxide)/PEO. The initial research was conducted using samples (viscosity molecular weights of 14k, 35k, 100k, 300k, 1000k g/mol) that were purchased from Sigma-Aldrich and are similar to those used by Tirtaatmadja et al. [1] in their research where the effect of polymer on drop formation in the dripping mode was investigated. These PEO samples have relatively large polydispersities, which are about 1.8 according to Tirtaatmadja et al. [1]. The initial research indicated that molecular weight is extremely important in DOD drop formation; however, the molecular weight distribution of the PEO obtained from Sigma-Aldrich was not available. Since molecular weight has a large effect on DOD drop formation, PEO samples with narrow molecular weight distributions were purchased from PolymerSource. These are listed in Table 1 along with their polydispersities.

Table 1 Properties of PEO samples.

Sample Number	Sample Name	Molecular Weight (g/mol)	PDI	Purchased from
N/A*	Poly Ethylene Oxide	14,000**	N/A*	Sigma-Aldrich
N/A*	Poly Ethylene Oxide	35,000**	N/A*	Sigma-Aldrich
N/A*	Poly Ethylene Oxide	100,000**	N/A*	Sigma-Aldrich
N/A*	Poly Ethylene Oxide	300,000**	N/A*	Sigma-Aldrich
N/A*	Poly Ethylene Oxide	1,000,000**	N/A*	Sigma-Aldrich
P2798-EO	Poly(ethylene glycol) methyl ether	59,000***	1.02	PolymerSource
P8846-4EOOH	Four-arm Poly ethylene Oxide	60,000***	1.15	PolymerSource
P5377-EG2OH	Poly Ethylene Oxide	95,000***	1.08	PolymerSource
P5656-EG2OH	Poly Ethylene Oxide	90,000***	2.5	PolymerSource
P4214-EG2OH	Poly Ethylene Oxide	203,000***	1.14	PolymerSource
P5617-EG2OH	Poly Ethylene Oxide	420,000***	1.12	PolymerSource
P5614-EG2OH	Poly Ethylene Oxide	700,000***	1.20	PolymerSource

* Not available.

**M_v, molecular weight is measured based on viscosity. PDI's are not provided by Sigma-Aldrich; however, Tirtaatmadja et al. [1] suggest that they are about 1.8.

***M_n, number average molecular weight.

Two of the polymers (P2798-EO and P8846-4EOOH) having similar molecular weights were obtained from PolymerSource to investigate the effect of shape of the polymer chains on DOD inkjet drop formation. P2798-EO is a linear chain polymer and P8846-4EOOH is a four-arm polymer.

Additional information (obtained from PolymerSource) on molecular weight distribution, synthesis and purification procedure, and results of thermal analysis can be found in the Appendix.

The solutions (weight concentration from 0.005wt% to 10wt%) were prepared by mixing distilled water and glycerin mixtures with PEO under room temperature and were held for at least 48 hours before using. The composition and basic properties of PEO aqueous solution used in this thesis are given in Table 2 and Table 3.

Table 2 Composition and basic properties of inks containing PEO, with relatively large polydispersities, purchased from Sigma-Aldrich.

Mw (g/mol)	c (wt%)	[η] (ml/g)	c/c*	η_s (mPa•s)	η (mPa•s)	λ_z (μs)	λ_{eff} (μs)	σ (mN/m)	Oh	t_{ca} (μs)	De
100,000	0.01	128.0	0.013	1.06	1.12	2.58	3.03	66.6	0.027	16.7	0.18
100,000	0.02	128.0	0.026	1.06	1.15	2.58	4.75	65.8	0.028	16.8	0.28
100,000	0.05	128.0	0.064	1.06	1.17	2.58	8.62	65.8	0.028	16.8	0.51
100,000	0.10	128.0	0.13	1.06	1.21	2.58	13.5	66.0	0.029	16.8	0.81
100,000	0.20	128.0	0.26	1.06	1.33	2.58	21.2	65.8	0.032	16.8	1.26
100,000	0.50	128.0	0.64	1.06	1.68	2.58	38.5	65.9	0.040	16.8	2.29
100,000	0.66	128.0	0.85	1.06	1.72	2.58	46.1	65.9	0.041	16.8	2.74
100,000	0.01	128.0	0.013	4.30	4.30	10.5	12.3	65.6	0.103	16.8	0.73
100,000	0.02	128.0	0.026	4.30	4.49	10.5	19.3	58.2	0.114	17.9	1.08
100,000	0.05	128.0	0.064	4.30	4.62	10.5	35.0	56.2	0.120	18.2	1.92
100,000	0.10	128.0	0.13	4.30	4.76	10.5	54.9	56.0	0.124	18.2	3.01
300,000	0.01	261.5	0.026	1.06	1.13	15.8	29.5	69.2	0.026	16.4	1.80
300,000	0.02	261.5	0.052	1.06	1.16	15.8	46.3	65.9	0.028	16.8	2.76
300,000	0.05	261.5	0.13	1.06	1.26	15.8	84.0	65.8	0.030	16.8	5.00
300,000	0.10	261.5	0.26	1.06	1.30	15.8	132	65.9	0.031	16.8	7.84
1000,000	0.00046	571.9	0.002	1.06	1.08	115	46.3	73.0	0.025	16.0	2.90
1000,000	0.005	571.9	0.029	1.06	1.08	115	228	73.0	0.025	16.0	14.28
1000,000	0.007	571.9	0.040	1.06	1.08	115	284	72.8	0.025	16.0	17.77
1000,000	0.01	571.9	0.057	1.06	1.13	115	358	72.7	0.026	16.0	22.36
1000,000	0.015	571.9	0.086	1.06	1.15	115	466	69.4	0.027	16.4	28.44
1000,000	0.02	571.9	0.11	1.06	1.18	115	561	66.4	0.028	16.7	33.53
1000,000	0.05	571.9	0.29	1.06	1.29	115	1020	65.8	0.031	16.8	60.57
1000,000	0.10	571.9	0.57	1.06	1.73	115	1600	65.5	0.042	16.9	94.82

Table 3 Composition and basic properties of inks containing PEO, with relatively small polydispersities, purchased from PolymerSource.

M_n (g/mol)	c (wt%)	[η] (ml/g)	c/c*	η_s (mPa•s)	η (mPa•s)	λ_z (μs)	λ_{eff} (μs)	σ (mN/m)	Oh	t_{ca} (μs)	De
59,000	0.1	90.9	0.09	1.06	1.16	1.08	4.53	67.50	0.027	16.6	0.27
59,000	0.5	90.9	0.45	1.06	1.68	1.08	12.9	67.70	0.040	16.6	0.78
95,000	0.01	123.8	0.12	1.06	1.26	2.37	12.2	67.70	0.030	16.6	0.73
95,000	0.10	123.8	1.24	1.06	3.18	2.37	54.3	67.40	0.075	16.6	3.27
203,000	0.05	202.9	0.10	1.06	1.20	8.29	37.4	64.70	0.029	17.0	2.20
203,000	0.1	202.9	0.20	1.06	1.31	8.29	58.7	67.70	0.031	16.6	3.54
203,000	0.2	202.9	0.41	1.06	1.58	8.29	92.1	66.40	0.038	16.7	5.50
203,000	0.4	202.9	0.81	1.06	2.03	8.29	144.4	67.70	0.048	16.6	8.71
203,000	0.6	202.9	1.22	1.06	2.60	8.29	188.0	67.90	0.061	16.6	11.36
203,000	0.8	202.9	1.62	1.06	3.50	8.29	226.7	68.00	0.082	16.5	13.70
203,000	1	202.9	2.03	1.06	4.20	8.29	342.51	67.90	0.099	16.6	15.83
203,000	0.05	202.9	0.10	5.88	6.00	46.0	207.0	58.00	0.153	17.9	11.58
420,000	0.01	325.4	0.03	1.06	1.15	27.5	59.3	69.00	0.027	16.4	3.61
420,000	0.02	325.4	0.07	1.06	1.16	27.5	93.0	68.00	0.027	16.5	5.62
420,000	0.05	325.4	0.16	1.06	1.28	27.5	168.7	68.50	0.030	16.5	10.23
420,000	0.1	325.4	0.33	1.06	1.52	27.5	264.7	67.90	0.036	16.6	15.99
420,000	0.15	325.4	0.49	1.06	1.78	27.5	344.5	67.40	0.042	16.6	20.73
420,000	0.2	325.4	0.65	1.06	1.91	27.5	415.4	67.90	0.045	16.6	25.09
700,000	0.005	453.6	0.02	1.06	1.11	63.9	108.9	70.30	0.026	16.3	6.69
700,000	0.01	453.6	0.05	1.06	1.14	63.9	170.8	70.90	0.026	16.2	10.54
700,000	0.02	453.6	0.09	1.06	1.20	63.9	268.1	68.90	0.028	16.4	16.31
700,000	0.05	453.6	0.23	1.06	1.37	63.9	486.3	68.70	0.032	16.5	29.55

4.5 Characterization Instrumentation

The properties of the liquid were characterized using available equipment at Georgia Tech. Dynamic surface tension was measured using a drop volume tensiometer LAUDA TVT2, and the static surface tension was measured using a Kruss bubble pressure tensiometer BP21was used to measure the static surface tension. The viscosity of the liquids was measured using a Brookfield DI-V+ Viscometer with LV spindle set.

The dynamic surface tensions (σ) of PEO dilute solutions are shown in Figure 6. There is not much difference between the dynamic surface tensions of solutions of PEO at different molecular weights and concentrations, except for the solutions containing very low concentration (0.01wt%).

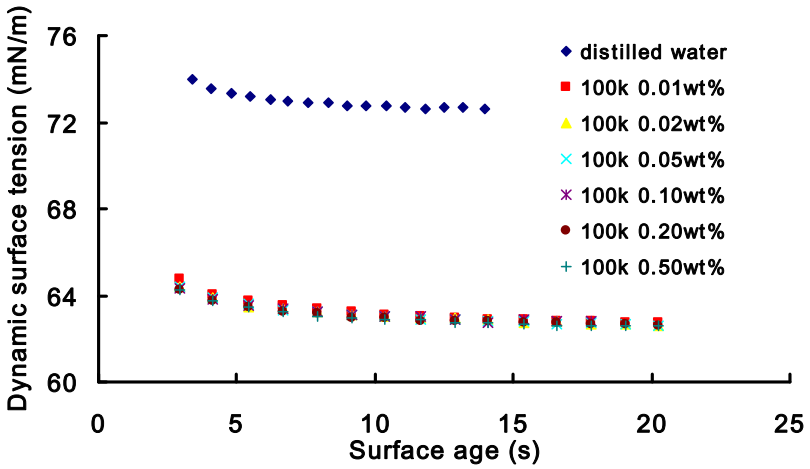

(A)

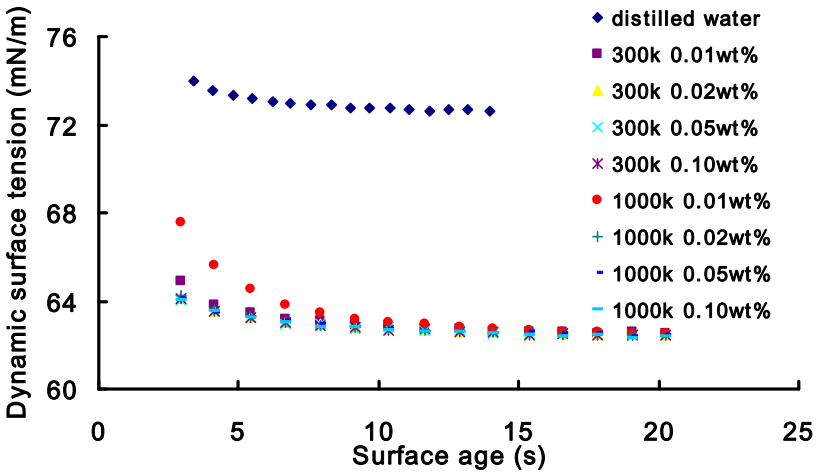

(B)

Figure 6 Dynamic surface tension of PEO aqueous solutions of (A) M_v = 100 kg/mol and (B) M_v = 300 kg/mol & 1000k g/mol at different concentrations.

CHAPTER 5

DOD DROP FORMATION OF POLYDISPERSED PEO SOLUTIONS

Results of the initial research using polydispersed PEO is presented in this chapter. The polymer was similar to the materials used in Tirtaatmadja et al. [1] in their research where the effect of polymer on drop formation in the dripping mode was investigated.

The effect of the addition of polymer to Newtonian fluid varies significantly depending on polymer concentration and molecular weight. For the lower molecular weight PEO (14k and 35k g/mol), the effects of the polymer are small for dilute solutions, even at c/c* = 1. On the other hand, for the higher molecular weight PEO (300K and 1000k g/mol), as PEO concentration is increased, the effect of polymer increases significantly until pinch off does not occur, i.e., polymer totally inhibits drop formation. For these two molecular weights, inhibition of pinchoff occurs for concentration below c/c* = 1.

First the effects that PEO can have are shown by comparing the DOD the stages of DOD Drop Formation for Newtonian base liquid with those of PEO aqueous solution. Then the effect of varying concentration and molecular weight will be discussed.

5.1 DOD Inkjet Drop Formation of PEO Aqueous Solution

A typical process of DOD drop formation of Newtonian fluid (see Figure 11) is composed of the following stages: (a) ejection of liquid, (b) stretching, necking and pinch-off of liquid thread from nozzle, (c) recoil and breakup of free liquid thread,

and (d) formation and recombination of primary drop and satellite [2]. The stages will be discussed in section 5.2.

Drop formation of a Newtonian liquid (distilled water) is shown in Figure 7. Stage (a), ejection of liquid, happens roughly before 10 μs. During ejection, liquid in the nozzle is accelerated and pushed out of the nozzle orifice. Initially, a liquid column is formed. After a short time the liquid flow rate from the nozzle decreases, and the difference in axial velocity between the column head and the liquid at the nozzle exit causes the liquid column to stretch. The speed of the liquid at the nozzle exit falls until no additional liquid flows into the column and possibly even some liquid is sucked back into the nozzle due to the negative pressure in the printhead. Since the volume of the liquid column remains nearly constant, the inertia of the liquid elongates the column, creating new surface with the corresponding increase in the surface energy. Stage (b), stretching, necking and pinchoff of liquid thread from nozzle, occurs between approximately 10 and 30 μs; stage (c), recoil and breakup of the free liquid thread, takes place between about 30μs and 60 μs; and stage (d), formation and recombination of satellites, starts at approximately 70 μs and ends at around 90 μs. After that, the primary drop and two satellites continue to move at approximately constant speeds, with the primary drop moving faster than the two satellites.

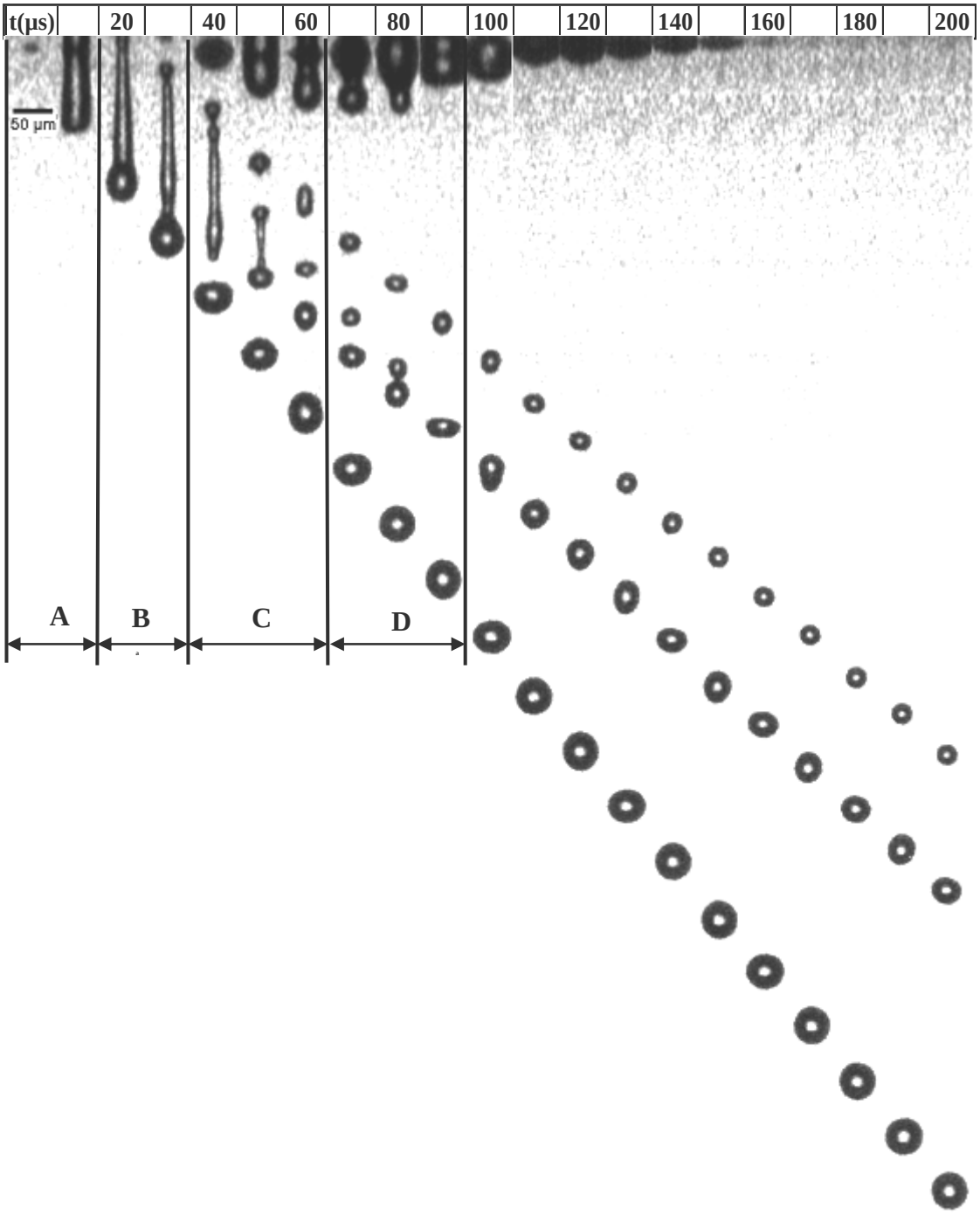

Figure 7 DOD Drop formation of distilled water including stages: (A) ejection of liquid, (B) stretching, necking and pinch-off of liquid thread from nozzle, (C) recoil of free liquid thread, breakup of the free liquid thread, and (D) formation and recombination of satellites. Images begin at 0 µs when liquid emerges from the nozzle and are shown for every 10 µs through 200 µs. Driving voltage = 44.2V and jetting frequency = 20Hz.

The effect of polymer on DOD drop formation will be shown by comparing the drop formation process of a polymer solution with that of the base liquid which is a Newtonian fluid. By adjusting polymer concentration and/or molecular the effects of polymer can be reduced or increased. In some cases, pinch off does not occur so that polymer total inhibits drop formation. The following four cases will be discussed where the effects were: (a) small, (b) moderate, (c) significant, and (d) extreme, resulting in no drop formation. After these are discussed, the stages of DOD Drop formation for PEO aqueous solution (case c where the effects are significant) are compared with those for the base solution.

5.1.1 Case A: Small Effects

In Figure 8, drop formation of aqueous solution containing PEO (Mw=300k g/mol, w%=0.01%, and c/c* = 0.026) is shown. The effects of polymer are small, but can be seen by comparing Figures 7 and 8. When drop formation of aqueous solution containing PEO is compared with that of distilled water, the following observations can be made concerning the polymer solution:

1. Breakup time increased from less than 30 μs to more than 60 μs;
2. Before pinchoff occurs near the nozzle, the long liquid thread below the nozzle pinches off from the bulbous head that becomes the primary drop;
3. Travelling speed of the primary drop containing PEO was slightly lower; and
4. Two satellites were generated in both cases; however, the satellites formation for the PEO solution was less reproducible.

The images shown in Figures 7 and 8 are based on flash photography which assumes that the phenomenon being observed is reproducible so that the process can be repeated many times and photographed at different times. Then the images can be shown in sequence to reveal information about the process. Notice that in Figure 8 the

primary drop moves smoothly downward with time; the first satellite also appears to move downward with time, but the movement appears to be a little irregular; the second satellite's change in position with time is very irregular, revealing that the satellite formation for the PEO solution is much less reproducible than for the distilled water DOD drop formation.

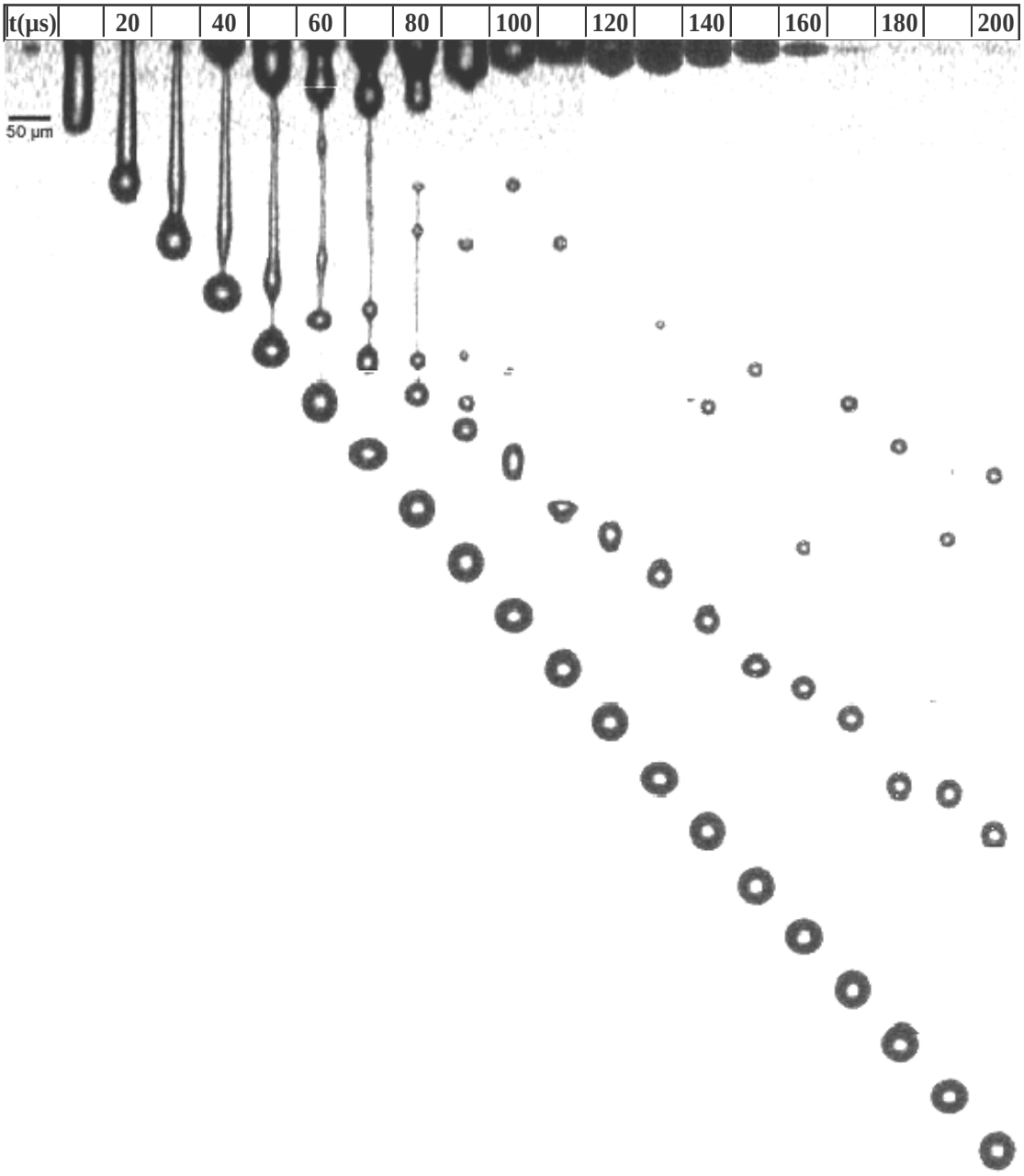

Figure 8 DOD Drop formation of PEO aqueous solution PEO (Mw = 300k g/mol, c = 0.01wt%, c/c* = 0.026). Images begin at 0 μs when liquid emerges from the nozzle and are shown for every 10 μs through 200 μs. Driving voltage = 44.2V and jetting frequency = 20Hz.

5.1.2 Case B: Moderate Effects

In Figure 9, images of drop formation of aqueous solution containing PEO (Mw=1000k g/mol, c=0.01wt%) are shown. The effects of polymer are larger than

observed in case A. By comparing Figures 7 and 9, the following observations can be made concerning the polymer solution:

1. Breakup time increased to more than 100 μs, and a long tail was formed and then broke up into small satellites, which later recombined with the one major satellite;
2. Pinchoff occurs near the nozzle at about the same time that the long liquid thread below the nozzle pinches off from the bulbous head that becomes the primary drop;
3. Travelling speed of the primary drop was lower than for case A; and
4. After recombination occurred, only one satellite was present.

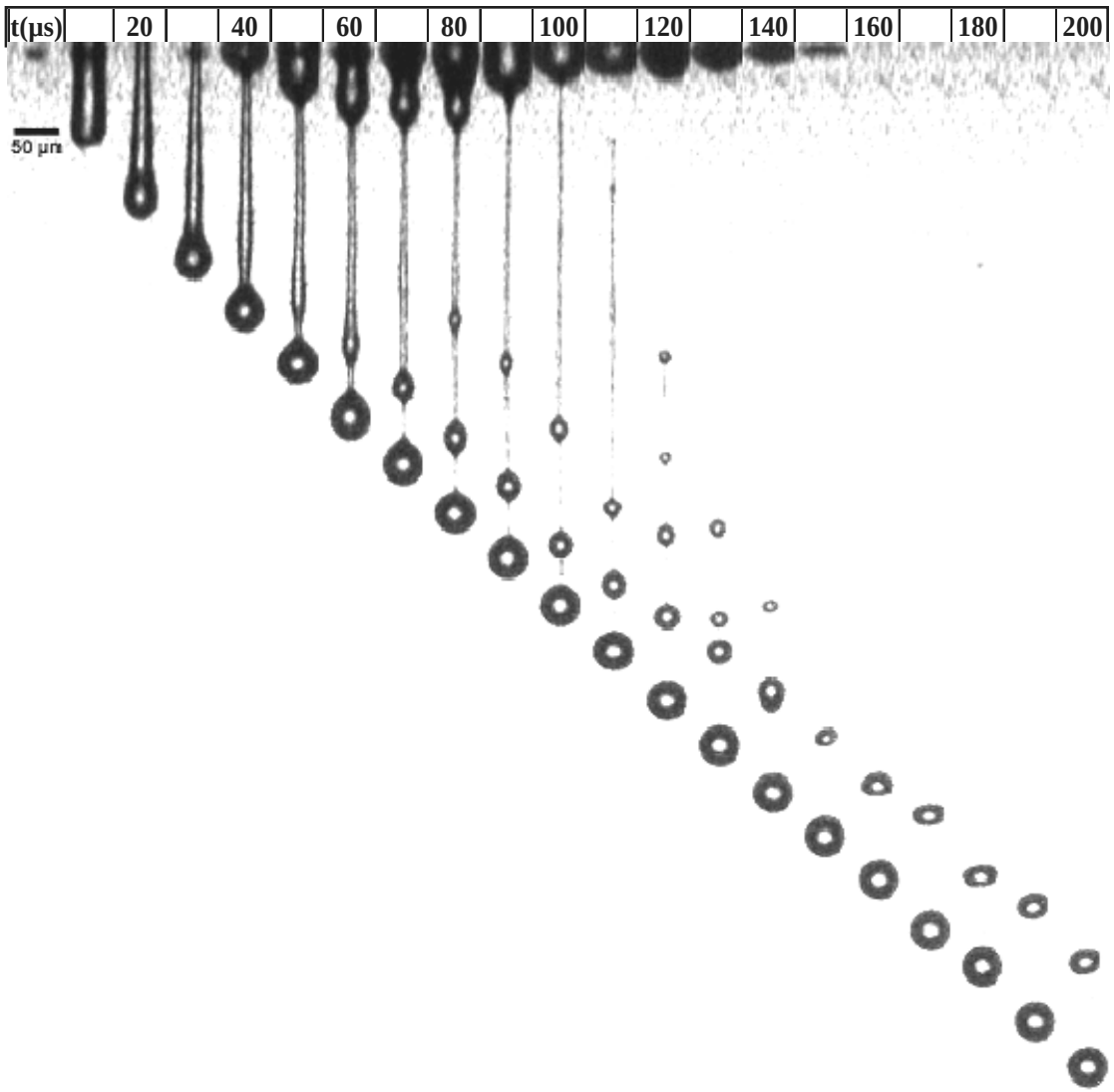

Figure 9 DOD Drop formation of PEO aqueous solution PEO (Mw = 1000k g/mol, c = 0.01wt%, c/c* = 0.057). Images begin at 0 µs when liquid emerges from the nozzle and are shown for every 10 µs through 200 µs. Driving voltage = 44.2V and jetting frequency = 20Hz.

5.1.3 Case C: Significant Effects

In Figure 10, drop formation of aqueous solution containing PEO (Mw=1000k g/mol, c=0.015wt%) is shown. The effects of polymer are significant.

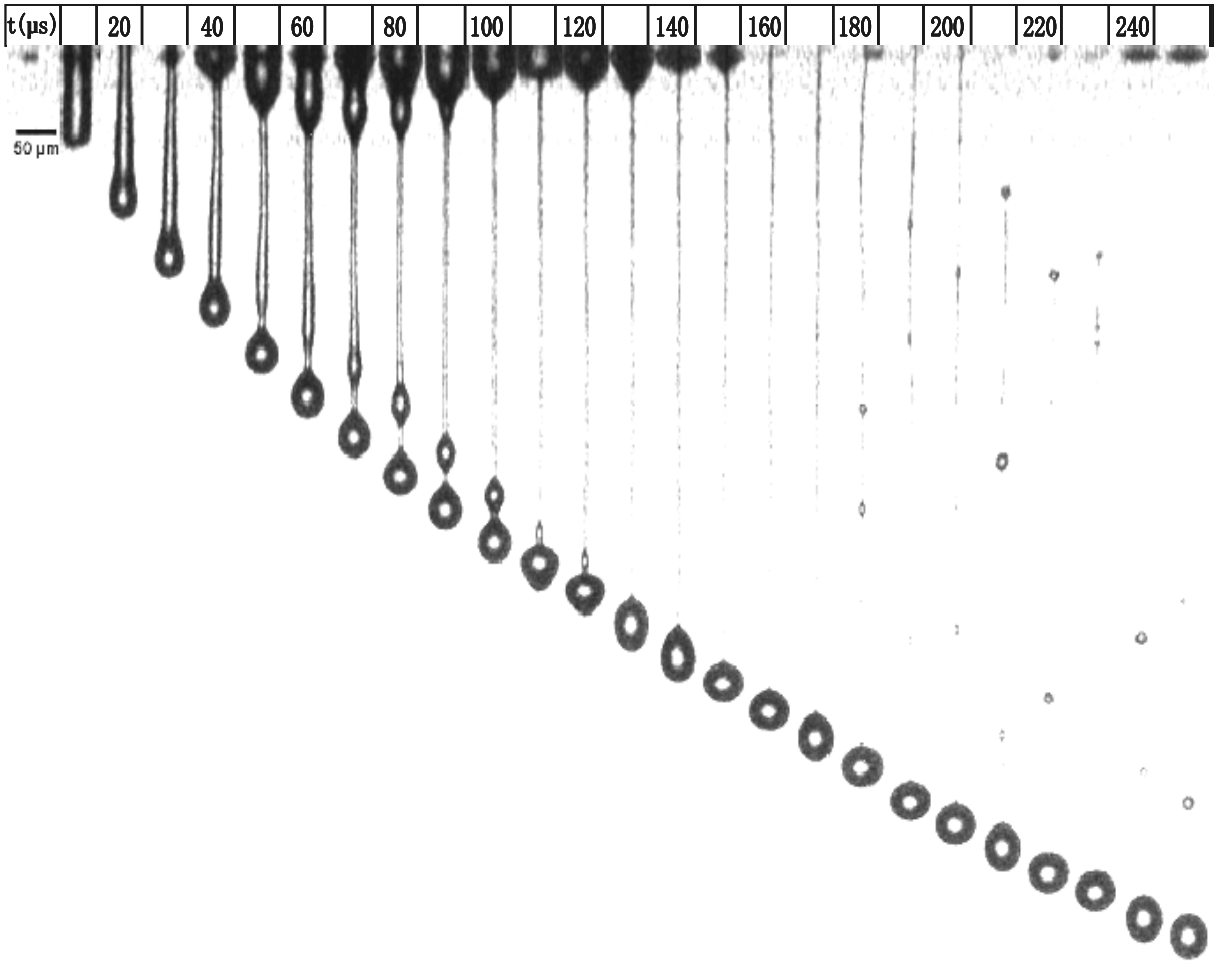

Figure 10 DOD Drop formation of PEO aqueous solution PEO (Mw = 1000k g/mol, c = 0.015wt%, c/c* = 0.086). Images begin at 0 μs when liquid emerges from the nozzle and are shown for every 10 μs through 200 μs. Driving voltage = 44.2V and jetting frequency = 20Hz.

By comparing Figures 7 and 10, the following observations can be made concerning the polymer solution:

1. Pinchoff is significantly delayed. A long tail forms between the bulbous head, which becomes the primary drop, and the liquid near the nozzle;
2. Breakup time occurs at about 200 μs, but the location of the breakup varies from drop to drop;
3. After the breakup, the long tail broke up into extremely small satellites, which

later usually disappeared, probably due to solvent evaporation and the small size of the remaining polymer;

4. Travelling speed of the primary drop was much lower than for previous cases; and
5. No major satellites were generated during the drop formation process.

5.1.4 Case D: Extreme Effects Resulting in No Drop Formation

In Figure 11, attempted drop formation of aqueous solution containing PEO (Mw=1000k g/mol) at three concentrations ((A) 0.02wt%, (B) 0.05wt%, (C) 0.1wt%) are shown.

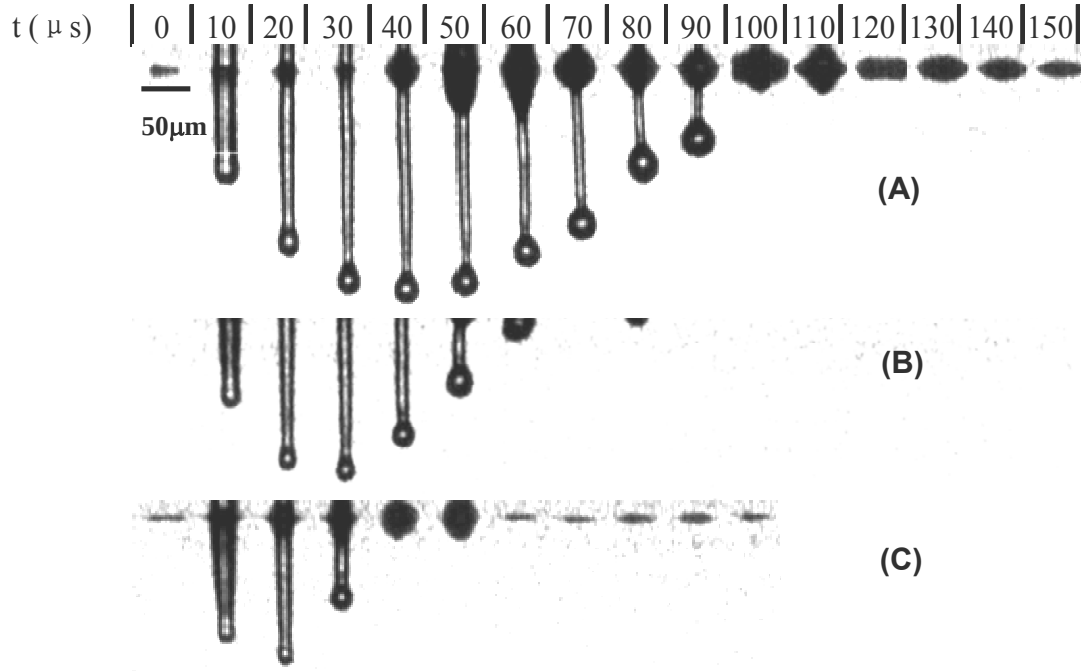

Figure 11 Attempted Drop formation of ink with PEO at Mw = 1000k and c = (A) 0.02wt%, (B) 0.05wt%, (C) 0.1wt%. Images begin at 0 μs when liquid emerges from the nozzle and are shown for every 10 μs through 150 μs. Driving voltage = 29.6V and frequency = 20Hz.

As shown in Figure 11, the liquid was pushed out of the nozzle, did not pinch off, and was sucked back into the nozzle. No drops were formed in these cases. As polymer concentration was increased, the time during which the liquid remain out of

the nozzle decreased, and the shape of the ligament changed. In Figure 11 (A), the shape of the ligament at 10 μs was a column which was similar to the previous three cases, and a bulbous head was also formed. The ligament did not form a separate drop before it was sucked back to the nozzle. In Figure 11 (C), at 10 μs, the radius of the ligament decreased with distance from the nozzle, and no obvious bulbous head was formed.

5.2 Comparison of Stages of DOD Drop Formation for Newtonian Liquid and PEO Aqueous Solution

In this section, the stages of DOD Drop formation for PEO aqueous solution are compared with those for the base solution which is a Newtonian liquid. Images of drop formation of distilled water and PEO aqueous solution for the same jetting parameters are shown in Figures 7 and 10, respectively. PEO concentration and molecular weight were selected so that the effects that polymer has on the stages of drop formation can be illustrated in detail.

5.2.1 Ejection of liquid

During the ejection stage, the drop formation process of PEO aqueous solution showed no obvious difference with that of water, as seen in Figure 12. When the piezo transducer expanded, liquid in the nozzle was pushed out of the nozzle orifice. After a short time, the liquid flow rate from the nozzle decreased. The difference in axial velocity between the column head and the liquid at the nozzle exit caused the liquid column to stretch. The speed of the liquid at the nozzle exit continued to fall until no additional liquid flowed into the column and possibly even some liquid was sucked back into the nozzle due to the negative pressure associated with the second pulse of the waveform causing contraction of the piezoelectric transducer. The

volume of the liquid column remained constant, and the inertia of the liquid continued to extend the column. The rate of extension decreased as new surface was created with the corresponding increase in the surface energy.

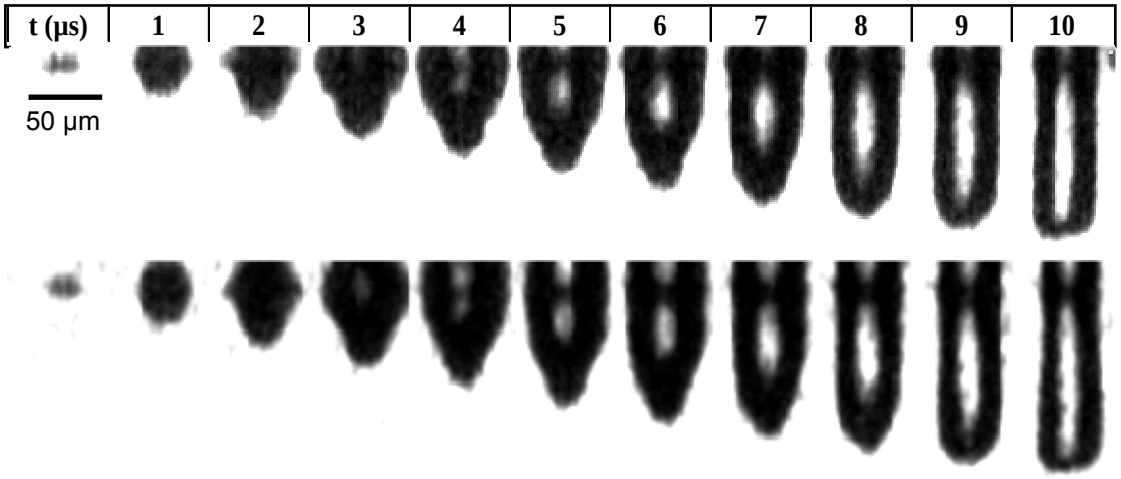

Figure 12 Sequence of images of DOD drop formation for PEO aqueous solution (upper row, Mw = 1000k g/mol, c = 0.015 wt%, c/c* = 0.086) and water (lower row) during the stage of ejection and stretch of fluid. Driving voltage = 44.2V and jetting frequency = 20Hz. Images begin at 0 μs when liquid emerges from the nozzle and are shown for every 1 μs through 10 μs.

5.2.2 Stretching, Necking and pinch-off from nozzle

During the stretching of the liquid column, the liquid at the nozzle exit necked. This necking position remained at the nozzle exit and the radius of the liquid thread here continuously thinned. For water, a second necking point began to appear toward the head of the column, eventually producing a bulbous head. Thus, a long transitional liquid column was created, reaching from the nozzle to the head. However, for PEO aqueous solution, no second necking was observed at this time. Finally, for water, the tail of the liquid thread pinched off at t = 28 μs from the nozzle exit, creating a free liquid thread with a bulbous head, while for PEO aqueous solution, the liquid column still remained at the necking stage at the nozzle exit, as seen in Figure 13. The pinch-

off for PEO aqueous solution did not happen until 200 μs at the same time when recoil and break up occurred for distilled water.

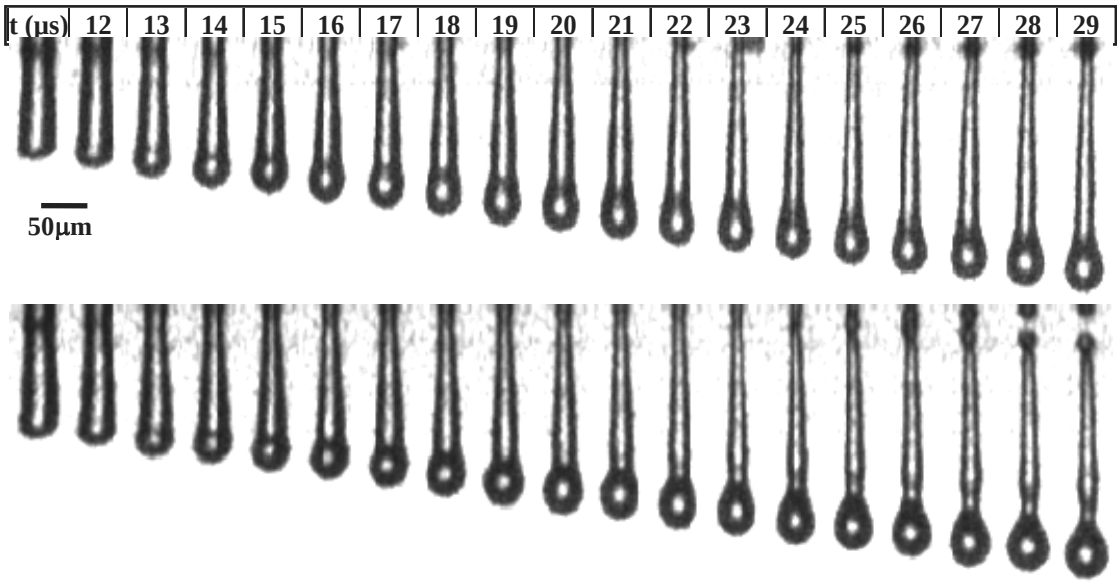

Figure 13 Sequence of images of DOD drop formation for PEO aqueous solution, (upper row, Mw = 1000k g/mol, c = 0.015 wt%, c/c* = 0.086) and water (lower row) during the stretching, necking and pinching-off from the nozzle. Driving voltage = 44.2V and jetting frequency = 20Hz. Images begin at 11 μs after liquid emerges from the nozzle and are shown for every 1 μs through 29 μs.

.

5.2.3 Recoil and break up of free liquid thread

For water, the surface contracted, and during the shrinkage of the liquid thread, a second neck near the bulbous head continued to evolve until the liquid thread broke up into two parts, a primary drop and a free secondary liquid thread. For the polymer aqueous solution, the liquid column still remained at the necking stage at the nozzle exit, as shown in Figure 14.

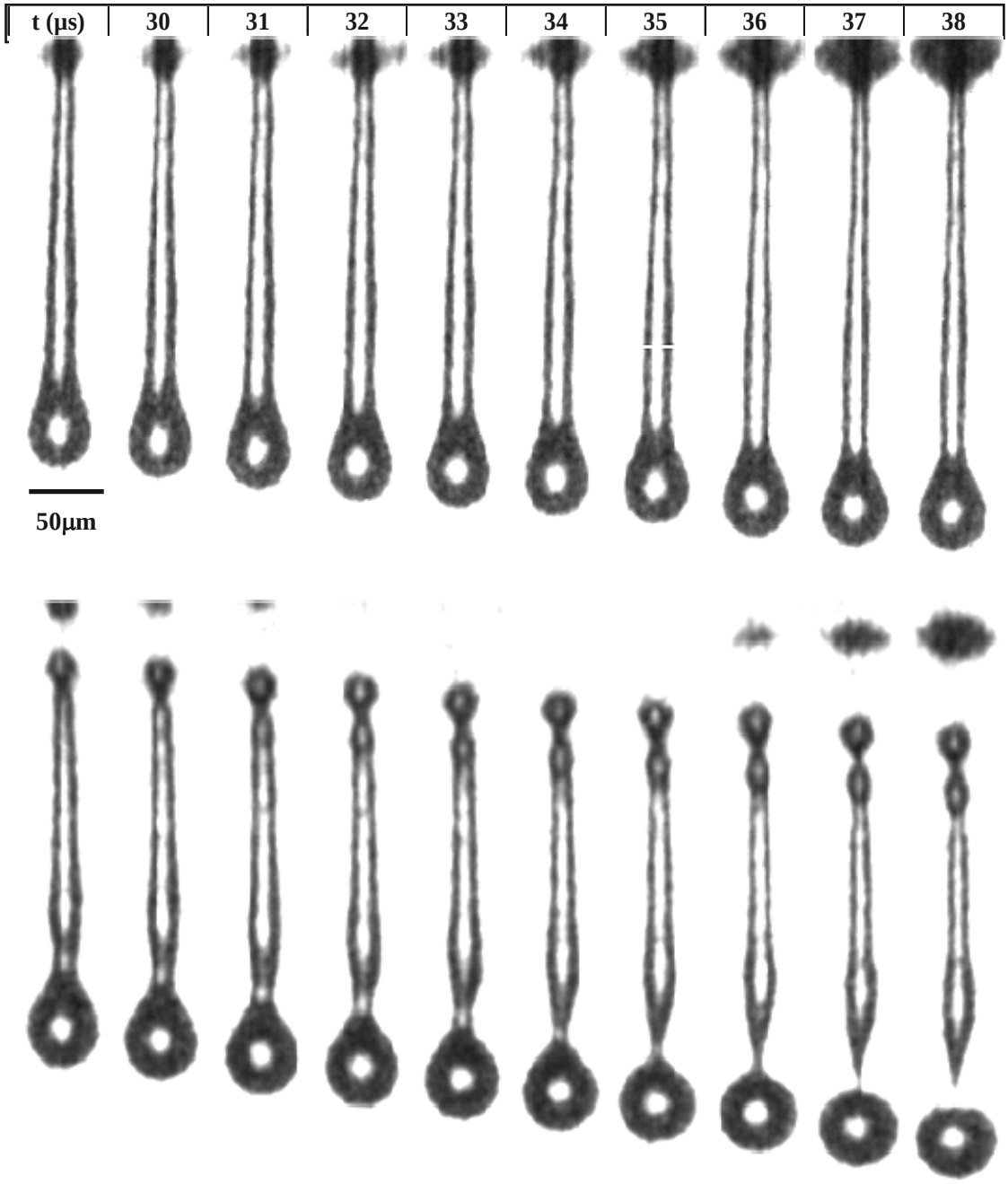

Figure 14 Sequence of images of DOD drop formation for PEO aqueous solution (upper row, Mw = 1000k g/mol, c = 0.015 wt%, c/c* = 0.086) and water (lower row) during the stage of recoil and break up of free liquid thread. Driving voltage = 44.2V and jetting frequency = 20Hz. Images begin at 29 μs after liquid emerges from the nozzle and are shown for every 1 μs through 38 μs.

5.2.4 Formation and recombination of satellites

For water, the stage involving formation and recombination of primary drop and satellites can be seen in Figure 7; however for the PEO solution, the stage was never reached. For water, depending on the length of the free secondary liquid thread, it broke up into several parts, three in this case. Because of the different speeds of the satellites, two of them recombined at about 80 μs and the excess kinetic energy and surface energy was transformed into oscillatory kinetic energy of the liquid. The satellite oscillated until surplus energy was viscously dissipated and an equilibrium state was reached. For the PEO aqueous solution, a second necking began at about 50 μs, and formed a bead-like structure on the liquid column. However, the bead on the column travelled faster than the bulbous head and joined it at about 110 μs. The excess kinetic energy and surface energy was transformed into oscillatory kinetic energy of the bulbous head, which oscillated until the surplus energy was viscously dissipated. At the same time the bulbous head continued to travel downward. The liquid column trailing the bulbous head was stretched until it was very long and thin. At about 200 μs, it broke up into several small pieces, most of which cannot be seen in Figure 10.

The effect of the varying pressure at the exit of the nozzle can be seen in Figures 7 and 10. For water, after pinch-off of liquid from the nozzle exit (see Figure 10), the oscillation of the pressure inside the liquid chamber alternately forced out liquid and then sucked it back into the chamber. Similar oscillatory behavior can be seen at the nozzle exit for the PEO aqueous solution; however, pinchoff did not occur until the oscillatory behavior had discontinued.

5.3 Effects of PEO Concentration and Molecular Weight on DOD Inkjet Drop Formation

The preliminary results showed clearly that both polymer concentration and molecular weight significantly influence DOD drop formation. The effect of concentration will be illustrated using PEO with molecular weight of 300k g/mol, and then the effect of molecular weight will be shown for a polymer concentration of 0.01wt%. The effects of both of these parameters are nonlinear for PEO and a relationship combining the two parameters will be related to important DOD drop formation parameters (first breakup time and primary drop speed) in section 5.5.

5.3.1 Effects of PEO Concentration on DOD Inkjet Drop Formation

The effects of concentration of PEO depend significantly on the molecular weight of the polymer. For the 14,000 and 35,000 g/mole PEO, the effects are much smaller than those of the larger molecular weight polymers and will be discussed in a later section. At $c/c^* \sim 1$, breakup time increased from 31 μs to 32 μs, and drop speed decreased from 6.9 m/s to 6.8 m/s, respectively.

Images of the drop formation process of PEO aqueous solution with molecular weight of 300k g/mol at four concentrations are shown in Figure 15. The pictures shown were taken every 20μs. The drops with lower PEO concentration travelled faster than those with higher PEO concentration. The leading edge of the liquid ejected from the nozzle later becomes the tip of the primary drop [2], and is referred to as the leading point in the Figure 17. When the PEO concentration is higher, breakup time is longer. For example, at a concentration of 0.01wt%, the ligament broke up at 63 μs, but at a concentration of 0.05wt%, the ligament had not broken up at 200 μs. However, the ligament for a concentration of 0.05wt% eventually broke at about 240 μs which is shown in Figure 16.

Data for PEO having molecular weights of 100k, 300k and 1000k g/mol were available. At low concentration, the effects of 100k g/mol PEO were small compared to those of 300k and 1000k g/mol PEO. On the other hand, the effects of the PEO with molecular weight of 1000k g/mol were so large that jetting did not occur for concentrations of 0.02 and 0.05 wt%. For that reason, the images of the DOD drop formation for the PEO with molecular weight of 300k g/mol are shown. In this section, the effect of increasing concentration for 300k g/mol when the solvent is distilled water is discussed. In Section 5.3.2, the effects of molecular weight for a constant concentration when distilled water is the solvent will be presented.

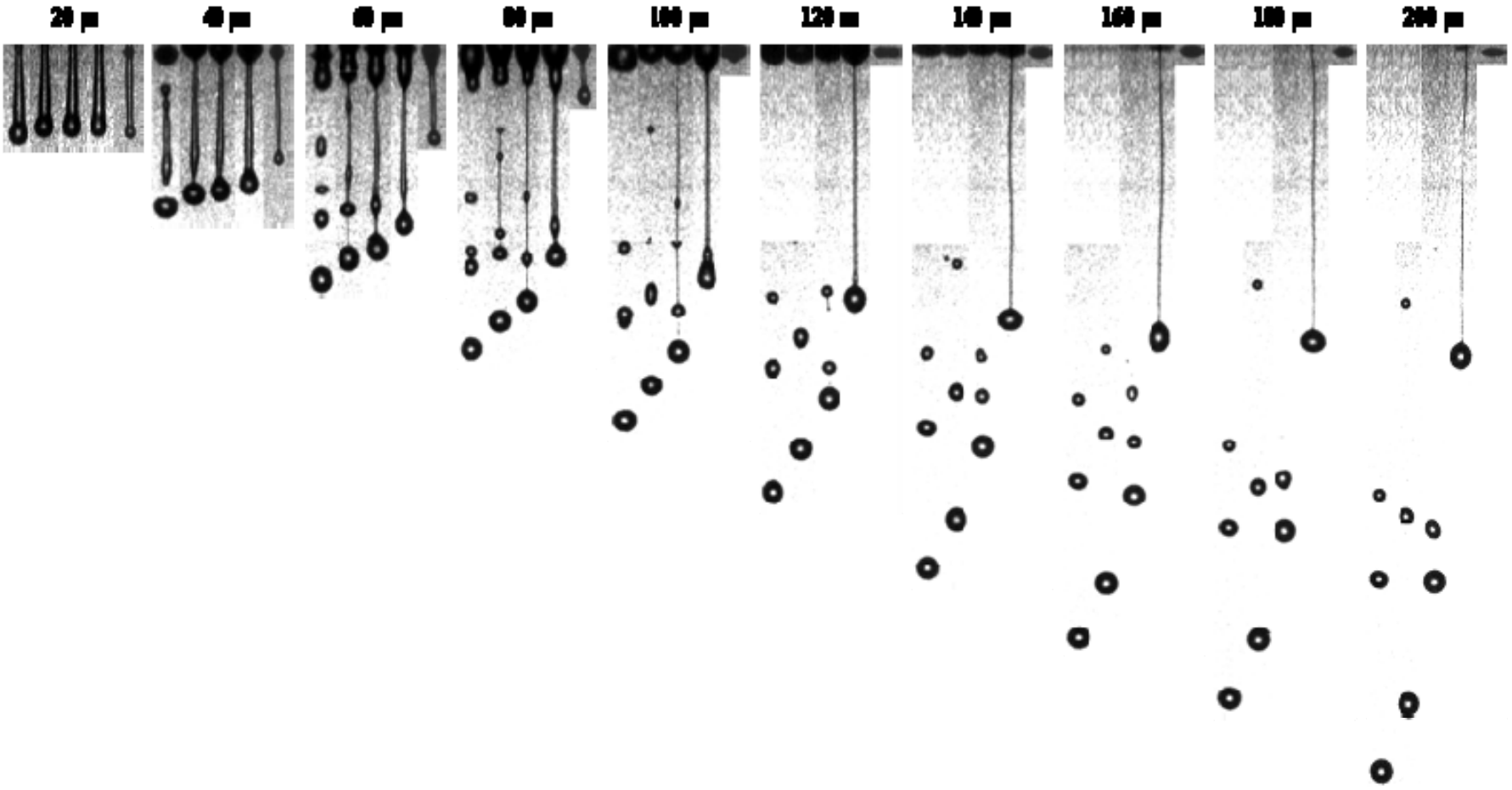

Figure 15 Drop formation of aqueous solution containing PEO with Mw of 300k g/mol at different concentrations (from left to right on each figure: c = 0, 0.01, 0.02, 0.05, 0.1wt% and c/c* = 0. 0.03, 0.05, 0.13, 0.26 respectively). Driving voltage = 44.2 V and frequency = 20 Hz.

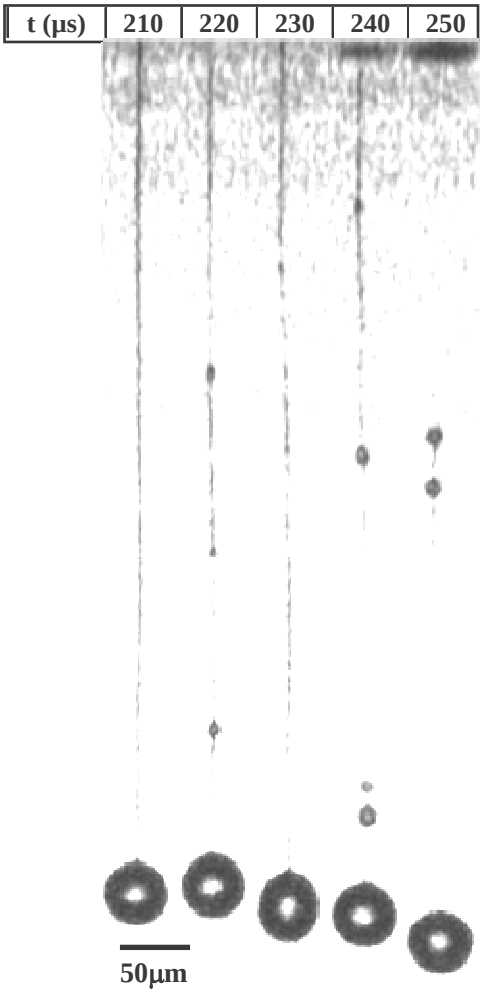

Figure 16 Continuation of Figure 15 for aqueous solution containing PEO with molecular weight of 300k g/mol at c = 0.1wt%. Driving voltage = 44.2V and jetting frequency = 20Hz. Images begin at 210 μs after liquid emerges from the nozzle and are shown for every 10 μs through 250 μs.

In Figure 17, leading point curves (distance from the leading point to the nozzle) are plotted versus time for different concentrations. The slope of the curve at a point is the velocity of the leading point at that time which is shown in Figure 18. The leading point curves at different concentrations were almost identical for times up to about 30 μs. Thus the velocities of the leading points at different concentrations were almost the same during the ejection stage of drop formation. As the liquid was stretched, the velocity of the leading point at higher concentration decreased much

faster than at lower concentrations. As a result, the primary drop speed at higher concentrations was much smaller than that at lower concentrations.

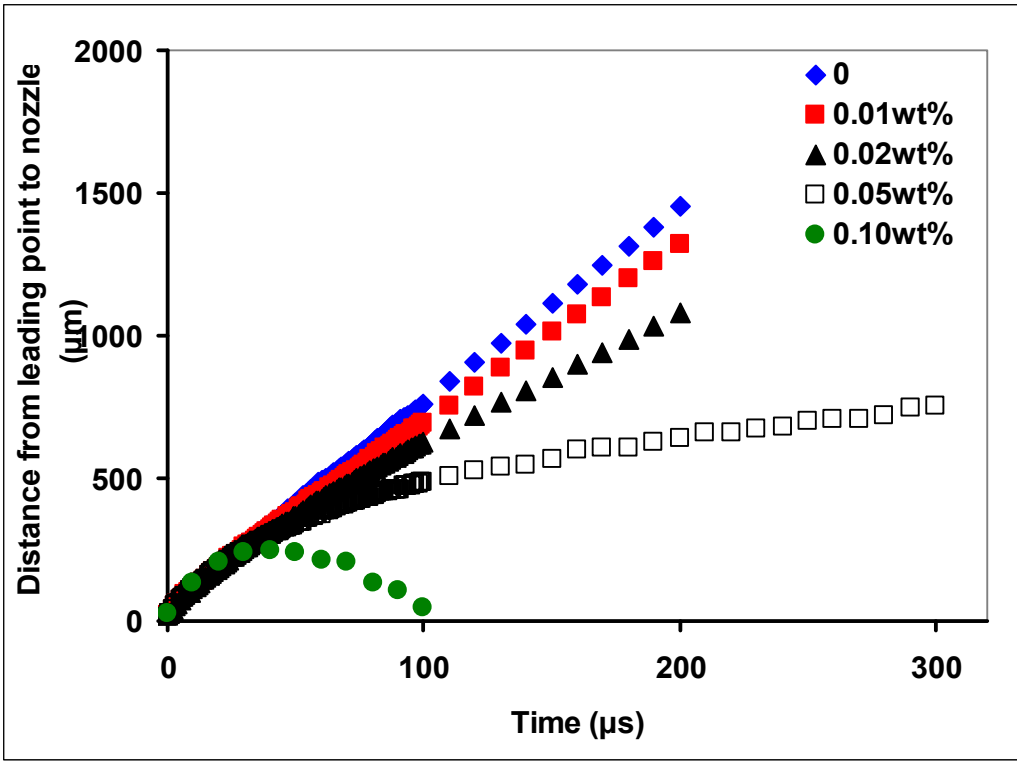

Figure 17 Leading point curves of drop formation process for aqueous solution containing PEO with Mw of 300k g/mol at different concentrations (wt%). Driving voltage = 44.2 V and frequency = 20 Hz.

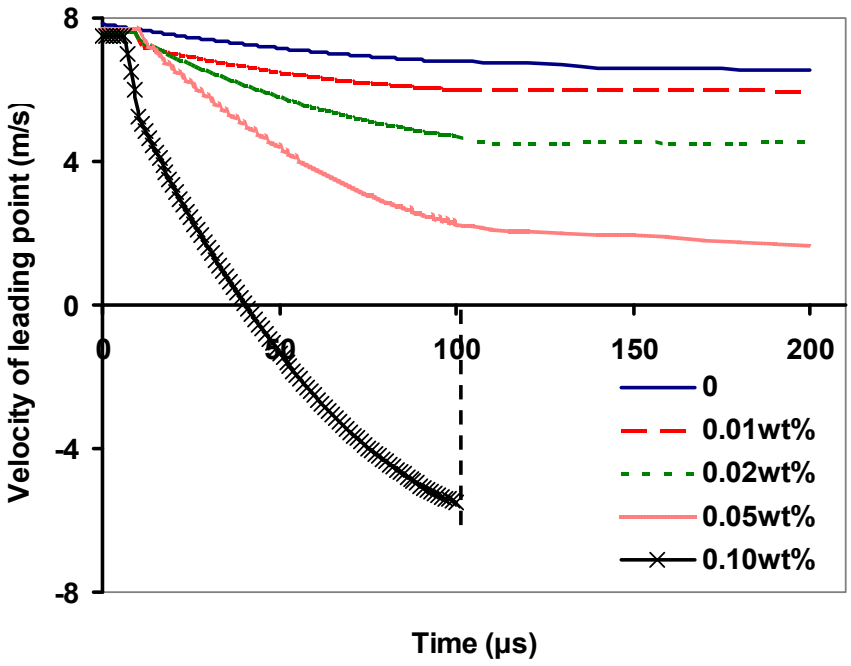

Figure 18 Velocity of leading point of drop formation process for aqueous solution containing PEO with Mw of 300k g/mol at different concentrations. Driving voltage = 44.2 V and frequency = 20 Hz.

Table 4 Concentration effect on drop formation of aqueous solution containing PEO with Mw of 300k g/mol. Driving voltage = 44.2 V and frequency = 20 Hz.

PEO Concentration (w%)	Initial ejection speed (m/s)	Primary drop speed (m/s)	Breakup time (µs)	Number of major satellites
0	8.3	7.5	28	2
0.01	7.6	6.2	62 to 64	2
0.02	7.7	4.6	100 to 120	1
0.05	7.6	1.1	230 to 250	0
0.1	7.5	0	No jetting	0

The primary drop speed (slopes of the curves in Figure 17) and other important parameters of the ink jet drop are listed in Table 4. When PEO concentration was increased, initial ejection speed decreased only slightly, but primary drop speed decreased significantly while breakup time increased greatly. No drop formation occurred for a PEO concentration of 0.1 wt%. Thus the effect of polymer was small during ejection. Apparently the polymer chains are not appreciably oriented and stretched during this stage. Once the ejection stage is over, the ligament attached to the nozzle is stretched due to the momentum of the liquid. The stretching causes the polymer molecules to become oriented and stretched in the flow direction, creating an elastic stress which reduces the speed of the leading point. The elastic stress in the ligament resists the capillary force tending to pinch off the ligament, delaying breakup. When PEO concentration is sufficiently high, breakup does not occur. If breakup occurs, the primary drop size is insignificantly affected by polymer concentration and/or molecular weight. Apparently primary drop size, for a given voltage and surface tension, is determined by nozzle pressure in the initial phase where elasticity effects are small.

Hoyt et al. [49] suggests that the addition of polymer to the ink can reduce the number and size of satellites. The PEO data support their observation; however, first breakup time is increased and drop speed is decreased. When the weight concentration reached 0.05wt%, there were no obvious satellites were formed, but drop speed was reduced to 1.1 m/s, which is probably too low for practical applications [65].

In Figures 19 and 20, primary drop speed is plotted versus PEO concentration and c/c*, respectively, for molecular weights of 100k, 300k, and 1000k g/mol. The figures show clearly that the effect of concentration on inkjet printing depends on the

molecular weight of the PEO. The molecular weight effect will be considered further in the next section.

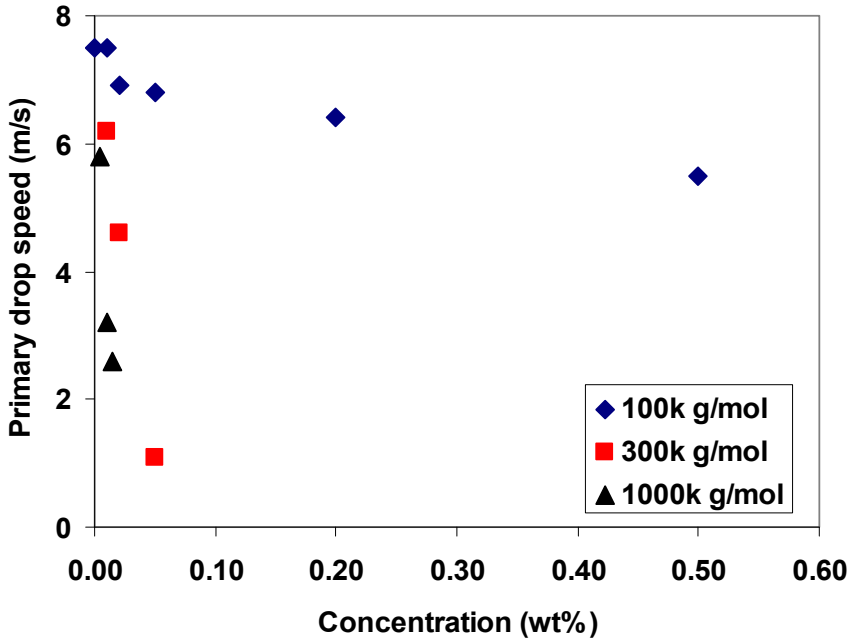

Figure 19 Primary drop speed versus PEO concentration for different molecular weights.

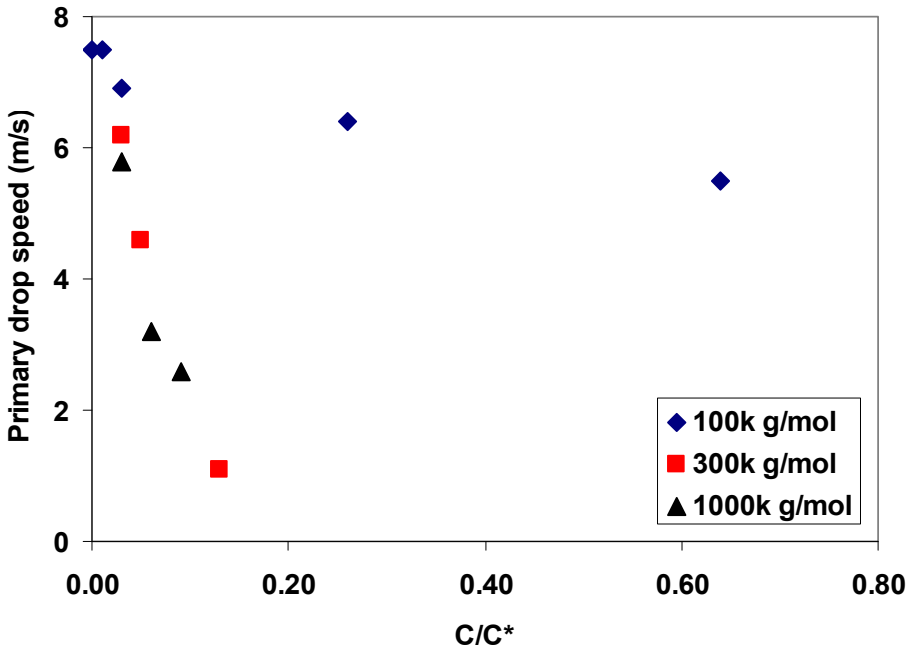

Figure 20 Primary drop speed versus c/c* for different molecular weights.

5.3.2 Effects of PEO Molecular Weight on DOD Inkjet Drop Formation

The previous section showed that the molecular weight of PEO in an aqueous solution greatly affects the DOD drop formation process. This can be seen in Figure 21 where images of the DOD drop formation process of aqueous solution containing PEO with different molecular weights (0, 100k, 300k, 1000k g/mol, sample A, B, C and D respectively) at a weight concentration of 0.01% are shown. The images are shown for every 20 μs following emergence of liquid from the nozzle.

The images for 20 μs are similar for all four molecular weights, but after 20μs, differences are apparent. At 40 μs, A and B already pinched off from the nozzle and each formed a primary drop and free ligament, while C and D had not pinched off. At 60 μs, the ligaments in A and B broke into several satellites, and the bulbous head in C was about to pinch off from the nozzle while D still stayed in the necking stage. At 80μs, two satellites in A began to recombine; three satellites were formed in B; the ligament in C broke up and a bead-like structure was formed in D. At 100μs, two satellites in A already recombined; one major satellite was formed in C and the bead-like structure in D began to recombine with the bulbous head. Between 120 and 180μs, two major satellites in A, B and C continued to travel downward, and the long tail in D continued to be elongated and thinned as the bulbous head traveled downward. At 200μs, the long ligament in D broke up and formed small satellites which cannot be seen in Figure 21.

In Figure 21, the effects of the oscillating pressure can be seen near the nozzle exit, beginning at about 40 μs and ending at about 160 μs. Liquid appeared to flow out of the nozzle and then be sucked back in. Drop formation in A and B was not affected by the pressure oscillation as the pinch off happened before the oscillation started. At about 60μs, pinchoff in C occurred between the thin thread and the thick liquid thread

(associated with the pressure oscillation) just below the nozzle exit. At 160 μs, a very thin thread stretched from the nozzle exit to the bulbous head, which became the primary drop. Between 160 and 200 μs, the long thin thread pinched off from both the nozzle exit and the primary drop and disappeared.

As molecular weight was increased, drop size increased slightly, the number of satellites decreased and breakup time increased. At molecular weight of 100k g/mol, the ligament broke up at 30μs, which was not much different from the break up time of distilled water (28μs). However, at a molecular weight of 1000k g/mol, the ligament did not break up until between 160 to 200μs. At the lower molecular weights, satellites occurred, but at molecular weight of 1000k g/mol, the long ligament was so thin that when it broke up due to capillary, there were no obvious satellites at 220 μs, which is not shown in Figure 21. It is conjectured that the surface area was so large relative to volume that the solvent evaporated so fast that no satellites could be seen in the image.

The leading point curves of the drop formation process for aqueous solutions containing 0.01wt% PEO with different molecular weights are shown in Figure 22. The leading point curves at different molecular weights were almost identical for times up to about 30 μs. Thus the velocities of the leading points were almost the same during the ejection stage. As the liquid was stretched, the velocity of the leading point at higher molecular weight decreased much faster than at lower molecular weight. As a result, the primary drop speed at higher molecular weights was much smaller than for lower molecular weights.

In Figure 22, there is a discontinuity in the slope of the curve for the 1000k g/mol solution at about 120 μs. This is due to a bead-like structure reaching the primary drop and recombining with it. After recombination occurred, the major drop

oscillated until the energy associated with the oscillation dissipated and the drop became almost spherically shaped.

The primary drop speeds (slopes of curves in Figure 22) and other important parameters of the ink jet drop produced from aqueous solution containing 0.01wt% PEO at different molecular weights are listed in Table 5.

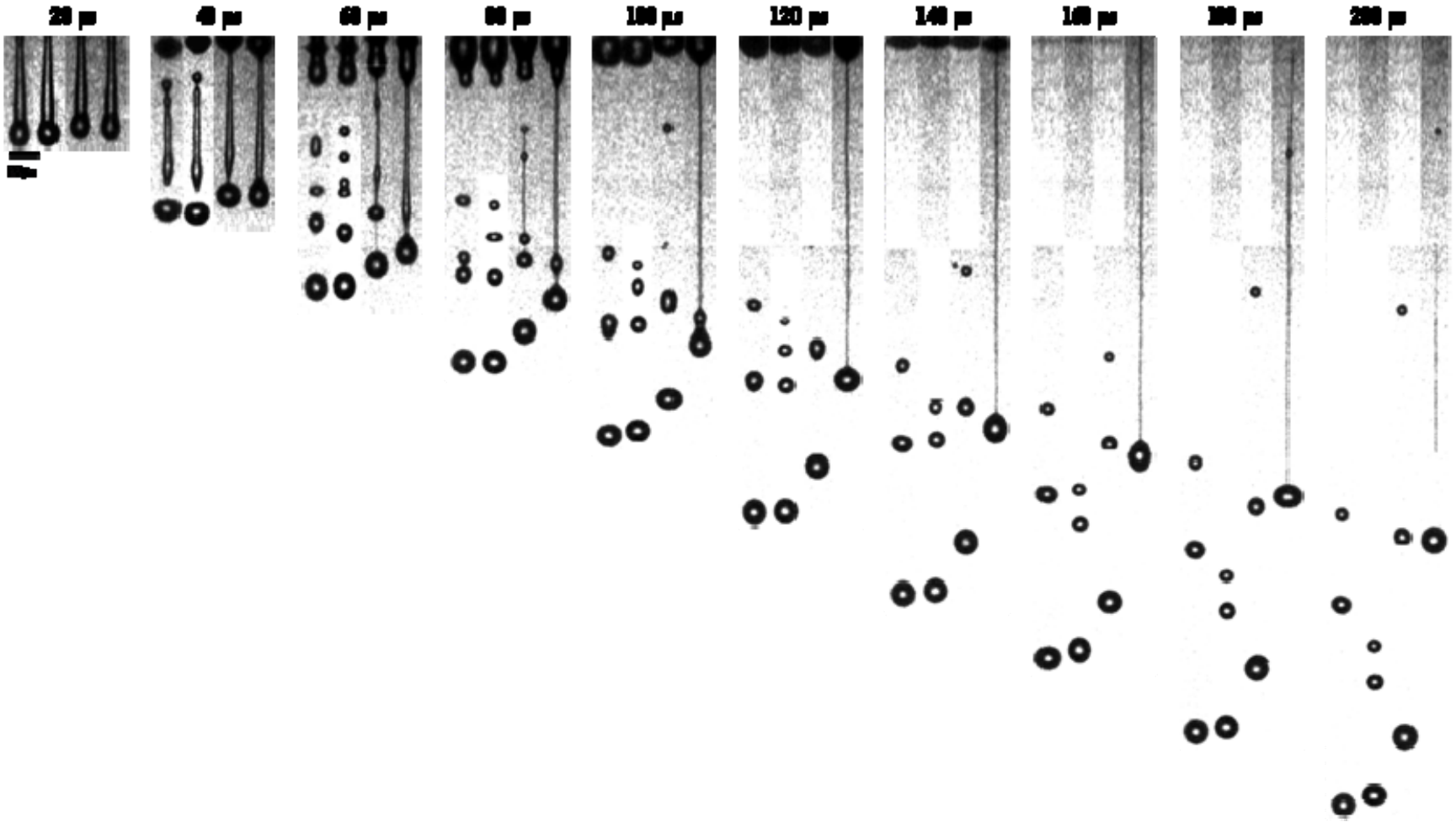

Figure 21 DOD drop formation process of aqueous solution containing PEO with different molecular weights (from left to right on each figure: Mw of 0, 100k, 300k, 1000k g/mol, sample A, B, C and D respectively) at a weight concentration of 0.01wt%. Driving voltage = 44.2 V and frequency = 20 Hz.

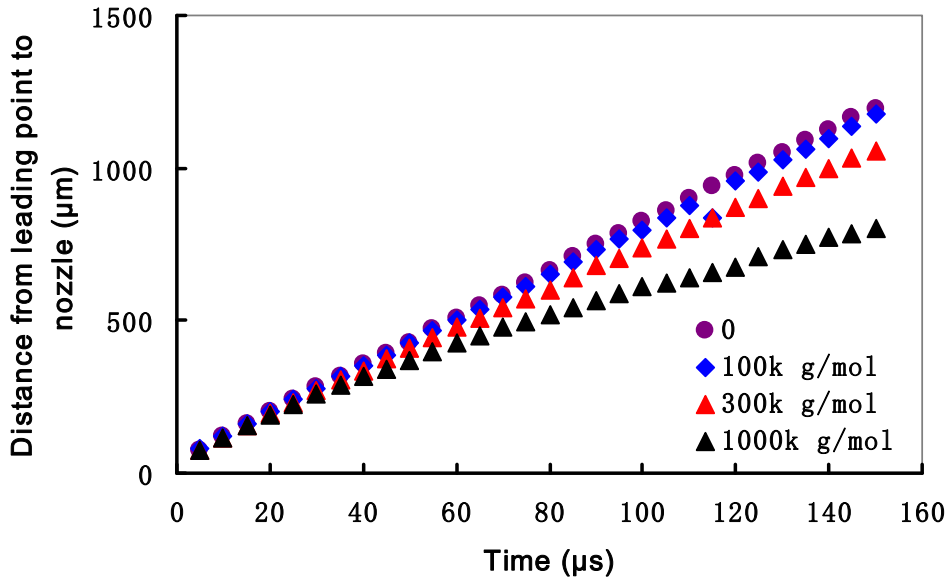

Figure 22 Leading point curves of drop formation process for aqueous solution of 0.01wt% PEO at different molecular weights.

Table 5 Molecular weight effects on drop formation of aqueous solution containing 0.01wt% PEO. Driving voltage = 44.2 V and frequency = 20 Hz.

Mw (g/mol)	Initial ejection speed (m/s)	Primary drop speed (m/s)	Breakup time (μs)	Number of major satellites
0	8.3	7.5	27	2
100k	8.2	7.5	30	2
300k	7.6	6.3	62-64	2
1000k	7.7	4.1	180 to 200	0

5.4 Discussion of Breakup Time in the DOD Drop Formation of PEO Solution

The addition of a small amount of PEO to fluids can have a significant effect on the DOD drop formation process. During the first two stages of DOD drop formation (see section 5.1), the liquid column is elongated and the polymer chains are stretched and oriented in the direction of flow. As a result, an elastic stress develops in the liquid column and resists capillarity-driven pinch off from the nozzle.

As elasticity in the liquid increases with increase in either polymer concentration or molecular weight, pinchoff time increases. During the DOD drop formation process of PEO dilute solution, break up time is a key parameter related to other process parameters such as primary drop speed and number of major satellites.

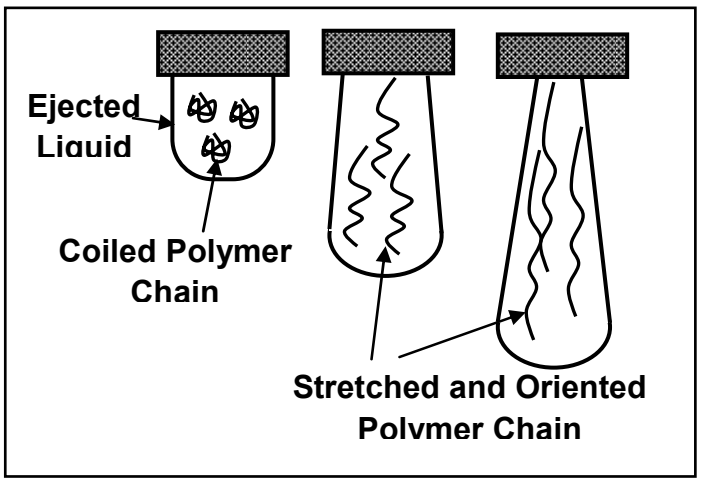

Figure 23 Schematic showing polymer orientation and stretching during stretching.

During the stretching of the liquid, the relative rates at which two opposing phenomena occur are important in determining the degree to which the polymer affects DOD drop formation. The degree to which the polymer chains are stretched and oriented depends on the relative rates at which two opposing phenomena occur. As the elongation of the liquid column causes the polymer chains to be stretched and oriented, Brownian motion tends to disorient the polymer chains. The time

characterizing Brownian motion is referred to relaxation time, λ. If λ is small relative to breakup time, t_0, for the base Newtonian liquid containing no polymer, Brownian motion prevents segments of the polymer chains to become sufficiently oriented to produce significant elastic effects. As λ increases, the elastic effects increase. If λ is sufficiently large, the polymer chains are stretched and oriented, and elastic effects may be significant, and in some cases large enough that pinchoff does not occur.

Several models, based on flexible chain molecule theories such as those of Rouse and Zimm, have been developed to predict the rheology of dilute polymer solutions [51-52]. In Zimm's model, a polymer chain is represented by a chain of beads connected by ideal springs. The chain consists of N identical segments joining N+1 identical beads with complete flexibility at each bead. Each segment, which is similar to a submolecule, has a Gaussian probability function for position. According to Zimm's model, if a chain is suspended in a viscous liquid, each bead j encounters three different forces: mechanical force, Brownian force, and the hydrodynamic drag force.

The longest relaxation time (λ_z) calculated by the Zimm model [1] is:

$$\lambda_z \cong \frac{1}{\zeta(3\nu)} \frac{[\eta] M_w \eta_s}{N_A k_B T} \qquad [3.3]$$

Investigations [1, 55, 58, 66] have shown that polymer solutions at different concentrations, but with identical relaxation times predicted by the Zimm model, behave differently in drop formation in the dripping mode. Tirtaatmadja et al. [1] suggest a modified equation for calculating effective relaxation time which includes

the following factor: $(c/c^*)^{0.65}$ where c is weight concentration and c* is the critical overlap concentration:

$$\lambda_{eff} \cong \frac{1}{\zeta(3\nu)} \frac{[\eta] M_w \eta_s}{N_A k_B T} \left(\frac{c}{c^*} \right)^{0.65}, \text{ for } 0.01 \le c/c^* \le 1 \qquad [5.1]$$

Since the a parameter relating the effect of the addition of PEO to DOD drop formation, the relationship between λ_{eff} and the first breakup time, t_b, was examined. In Figure 24, $t_b - t_{b0}$ is plotted against λ_{eff} for polydispersed PEO at various concentrations in distilled water and a mixture of distilled water and glycerin. Here t_b is the break up time of the PEO solution, and t_{b0} is the break up time of the base Newtonian solvent containing no PEO. The figure shows that the breakup time increases with λ_{eff}. However, the data of 1000k g/mol PEO do not lie close to the data of the 100k and 300k g/mol PEO. The polymer was purchased from Sigma Aldrich, and only viscosity average molecular weights were provided. Stokes [67] measured the molecular weight of the 1000k g/mol PEO and found that it had a polydispersity of about 1.8. Tirtaatmadja et al. [1] used PEO from the same source and assumed that the other PEO samples had similar polydispersities; however, since molecular weight has a very large effect on DOD drop formation and the data do not correlate for our tests, the polydispersities of the different molecular samples may be different. For that reason, we purchased PEO with known low polydispersities for further testing. Results of tests with the low polydispersities are discussed in Chapter 6.

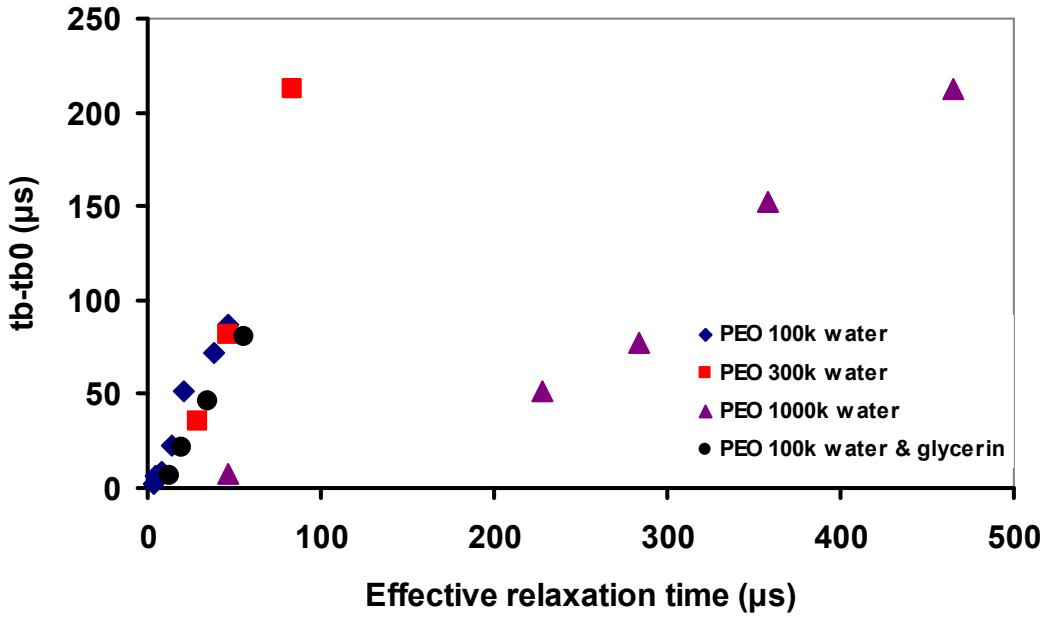

Figure 24 Plots of t_b/t_{b0} versus effective relaxation time (defined in Equation 5.1) for PEO at various concentrations in different solvents.

In Figure 25, primary drop speed is plotted against $t_b - t_{b0}$. When the solvent is fixed, there is a linear relationship between the first breakup time and primary drop speed. As effective relaxation time of PEO in the solution increases, first breakup time increases and primary drop speed decreases. These occur because as elastic effects increase, inertial energy expended in orienting and stretching the long chain molecules increases. Brownian motion returns the oriented and stretched molecules to more random configurations and the inertial energy consumed in orienting and stretching the molecules is converted to heat. As a result, the primary drop speed of the solutions with PEO is lower than for the base solution containing no polymer. The number of satellite is related to the break up time and the viscosity of the solvent.

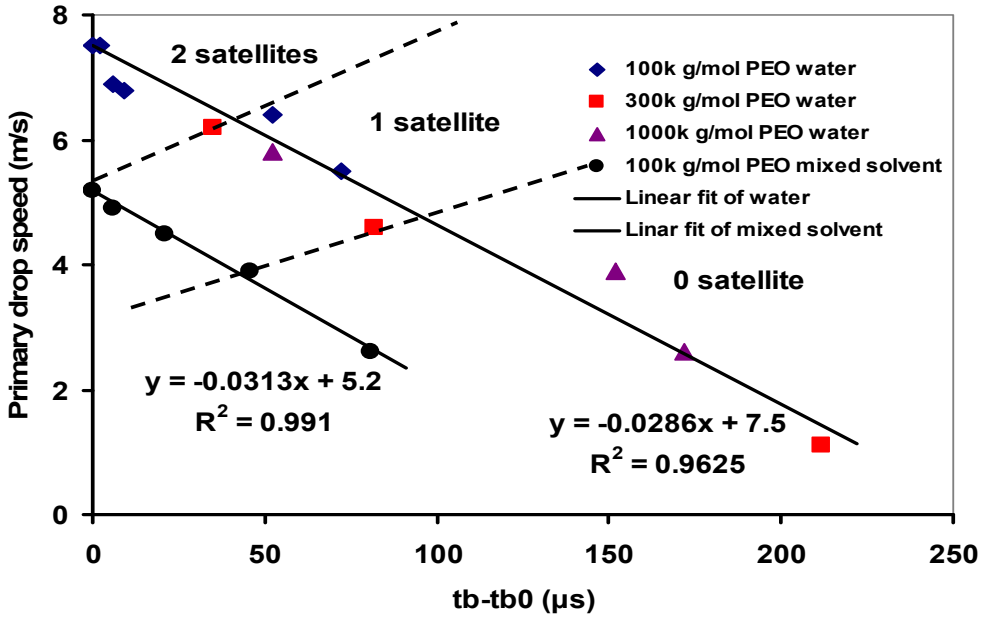

Figure 25 Relationship between t_b - t_{b0} and primary drop speed. Driving voltage=44.2 V and frequency=20 Hz.

Thus for DOD inkjet drop formation, the primary drop speed can be estimated from breakup time from the following relationship:

$$v - v_0 = -0.03(t_b - t_{b0}) \qquad [5.2]$$

or

$$. \; v / v_0 = 1 - 0.03(t_b - t_{b0}) / v_0$$

The effect of viscosity on primary drop speed can be evaluated by plotting dimensionless primary drop speed versus $(t_b - t_{b0})/v_0$, as shown in the Figure 26, and regression analysis. The resulting relationship is

$$v / v_0 = 1 - 0.03(t_b - t_{b0}) / (7.7 - 0.5\eta_s) \qquad [5.3]$$

where η_s is the solvent viscosity.

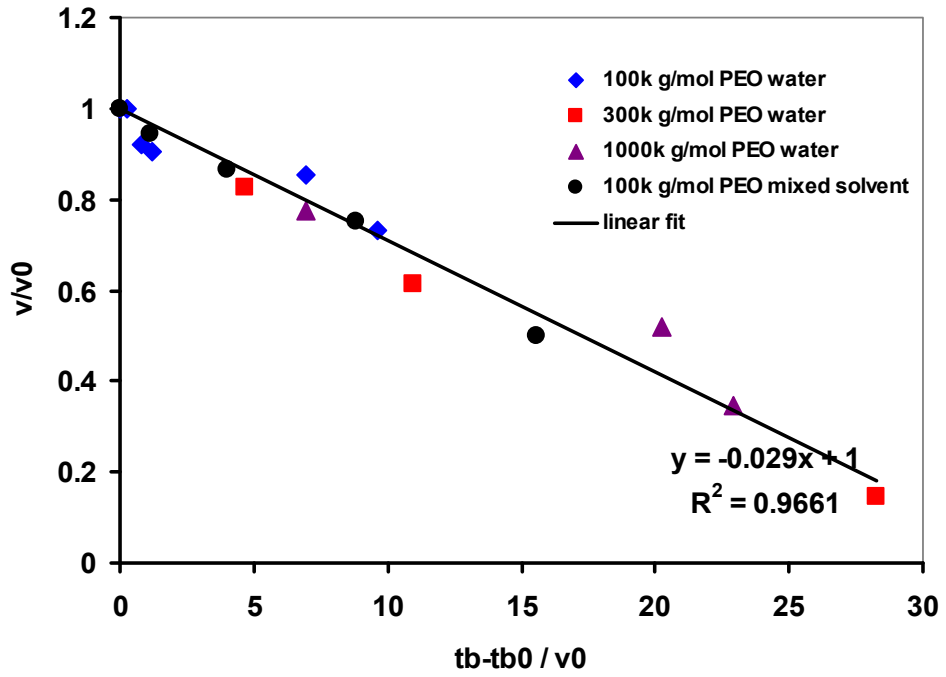

Figure 26 Relationship between $(t_b - t_{b0})/v_0$ and v/v_0. Driving voltage = 44.2 V and frequency = 20 Hz

5.5 DOD Drop Formation of Lower Molecular Weight PEO Solution

The DOD drop formation process for lower molecular weight PEO aqueous solutions was also observed. The basic properties of the solutions, as well as first breakup times, are shown in Table 6. Breakup times for Newtonian liquid having different shear viscosity are given in Table 7. Comparison of the breakup times for the PEO solutions with those for Newtonian liquids having similar shear viscosities reveals that the breakup time did not increase with PEO concentration, even at concentrations large enough that the solution does not fall in the dilute regime.

Table 6 Basic properties of aqueous solutions containing lower molecular weight PEO

Mw (g/mol)	c (wt%)	c/c*	η (mPa•s)	λeff (μs)	Surface tension (mN/m)	Breakup time (μs)	Primary drop speed (m/s)
0	0	0	1.06	0	72.0	28	7.5
14000	2	0.71	1.76	1.61	66.2	31	6.8
14000	2.8	1.00	1.88	2.00	66.3	31	6.9
14000	5	1.78	2.87	2.92	66.6	31	6.2
14000	7	2.50	3.50	3.64	66.1	31	5.8
14000	10	3.57	6.25	4.59	66.5	34	3.8
35000	1	0.65	1.86	6.86	66.2	32	6.7
35000	1.5	0.97	2.14	8.93	66.7	32	6.8
35000	3	1.94	3.90	14.0	65.9	32	6.1
35000	5	3.24	6.36	19.5	66.5	36	4.7
35000	7	4.53	11.6	24.3	65.9	48	1.3

Table 7 Breakup times for Newtonian liquid having different shear viscosities

Shear viscosity (mPa•s)	1.06	3.60	4.30	6.48	11.50
Breakup time (μs)	28	30	30	33	45

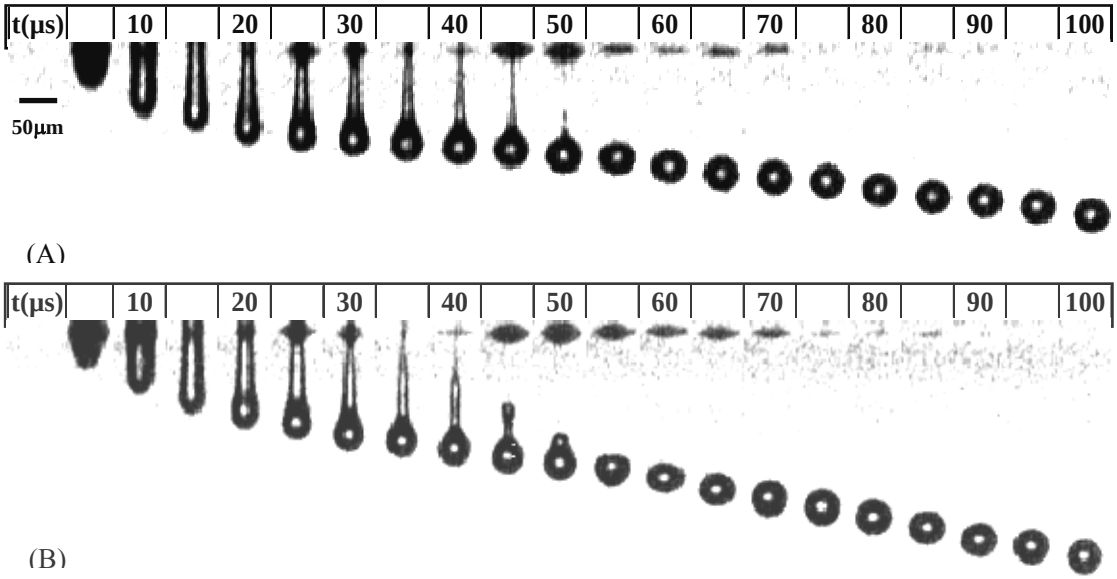

Figure 27 Drop formation process from 0 to 100 μs of (A) PEO aqueous solution (Mw = 35,000 g/mol, c = 7wt%, c/c*=4.5) and (B) Water and glycerin mixture η = 11.5 mPa•s. Images begin at 0 μs after liquid emerges from the nozzle and are shown for every 5 μs through 100 μs. Driving voltage = 44.2 V and frequency = 20 Hz

Images of the drop formation process for lower molecular weight PEO solution and Newtonian fluid with similar shear viscosity are shown in Figure 27. The jetting behavior of PEO aqueous solution at lower molecular weight was similar to that of the Newtonian fluid. The effective relaxation times of the lower molecular weight PEO were of the same order as the capillary time, but even at high concentrations, elastic effects were not important. The drop formation process was similar to that of Newtonian liquid where DOD drop formation is determined by viscous, capillary and inertial effects. Since the shear viscosity and the surface tension of A and B (in Figure 27) were similar, the jetting behavior was similar.

Jettability is acceptable for the aqueous solutions containing lower molecular weight PEO. For that reason, if a large amount of polymer needs to be deposited on a substrate, the lowest molecular weight polymer giving acceptable properties should be selected.

5.6 Conclusions

The addition of PEO increases the shear viscosity at all molecular weights, but the change is small for dilute solutions. However, the addition of a small amount of PEO can have a significant effect on the DOD drop formation process, increasing breakup time and decreasing primary drop speed and the number of satellites. The effects depend on both molecular weight and concentration. At lower molecular weights, the effect of PEO over the dilute solution regime was small when the drop formation process for the dilute solution was compared with that of a Newtonian liquid having similar shear viscosity, and the effect of PEO was small even at concentrations large enough that the solution does not fall in the dilute regime.

As molecular weight was increased, the effects of PEO on the DOD drop formation process increased significantly, and the effects of concentration became important. These effects are explained by the fluid elasticity which increases with increasing in molecular weight and concentration. When the liquid jets out of the nozzle, the polymer chains are stretched and oriented, and thus depart from their ideal coiled state. As a result, an elastic stress develops in the liquid column and resists capillarity-driven pinch off from the nozzle and is responsible for the decrease in drop speed and longer breakup time.

Modified Zimm longest relaxation time, λ_{eff}, was shown to be related to breakup time and primary drop speed. However, when breakup time was plotted versus λ_{eff}, the data for 1000k g/mol PEO did not lie close to that for the 100k and 300k g/mol PEO. Since molecular weight had a very large effect on DOD drop formation and polydispersities of the different molecular samples were not known, further testing with PEO with known low polydispersities were conducted, and the results are discussed in Chapter 6.

CHAPTER 6

DOD DROP FORMATION OF MONODISPERSED PEO SOLUTIONS

As discussed in the previous chapter, the addition of a small amount of polydispersed PEO to Newtonian liquids may have a significant effect on the DOD drop formation process, depending on PEO molecular weight and concentration. The degree to which the polymer chains are stretched and oriented depends on the relative rates at which two opposing phenomena occur. The elongation of the liquid causes the polymer chains to be stretched and oriented. At the same time, Brownian motion tends to disorient the polymer chains. Thus it is reasonable to expect that the effects of addition of a small amount of polydispersed PEO to Newtonian liquids depend on the relaxation time characterizing Brownian motion.

An effective relaxation time, λ_{eff}, was measured by Tirtaatmadja et al. [1] for PEO solution in a study of drop formation in the dripping mode. In their study, they obtained relaxation times, λ_{eff}, of PEO solutions of varying concentrations and molecular weights and found that the values were significantly higher than relaxation times, λ_z, estimated from Rouse-Zimm theory, which is independent of concentration for dilute polymer solutions. They correlated λ_{eff} with λ_z and c/c* and obtained a relationship for calculating λ_{eff}, which includes the effects of molecular weight and concentration.

As discussed in Chapter 5, attempts were made to correlate drop formation parameters in DOD drop formation of polydispersed PEO solutions with λ_{eff}. When pinchoff time was plotted versus effective relaxation time, the data for a given molecular weight PEO appeared to fall on a line; however, the data for aqueous solution containing PEO with 1000k g/mol did not correlate with the rest of the data.

This is believed to be associated with the molecular weight distributions of the polydispersed PEO used, which were not available. It was conjectured that the effect of the larger molecular weight molecules is greater than accounted for by molecular weight based on viscosity measurement. For that reason, drop formation tests were conducted using PEO with polydispersities close to one, referred to in this chapter as monodispersed PEO. Tests were first conducted using one monodispersed PEO at a time at several concentrations to study the interaction of molecular weight and concentration. Then by combining samples of monodispersed PEO with different molecular weights, the effect of polydispersity on DOD inkjet drop formation was investigated by adding various PEO concentrations to Newtonian solvents. The results of the monodispersed PEO tests are presented in this chapter.

6.1 Effects of Monodispersed and Polydispersed PEO with Similar M_n

Two samples with similar number average molecular weights, but different polydispersities (PDI) were used to test the effect of polydispersity on DOD inkjet drop formation. The PDI's of the monodispersed and polydispersed PEO's are shown in Table 1 in Chapter 4. In Figure 28, images of drop formation for the two samples are shown. The drop formation dynamics of low (1.08) PDI PEO solution (see Figure 28 A) was similar with that of water (see Figure 7 and discussion in Section 5.1). The breakup time was 30 μs, two satellites were generated during the drop formation process, and thus the effects of monodispersed PEO were small. However, the effects of the high (2.5) PDI PEO solution were larger, see Figure 28 B. Breakup time increased to 80 μs, and the primary drop speed decreased correspondingly. Only one satellite was generated. It is not surprising that the PEO with a larger polydispersity has a larger effect since it has a fraction of longer chain molecules with corresponding longer relaxation times.

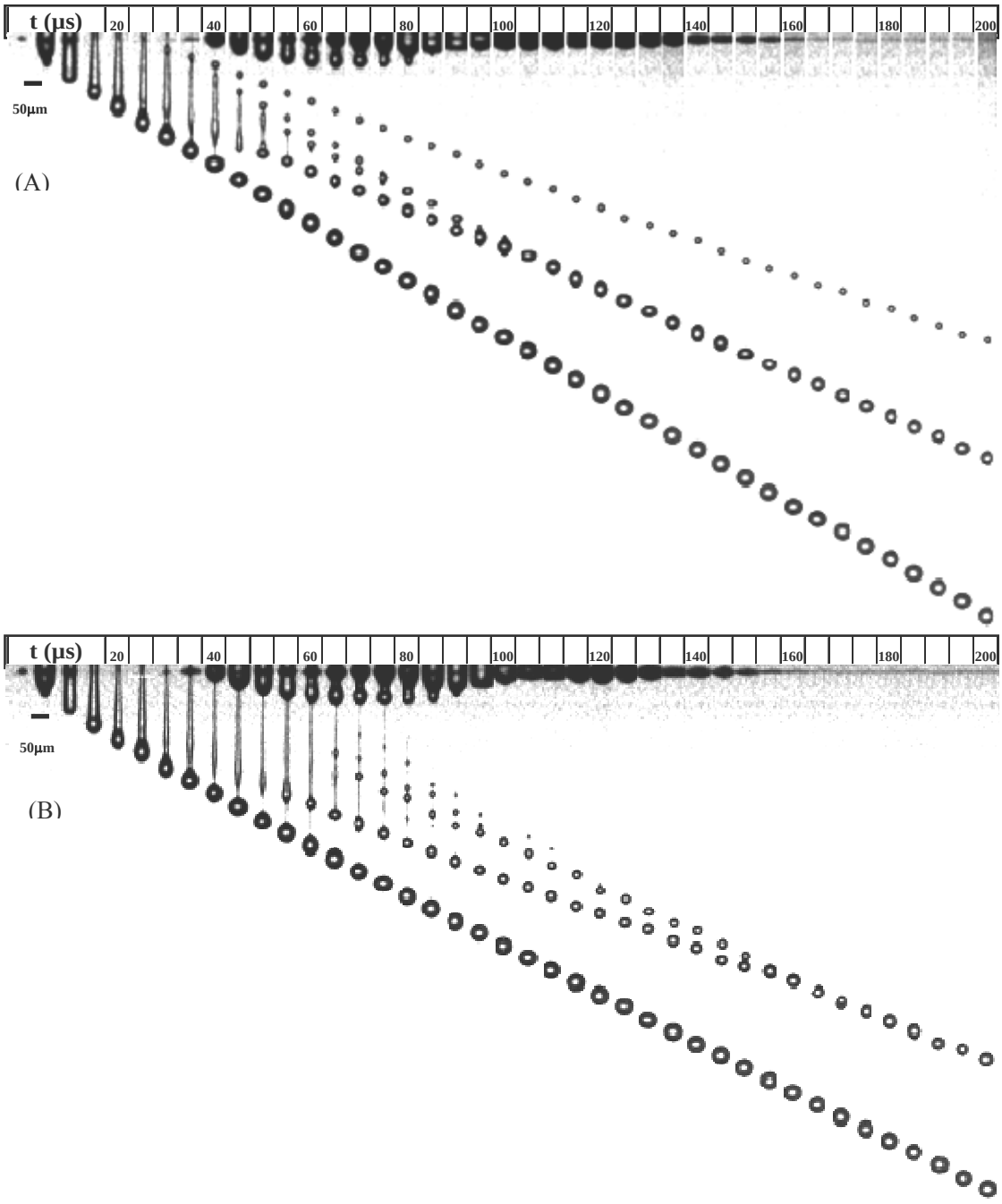

Figure 28 Images of DOD Drop formation of aqueous solution containing PEO. (A) M_n = 95k g / mol, c = 0.1wt% and PDI = 1.08. (B) M_n = 90k g / mol, c = 0.1wt% and PDI = 2.5. Time interval = 5 μs, driving voltage = 44.2 V and frequency = 20 Hz. Images begin at 0 μs when liquid emerges from the nozzle and are shown for every 5 μs through 200 μs.

6.2 DOD Inkjet Drop Formation Dynamics of Monodispersed PEO Solutions

The drop formation dynamics of monodispersed PEO solutions were tested, and the results are given in Table 8. The addition of a small amount of monodispersed PEO to fluids may have a significant effect on the DOD drop formation process, depending on molecular weight and concentration.

The effects of polymer addition on the DOD drop formation process for the monodispersed PEO were similar to those observed for polydispersed PEO. As either molecular weight or concentration increased sufficiently, breakup time increased and primary drop speed and the number of satellites decreased. The drop formation process became less repeatable as the molecular weight and concentration increased, which was reflected in the variation of breakup time. However the repeatability was better than for polydispersed PEO solutions. For example, the variation in breakup time was about ± 3 μs for monodispersed PEO (M_n = 700,000 g/mol, c = 0.01wt%) solution with an average breakup time of about 160 μs while the variation in breakup time was about ± 10 μs for polydispersed PEO (Mw = 1,000,000 g/mol, c = 0.01wt%) solution with an average breakup time of about 180 μs.

Table 8 Breakup time, primary drop speed and number of satellites of monodispersed PEO solutions during DOD drop formation. Driving voltage=44.2 V and frequency=20 Hz.

M_n (g/mol)	PDI	c (wt %)	c/c*	Breakup time (μs)	Primary drop speed (m/s)	Number of major satellites
59,000	1.02	0.1	0.09	31	6.5	2
59,000	1.02	0.5	0.45	31	6.5	2
95,000	1.08	0.1	0.12	35	6.3	2
95,000*	1.08	1.0	1.24	75	4.8	2
203,000	1.14	0.05	0.10	52	6.3	2
203,000	1.14	0.1	0.20	70	5.9	2
203,000	1.14	0.2	0.41	90	5.4	1
203,000	1.14	0.4	0.81	120 ± 3	4.2	1
203,000*	1.14	0.6	1.22	150 ± 3	1.4	0
203,000*	1.14	0.8	1.62	190 ± 5	0.87	0
203,000*	1.14	1.0	2.03	No jetting	0	0
420,000	1.12	0.01	0.03	61	6	1
420,000	1.12	0.02	0.07	81	5.7	1
420,000	1.12	0.05	0.16	125 ± 3	4.3	1
420,000	1.12	0.1	0.33	190 ± 5	1.9	0
420,000	1.12	0.15	0.49	225 ± 5	0.64	0
420,000	1.12	0.2	0.65	No jetting	0	0
700,000	1.20	0.005	0.02	80	5.2	1
700,000	1.20	0.01	0.05	160 ± 3	3.4	0
700,000	1.20	0.02	0.09	No jetting	0	0
700,000	1.20	0.05	0.23	No jetting	0	0

* When c/c* is larger than 1, the PEO solution can not be considered as dilute.

6.3 Predictive Equations for Breakup Time and Drop Speed for DOD Inkjet Drop Formation of Monodispersed PEO Solutions

Efforts were made to find a scaling factor that included the effects of PEO molecular weight and concentration that could be use to predict important DOD drop formation parameters such as breakup time and primary drop speed.

Since the breakup time increased with the increase of molecular weight and concentration, the following equation was use to fit the experimental data for the monodispersed PEO:

$$t_b - t_{b0} = A \cdot M_n{}^a c^b \qquad [6.1]$$

where t_b is the breakup time (μs) of PEO solution; t_{b0} is the breakup time (μs) of base solvent; M_n is the number average molecular weight (g/mol) of PEO; c is the PEO concentration (wt fraction); and A, a, and b are constants. Using the data in Table 8, the constants were obtained by regression analysis ($R^2 = 0.9623$), and the following relationship was obtained:

$$t_b - t_{b0} \cong 6.45 \times 10^{-9} \times M_n{}^{2.19} \times c^{0.65} \qquad [6.2]$$

Tirtaatmadja et al. [1] found that relaxation time (referred to as effective relaxation time, λ_{eff}) measured during drop formation in the dripping mode could be related to the longest relaxation time from the Zimm model by the following relationship:

$$\lambda_{eff} = \lambda_z \cdot \left(\frac{c}{c^*}\right)^{0.65} = \frac{1}{\zeta(3\nu)} \frac{[\eta] M_v \eta_s}{N_A k_B T} \left(\frac{c}{c^*}\right)^{0.65}, \text{ for } 0.01 \le c/c^* \le 1 \qquad [6.3]$$

When this expression for effective relaxation time for aqueous solution is written in the format similar to that of Equation 6.2 with M_n used as molecular weight instead of M_v, the following equation is obtained:

$$\lambda_{eff} \cong 5.38 \times 10^{-8} \times M_n{}^{2.07} \times c^{0.65} \text{ (μs)} \qquad [6.4]$$

Notice that the exponents of M_n and c are similar in Equations 6.2 and 6.4., indicating that $t_b - t_{b0}$ may correlate with λ_{eff}. For that reason, t_b-t_{b0} was plotted against λ_{eff} in Figure 29. A linear relationship fitted the data well ($R^2 = 0.9775$):

$$t_b - t_{b0} = 0.6029\lambda_{eff} \qquad [6.5]$$

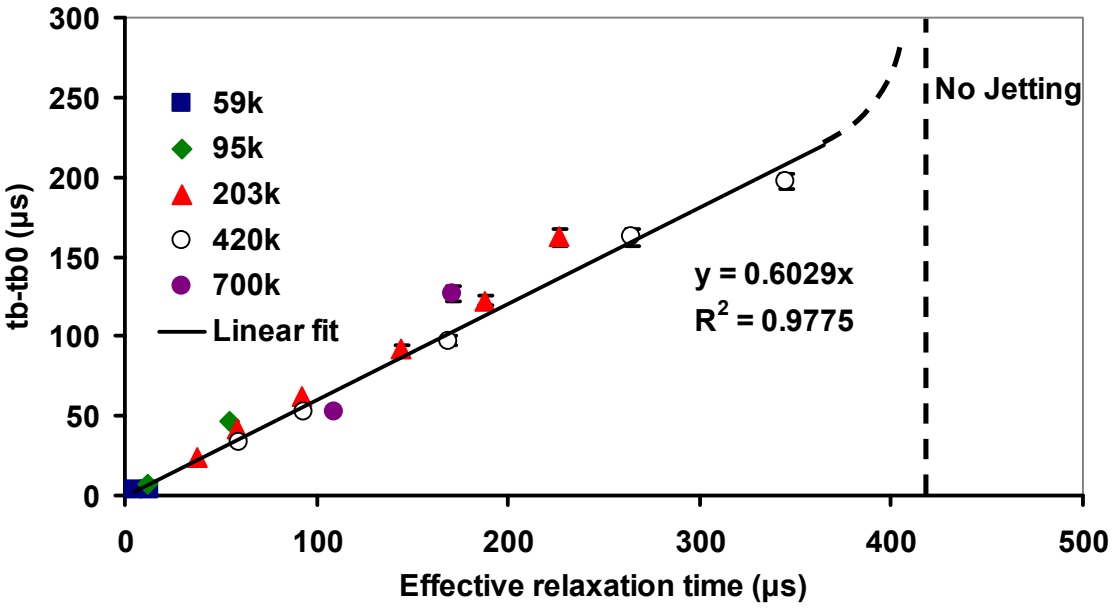

Figure 29 Breakup time versus effective relaxation time in DOD inkjet drop formation of dilute PEO solutions. Driving voltage = 44.2 V and frequency = 20 Hz.

In Newtonian liquids, first breakup time can be scaled by capillary time, $(\rho R^3_{noz}/\gamma)^{1/2}$ [16]. When PEO is added to distilled water, capillary time does not change much; however, the fluid may have Non-Newtonian behavior, i.e., the solution exhibits elasticity, which affects breakup time. The polymer chains may be stretched and oriented during the elongation of the liquid thread, producing an elastic stress in the liquid thread which opposes pinchoff. The degree to which the polymer chains are stretched and oriented depends on the relative rates at which two opposing

phenomena occur. The elongation of the liquid column causes the polymer chains to be stretched and oriented. At the same time, Brownian motion disorients the polymer chains. The time characterizing Brownian motion is referred to relaxation time, λ. If λ is small relative to breakup time, t_0, for the base Newtonian liquid containing no polymer, Brownian motion prevents segments of the polymer chains to become sufficiently oriented to produce significant elastic effects. As λ increases, the elastic effects increase. If λ is sufficiently large, the polymer chains are stretched and oriented, and elastic effects may be significant, and in some cases large enough that pinchoff does not occur. Thus, the increase in breakup time (t_b - t_{b0}) with the addition of PEO might be expected to scale with the relaxation time of the polymer chains. Based on the results shown in Figure 29, λ_{eff} was used in this study.

As liquid is ejected from the nozzle and stretched, some of the inertial energy in the ejected liquid is consumed in orienting and stretching the polymer chains. As a result, primary drop speed decreases. Thus it may be expected that the primary drop speed correlates with relaxation time. The ratio of primary drop speed (v) of PEO solution to the primary drop speed of distilled water (v_0) is plotted versus effective relaxation time in Figure 30. A linear relationship between v/v_0 and effective relaxation time was found to fit the data well ($R^2 = 0.9753$);

$$v / v_0 = 1 - 0.0026\lambda_{eff} \qquad [6.6]$$

The relationship predicts that no jetting will occur for an effective relaxation time greater than about 384 μs. In a jetting experiment, no pinchoff occurred for effective relaxation time of about 415 μs.

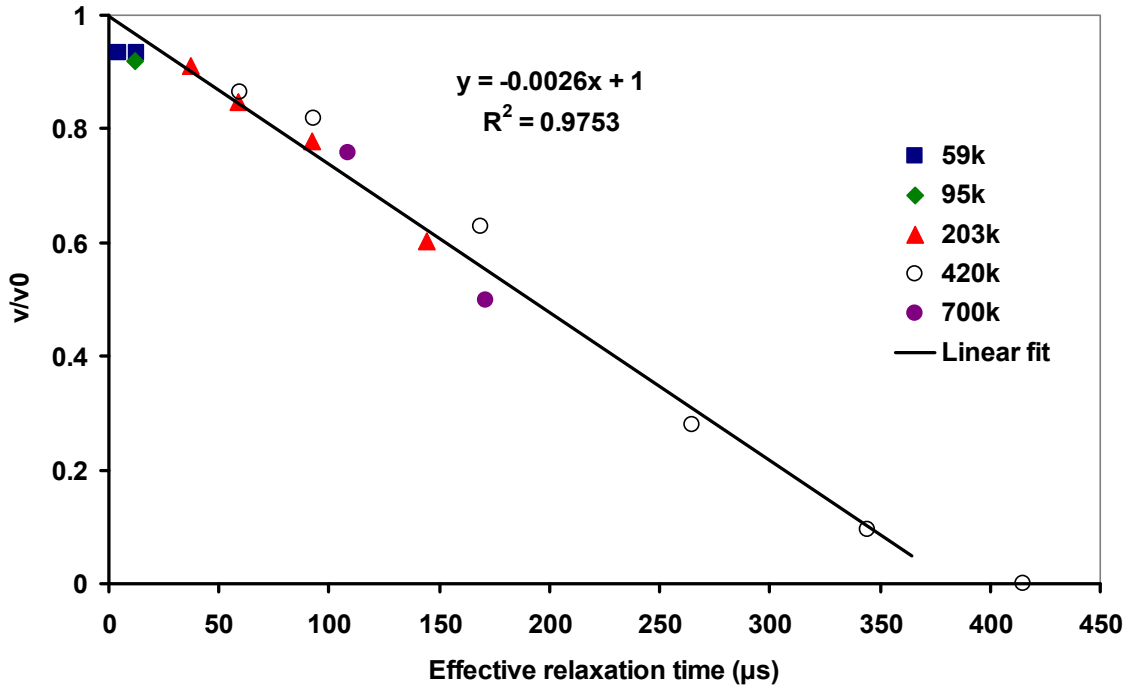

Figure 30 Variation of v/v_0 with effective relaxation time in DOD inkjet drop formation of dilute PEO solutions. Driving voltage=44.2 V and frequency=20 Hz.

By combining Equations 6.5 and 6.6,

$$v / v_0 = 1 - 0.03 (t_b - t_{b0}) / v_0 \qquad [6.7]$$

which is identical to the relationship obtained from polydispersed PEO (Equation 5.2). Breakup time and primary drop speed for both polydispersed and monodispersed PEO aqueous solution are plotted against $t_b - t_{b0}$ in Figure 31. The predictions of Equation 6.7 are also shown in the figure, and the fit is good ($R^2 = 0.9449$).

Thus, for the monodispersed PEO solutions, two important DOD printing parameters, breakup time and dimensionless primary drop speed were shown to be linearly related to λ_{eff}, which can be calculated from the basic properties of PEO solutions.

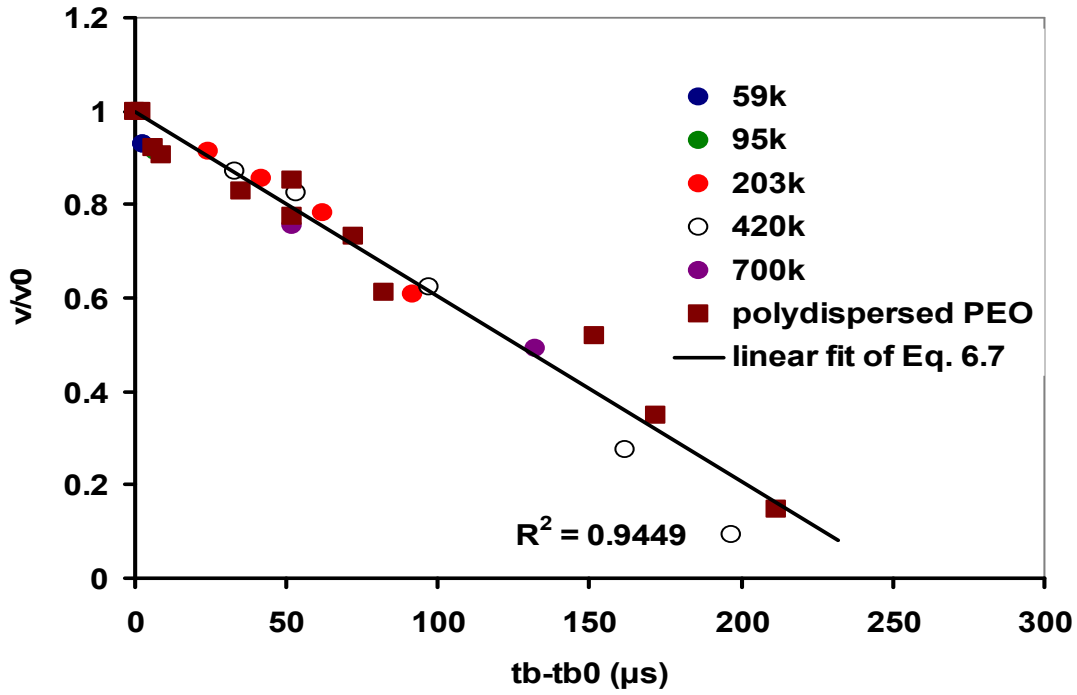

Figure 31 Relationship between t_b - t_{b0} and v/v_0. Driving voltage=44.2 V and frequency=20 Hz

6.4 DOD Inkjet Drop Formation Dynamics of Monodispersed PEO Solutions with High Viscosity

Effective relaxation time varies directly with the viscosity of the base solvent, η_s, as can be seen in Equation 6.3. Thus the effect of adding polymer on DOD jetting can be expected to increase with viscosity of the base solvent. DOD inkjet drop formation of PEO solutions having a mixed solvent of water and glycerin were compared with that for water as the solvent. The shear viscosity of the base solvent of water and glycerin was 5.88 cP. In Figure 32, the drop formation process for the mixed solvent with and without PEO is compared with that of water with and without PEO. For both PEO solutions, M_n was 203,000 g/mol, and concentration was 0.05wt%. Breakup time, primary drop speed and number of satellites are listed in Table 8.

By comparing Figures 33 A (5.88 cP) and C (1.06 cP), it can be seen that increase in viscosity for a Newtonian liquid affects DOD drop formation. When shear viscosity increased from 1.06 to 5.88 cP, breakup time increased only slightly, but drop speed decreased significantly (6.9 versus 4.6 m/s) and the number of satellites decreased from two to one.

The addition on PEO to both Newtonian solvents affected DOD drop formation, but the effect was much greater for the higher viscosity solution. For example, breakup time increased from 28 and 30 μs for the pure solvents to about 55 and 175 μs for base solution viscosities of 1.06 and 5.88 cP, respectively. Apparently, the increased viscosity and elasticity retarded pinchoff. For the higher viscosity solution, a bead-like structure was formed at about 100 μs, and the bead recombined with the bulbous head at about 150 μs.

In Figure 31 D, the position on the upper satellite does not move uniformly down in the sequence of images. This indicates that the satellite formation is less reproducible than other parts of the drop formation process.

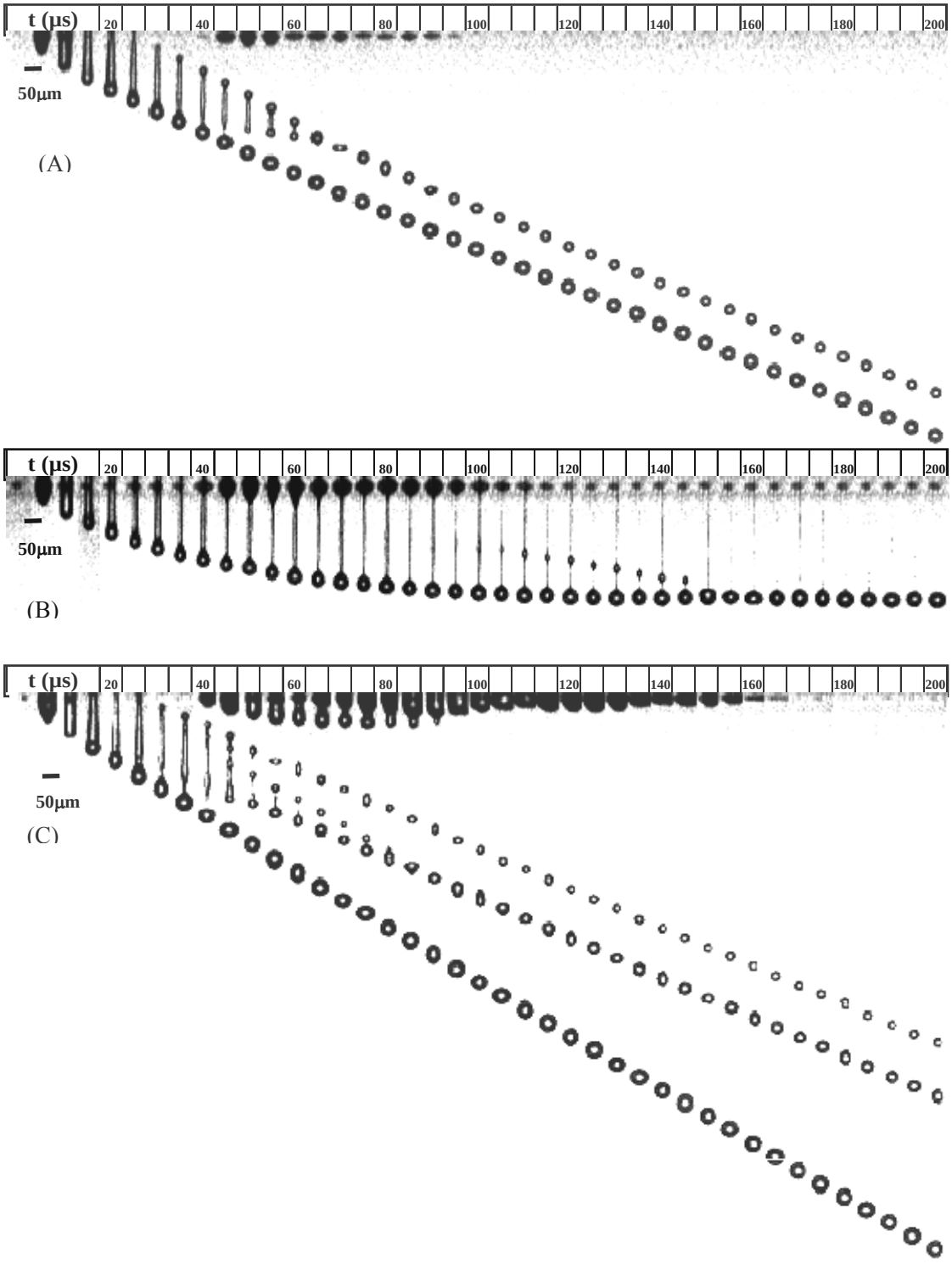

Figure 32 Images of drop formation for: (A) distilled water and glycerin mixture with a shear viscosity of 5.88 cp; (B) PEO solution with water and glycerin mixture (C) distilled water with a shear viscosity of 1.06 cp; and (D) PEO in distilled water. For B and D, PEO had M_n = 203,000 g/mol at c = 0.05wt%, c/c* = 0.10. Driving voltage = 44.2 V and frequency = 20 Hz. Images begin at 0 μs when liquid emerges from the nozzle and are shown for every 5 μs through 200 μs.

Figure is continued on next page.

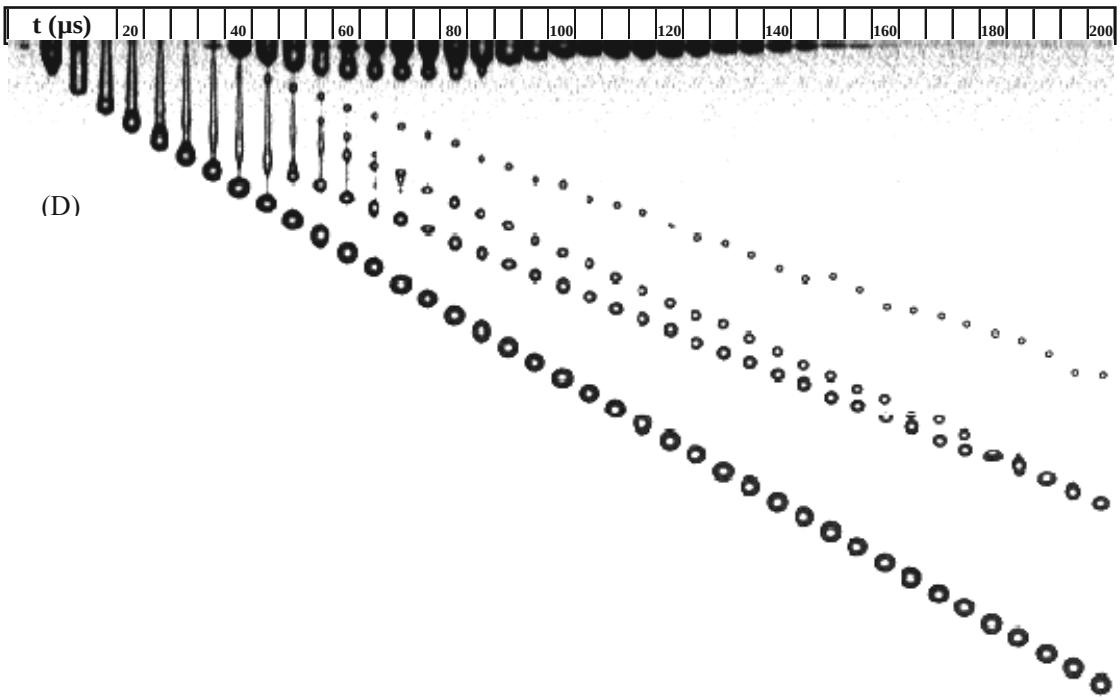

Figure 32 (continued) (D) PEO in distilled water. For B and D, PEO had M_n = 203,000 g/mol at c = 0.05wt%, c/c* = 0.10. Driving voltage = 44.2 V and frequency = 20 Hz. Images begin at 0 μs when liquid emerges from the nozzle and are shown for every 5 μs through 200 μs.

Equation 6.4 was written for aqueous solution with η_s of 1.06 cP. When the equation is modified to include viscosity (cP) of the base solution, the following relationship is obtained:

$$\lambda_{eff} \cong 5.08 \times 10^{-8} \times \eta_s \times M_n^{2.07} \times c^{0.65} \ (\mu s) \qquad [6.8]$$

where η_s is in units of cP.

When effective relaxation time for the PEO solution with for the 5.88-cP solvent was calculated using Equation 6.8 and substituted into Equation 6.5, predicted breakup time was 155 μs, which is reasonably close to the measured value of 175 μs. Also, when Equation 6.7 was used to calculate the primary drop speed, the predicted

value of 0.25 m/s was obtained. This agrees closely with the measured value of 0.24 m/s.

*6.*5 DOD Inkjet Drop Formation of Solutions Containing Mixtures of Different Molecular Weight Monodispersed PEO

The experimental results for polydispersed PEO solutions did not correlate well with effective relaxation time; however, the polydispersities of the polymers were not known and thus could not be used to help explain the results. For that reason, the monodispersed polymers were used to produce mixtures of PEO solutions. A series of solutions of PEO containing up to three different molecular weight monodispersed PEO was used to investigate the drop formation process. The properties of the solution are shown in Table 9. The values of c/c* are smaller than 1, and all of the four samples can be considered as dilute solutions.

Table 9 Basic properties of PEO solutions with mixtures of PEO of different molecular weight in DOD drop formation.

Mixture number	$M_{n,i}$ (g/mol)	$M_{w,i}$ (g/mol)	c_i (wt%)	For mixture M_n (g/mol)	For mixture M_w (g/mol)	For mixture PDI[a]	For mixture c/c*[b]	η_s (mPa•s)	For mixture η (mPa•s)	For mixture λ_{eff}[c] (μs)
A	203,000 420,000	231,000 441,000	0.1 0.01	213,000	250,000	1.17	0.26	1.06	1.36	92.5
B	59,000 203,000 420,000	60,000 231,000 441,000	0.5 0.1 0.01	68,000	94,000	1.39	0.75	1.06	1.81	95.4
C	203,000 420,000	231,000 441,000	0.1 0.02	222,000	266,000	1.20	0.29	1.06	1.43	120.6
D	203,000 420,000	231,000 441,000	0.1 0.1	274,000	336,000	1.23	0.56	1.06	1.74	281.1

a. PDI=M_w / M_n
b. When calculating c*, the weight average molecular weight of the mixture was used,
c. For aqueous solution containing mixtures of monodispersed PEO, λ_{eff} was calculated using Equation 6.12.

The number average molecular weight for the mixture of PEO can be calculated as follows:

$M_n = \sum_i x_i M_{n,i}$, where x_i is the mole fraction of each species.

For a mixture made up of two (A and B) samples of PEO:

$$M_n = \frac{1}{n_T}\sum_i n_i M_{n,i} = \frac{1}{n_T}\sum n_A M_{n,A} + \frac{1}{n_T}\sum n_B M_{n,B} = \sum x_A M_{n,A} + \sum x_B M_{n,B}$$

Generalizing, the weight average molecular weight (M_w) for a mixture of made up of N samples (A, B, C, …, N) of PEO, weighing w_A, w_B, w_c, …, w_N, and having weight average molecular weights M_{wA}, M_{wB}, M_{wC}, …, M_{wN}, respectively, can be calculating using the following equation:

$$M_n = \sum_{i=A}^{N} x_i M_{n,i}$$

The weight average molecular weight for the mixture of PEO can be calculated using the weight average molecular weights of the components constituting the mixture. This can be shown by starting with the definition of weight average molecular weight of the mixture:

$$M_w = \sum_i \omega_i M_i$$

where ω_i is the weight fraction of each species based on the total weight (w_T) of the mixture. For a mixture made up of two (A and B) samples of PEO, weighing w_A and w_B, respectively,

$$M_w = \sum_i \omega_i M_i = \frac{\sum_i w_i M_i}{w_T} = \frac{\sum_i w_{A,i} M_{A,i}}{w_T} + \frac{\sum_i w_{B,i} M_{B,i}}{w_T}$$
$$= \frac{w_A}{w_T} \cdot \frac{\sum_i w_{A,i} M_{A,i}}{w_A} + \frac{w_B}{w_T} \cdot \frac{\sum_i w_{B,i} M_{B,i}}{w_B} = \omega_A M_{w,A} + \omega_B M_{w,B}$$

Generalizing, the weight average molecular weight (M_w) for a mixture made up of N samples (A, B, C, …, N) of PEO, weighing w_A, w_B, w_c, …, w_N, and having weight average molecular weights $M_{w,A}$, $M_{w,B}$, $M_{w,C}$, …, $M_{w,N}$, respectively, can be calculating using the following equation:

$$M_w = \omega_A M_{w,A} + \omega_B M_{w,B} + \omega_C M_{w,C} + \ldots + \omega_N M_{w,N} = \sum_{i=A}^{N} \omega_i M_{w,i} \qquad [6.9]$$

The effective relaxation times (λ_{eff}) of the mixtures shown in Table 9 were calculated by modifying the relationship for monodispersed PEO given in Equation 6.4:

$$\lambda_{eff} \cong 5.38 \times 10^{-8} \times M_n{}^{2.07} \times c^{0.65} \ (\mu s) \qquad [6.4]$$

The relationship can be rewritten as follows:

$$\lambda_{eff} \cong 5.38 \times 10^{-8} \times M_n{}^{2.07} \times c^{0.65} = 5.38 \times 10^{-8} \times \left(M_n{}^{3.185} c\right)^{0.65} \qquad [6.10]$$

When a mixture made up of N samples of PEO, $\left(M_n{}^{3.185} c\right)_{eff}$ was calculated as follows:

$$\left(M_n{}^{3.185} c\right)_{eff} = \sum_{i=A}^{N} \left(M_{ni}{}^{3.185} c_i\right) \qquad [6.11]$$

When Equation 6.11 is substituted into Equation 6.4, the following relationship is obtained.

$$\lambda_{eff} \cong 5.38 \times 10^{-8} \times \left(M_n{}^{3.185} c\right)_{eff}{}^{0.65} = 5.38 \times 10^{-8} \times \left(\sum_{i=A}^{N} M_{ni}{}^{3.185} c_i \right)^{0.65} \qquad [6.12]$$

Table 10 Breakup time and primary drop speed of aqueous solutions containing formation. Driving voltage=44.2 V and frequency=20 Hz.

Sample	Breakup time (μs)	Predicted breakup time (μs)	Primary drop speed (m/s)	Predicted primary drop speed (m/s)
A	80 ± 5	83.8	5.8	5.2
B	80 ± 5	85.5	5.6	5.2
C	100 ± 5	100.7	5.2	4.7
D	190 ± 10	197.5	2.0	1.9

The breakup time and primary drop speed of several mixtures of PEO were predicted by substituting λ_{eff} (calculated using Equation 6.12) into Equations 6.5 and 6.6, respectively. The experimental data are compared with predicted values in Table 10, and the agreement is good. These results are can also be seen in Figure 33, where breakup times for the mixtures are plotted with those for the monodispersed PEO mixtures of monodispersed PEO of different molecular weight in DOD drop solutions, previously shown in Figure 29. Thus, the relationship derived for the monodispersed PEO solutions predicts well the results for the mixtures containing monodispersed PEO. As shown in Table 11, the repeatability of drop formation of mixtures of monodispersed PEO is more like that of polydispersed PEO.

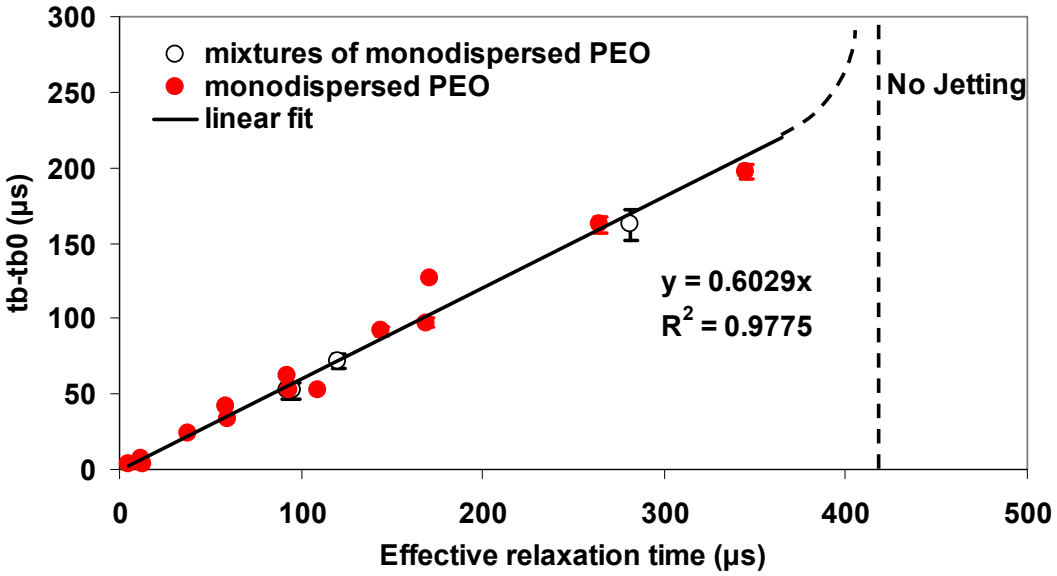

Figure 33 Breakup time versus effective relaxation time in DOD inkjet drop formation of dilute PEO solutions and PEO mixture solutions. Driving voltage=44.2 V and frequency=20 Hz.

Table 11 Variation in Breakup time of PEO solutions

Molecular Weight (g/mol)	PDI	c (wt %)	c/c*	Breakup time t_b (µs)
300,000[a] (polydispersed)	c	0.02	0.05	110 ± 10
1,000,000[a] (polydispersed)	c	0.01	0.06	190 ± 10
203,000[b] (monodispersed)	1.14	0.2	0.41	90 ± 1
700,000[b] (monodispersed)	1.20	0.01	0.05	160 ± 3
Mixture of 203,000[b] (monodispersed) 420,000[b] (monodispersed)	1.17	0.1 0.01	0.26	80 ± 5
Mixture of 203,000[b] (monodispersed) 420,000[b] (monodispersed)	1.23	0.1 0.1	0.56	190 ± 10

a. Viscosity average molecular weight

b. Number average molecular weight

c. The PDIs of the samples referred to as polydispersed PEO are not known, but Tirtaatmadja et al. [1] indicate that they are about 1.8 based on the GPC test of 1,000,000 g/mol PEO.

6.6 DOD Inkjet Drop Formation Dynamics of Monodispersed PEO Solutions with Similar Effective Relaxation Time

Drop formation process of four aqueous solutions containing PEO which have similar effective relaxation times are shown in Figure 34. Important DOD drop formation parameters are listed in Table 12. Two of the solutions contain monodispersed PEO and the other two contain mixtures of monodispersed PEO. In general, the drop formation processes were similar, and the breakup times and primary drop speeds were nearly the same. The images of drop formation show that while one major satellite was formed for the four cases, there were some differences in the satellite formation process. Notice that, in all four cases, several satellites were formed due to capillarity, but they recombined into one major satellite except for (D), where one small satellite did not recombine with the major satellite.

Table 12 Breakup time, primary drop speed and number of satellites of PEO solutions with similar effective relaxation time in DOD drop formation. Driving voltage=44.2 V and frequency=20 Hz.

Sample in Figure 34	M_n (g/mol)	c (wt%)	Effective relaxation time* (μs)	Breakup time t_b (μs)	Primary drop speed (m/s)	Number of major satellites
A Monodispersed PEO	203,000	0.2	92.1	90	5.4	1
B Monodispersed PEO	420,000	0.02	93.0	81	5.7	1
C** Mixture of monodispersed PEO	203,000	0.1	92.5	80 ± 5	5.8	1
	420,000	0.01				
D*** Mixture of monodispersed PEO	59,000	0.5	95.4	80 ± 5	5.6	1
	203,000	0.1				
	420,000	0.01				

* Calculated using Equation 6.3.

** Mixture has a M_n of 213,000 g/mol, M_w of 250,000g/mol and PDI of 1.17.

*** Mixture has a M_n of 68,000 g/mol, M_w of 94,000g/mol and PDI of 1.39.

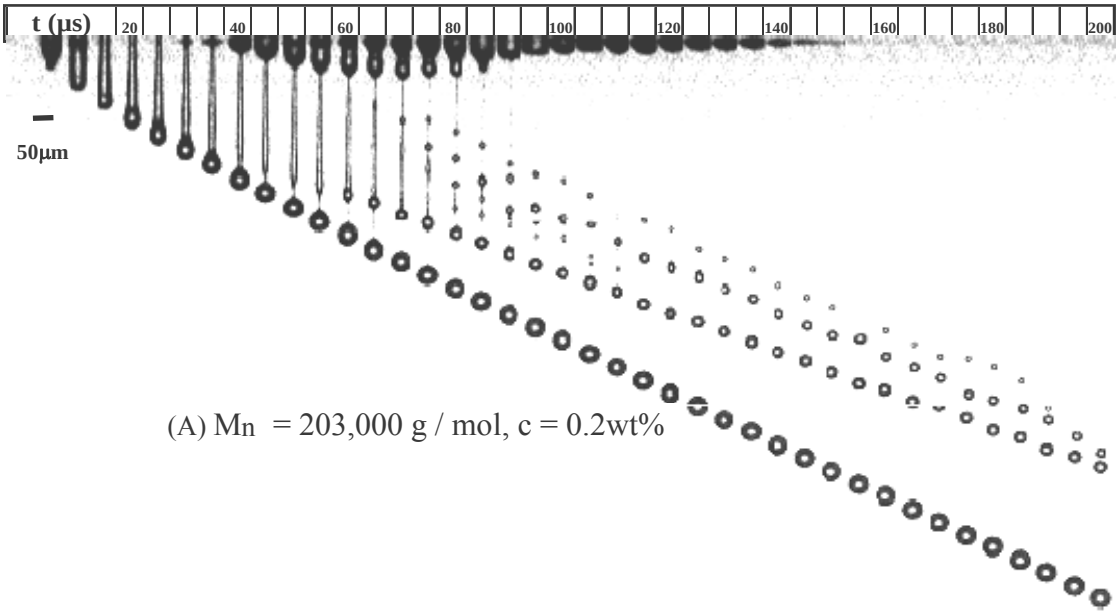

(A) M_n = 203,000 g / mol, c = 0.2wt%

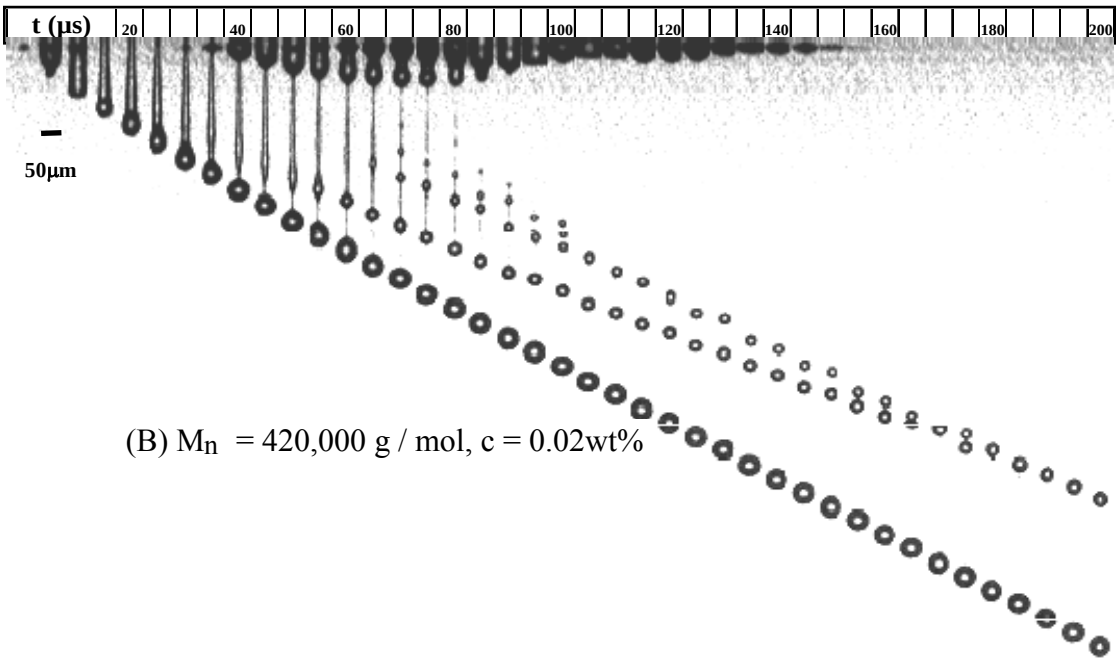

(B) M_n = 420,000 g / mol, c = 0.02wt%

Figure 34 Images of drop formation of aqueous solution containing PEO. (A) M_n = 203,000 g / mol, c = 0.2wt%; (B) M_n = 420,000 g / mol, c = 0.02wt%; (C) Mixture A (M_n =203,000 g/mol, c = 0.1wt% and M_n = 420,000 g/mol c = 0.01wt%); (D) Mixture B (M_n =203,000 g/mol, c = 0.1wt%, M_n = 420,000 g/mol c = 0.01wt% and M_n = 59,000 g/mol c = 0.5wt%) Time interval = 5 μs, driving voltage = 44.2 V and frequency = 20 Hz. Images begin at 0 μs when liquid emerges from the nozzle and are shown for every 5 μs through 200 μs.

Figure is continued on next page.

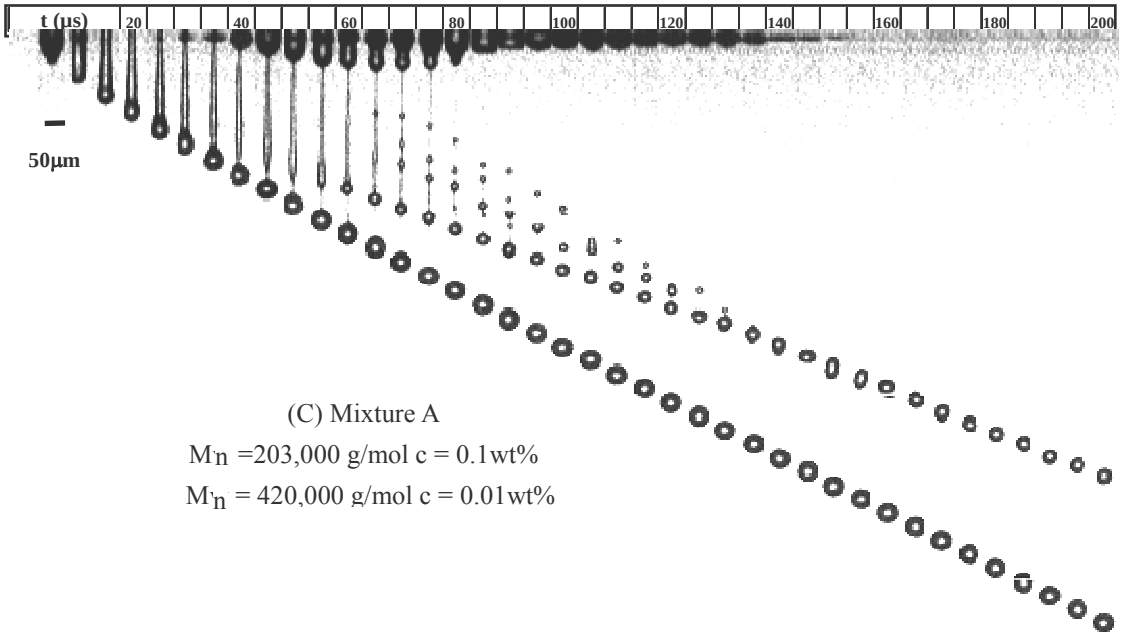

(C) Mixture A
M_n =203,000 g/mol c = 0.1wt%
M_n = 420,000 g/mol c = 0.01wt%

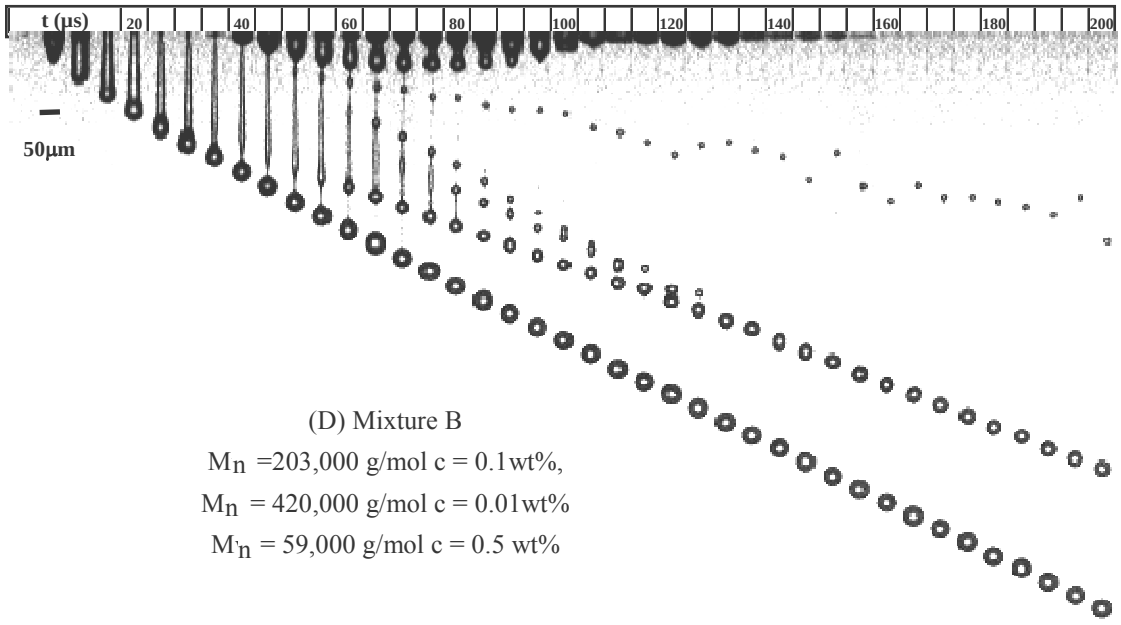

(D) Mixture B
M_n =203,000 g/mol c = 0.1wt%,
M_n = 420,000 g/mol c = 0.01wt%
M_n = 59,000 g/mol c = 0.5 wt%

Figure 34 (Continued) Images of drop formation of aqueous solution containing PEO. (A) M_n = 203,000 g / mol, c = 0.2wt%; (B) M_n = 420,000 g / mol, c = 0.02wt%; (C) Mixture A (M_n =203,000 g/mol, c = 0.1wt% and M_n = 420,000 g/mol c = 0.01wt%); (D) Mixture B (M_n =203,000 g/mol, c = 0.1wt%, M_n = 420,000 g/mol c = 0.01wt% and M_n = 59,000 g/mol c = 0.5wt%) Time interval = 5 μs, driving voltage = 44.2 V and frequency = 20 Hz. Images begin at 0 μs when liquid emerges from the nozzle and are shown for every 5 μs through 200 μs.

6.7 DOD Inkjet Drop Formation Dynamics of Monodispersed PEO Solutions with Different Molecule Structures

Two of the polymers (P2798-EO and P8846-4EOOH) having similar molecular weights were obtained from PolymerSource to investigate the effect of shape of the polymer chains on DOD inkjet drop formation. Sample A (P2798-EO) is a linear chain polymer with a M_n of 59k g/mol and a polydispersity of 1.02; Sample B (P8846-4EOOH) is a four-arm polymer with a M_n of 60k g/mol and a polydispersity of 1.15, see Table 1 in Chapter 4. Images of the DOD drop formation of these two PEO solutions are shown in Figure 35. Since the molecular weights of the two polymers are low, both DOD drop formation of these two solutions have small polymer effects, and the difference between DOD drop formation of two different structures are small. However, despite the linear chain PEO having a smaller polydispersity which suggests smaller polymer effects, the breakup time of A (34 μs) is slightly larger than that of B (33 μs), and the primary drop speed of A is smaller than that of B, which indicates that the effects of A are larger than those of B. For the same M_n, the linear structure of polymer gives a longer molecule chain compared to the 4-arm shaped structure.

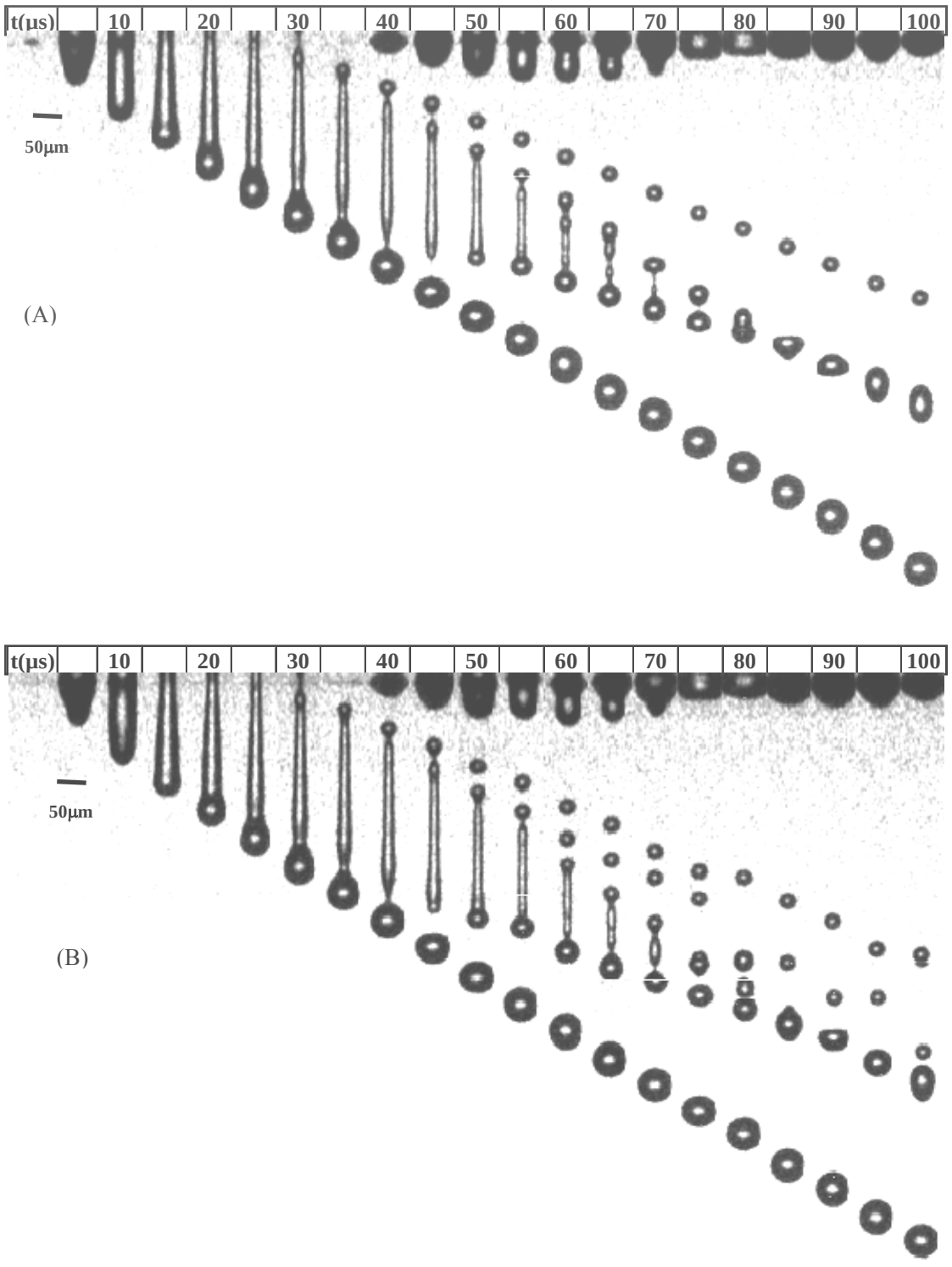

Figure 35 Drop formation process of aqueous solution containing PEO. (A) M_n = 59,000 g / mol, c = 1wt%; (B) M_n = 60,000 g / mol, c = 1wt%, driving voltage=44.2 V and frequency=20 Hz. Images begin at 0 μs when liquid emerges from the nozzle and are shown for every 5 μs through 100 μs.

6.8 Conclusions

DOD drop formation data were shown to correlate closely with effective relaxation time, λ_{eff}, proposed by Tirtaatmadja [1] based on Rouse-Zimm theory. Breakup time and primary drop speed for solutions containing monodispersed PEO and aqueous solutions containing mixtures of monodispersed PEO were closely predicted by the following equations:

$$t_b - t_{b0} = 0.6029\lambda_{eff} \quad [6.5]$$

$$v / v_0 = 1 - 0.0026\lambda_{eff} \quad [6.6]$$

The dimensionless primary drop speed, v/v_0, correlated closely with (t_b - tb_0) and was closely predicted by the following relationship:

$$v / v_0 = 1 - 0.03 (t_b - t_{b0}) / v_0 \quad [6.7]$$

These equations also predicted well for solutions with base solvent having a viscosity of 5.88 cP.

When solutions containing monodispersed PEO and aqueous solutions containing mixtures of monodispersed PEO had similar effective relaxation time, the drop formation processes were similar. In calculating relaxation time for mixtures of monodispersed PEO, the concentration and molecular weight of each species was accounted for by using the following mixture rule:

$$\lambda_{eff} \cong 5.38 \times 10^{-8} \times \left(M_n{}^{3.185} c \right)_{eff}{}^{0.65} = 5.38 \times 10^{-8} \times \left(\sum_{i=A}^{N} M_{ni}{}^{3.185} c_i \right)^{0.65} \quad [6.12]$$

which indicated that weight average and viscous average molecular weight underestimated the effect of the molecular weight of each of the species in the mixture.

The addition of polydispersed PEO had a greater effect on DOD drop formation compared to that of monodispersed PEO with similar number average

molecular weight. This is due to the polydispersed PEO having a fraction of longer chain molecules with corresponding longer relaxation times. The repeatability of breakup time in DOD drop formation on monodispersed PEO solutions was better than that of solutions containing mixtures of monodispersed PEO. The repeatability of breakup time containing mixtures of monodispersed PEO was similar with that of the polydispersed PEO solutions.

When different structures of monodispersed PEO with similar number average molecular weight were compared, little difference was observed because the molecular weights of the samples were too low.

CHAPTER 7

EFFECTS OF WAVEFORM AND JETTING FREQUENCY ON DOD DROP FORMATION OF DILUTE PEO SOLUTIONS

When a signal (or waveform) is sent to the piezoelectric actuator of a typical DOD inkjet printer, the actuator responds, producing a pressure wave inside the printhead. As a result, ink inside the chamber is ejected from the nozzle. DOD drop formation dynamics is highly affected by the actuating waveform, including the driving voltage, waveform shape, and frequency [60]. In this chapter, the effects of parameters (jetting frequency, voltage amplitude and the shape of waveform) characterizing the signal are investigated. The open time and first drop problem [2] are also discussed.

7.1 First Drop Problem

The method used in this study for visualizing of the DOD drop formation is based on flash photography [2]. The reproducibility of the process under study is the major concern for flash photography, because it is assumed that taking images at different times in individual tests in a series of tests will allow reconstruction of the dynamics representing the process (single drop formation and impaction). Several factors which can may make drop formation dynamics of the first few drops inconsistent are fluctuation of signal amplitude, accuracy of time setting, surrounding air currents, wetting of nozzle plate, and the “first drop problem” of inkjet printing. Although all of the factors may affect reproducibility, the “first drop problem” is the most significant in the present experiments. It is caused by the evaporation of ink at the nozzle exit for inks containing more than one material because evaporation

changes concentrations of ink constituents at the nozzle. The severity of the problem depends on the idle time of the nozzle. In order to minimize the "first drop problem", Dong et al. [2] used a pulse train from an external waveform generator (Agilent 33220A), instead of a single pulse, to trigger the whole system. Hence, for each trigger, not a single drop, but a drop stream is generated, and the idle time between two drops is constant. After several drops, the drop formation becomes consistent with a position variation less 1 μm.

In Figure 36, the severity of the "first drop problem" in the drop formation process of DOD inkjet printing is compared for three inks. Since ink composed of water has only one constituent, evaporation does not cause a problem. Thus, for water, there is no "first drop problem", all 20 drops look identical in Figure 36 (A). However, for water and glycerin mixture (see Figure 36 (B)), there is an obvious "first drop problem" because water evaporates faster than glycerin. Similarly, for PEO solution (see Figure 36 (C), there are several drops jetted before the images look identical. For PEO solutions, the time taken for the images to look identical depends on the idle time of the printhead. If the idle time is increased, it takes longer for concentrations at the end of the nozzle to stabilize and for the drop formation process to become reproducible. If the idle time is too long, the nozzle does not jet. In the inkjet industry, the idle time that allows the printing system to jet well is referred to as "open time", which is an important parameter of the printhead and inks. In DOD inkjet printing of PEO solutions, as molecular weight or concentration is increased, the open time is shortened.

In order to get a good repeatability in DOD drop formation of polymer solutions, a series of non-stop signal in a certain frequency was used to trigger the printhead to avoid the first drop problem.

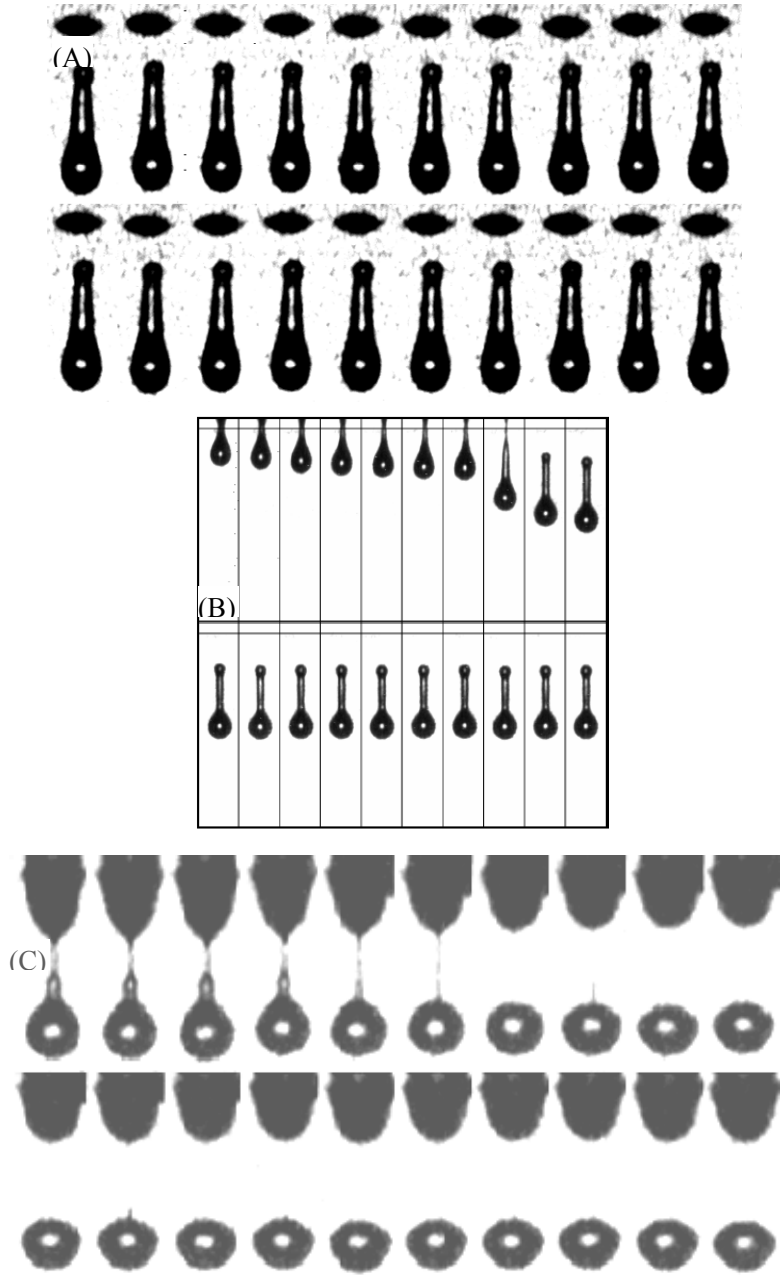

Figure 36 Comparison of "first drop problem" in the drop formation process of DOD inkjet printing for three inks: (A) first 20 drops of water viscosity = 1 cp, surface tension = 72 mN/m; (B) first 20 drops of water and glycerin mixture viscosity = 4.7 cp [2]; and (C) first 20 drops of PEO solution (Mw=300k g/mol, w% = 0.01wt%). Jetting frequency = 20Hz.

7.2 Effects of Jetting Frequency on DOD Drop Formation

Jetting frequency can significantly affect DOD drop formation dynamics. Since the time between two consecutive signals decreases as jetting frequency increases, the time interval between two consecutive signals may not be long enough for pressure variation inside the nozzle chamber due to the previous pulse to be fully damped by viscous dissipation before the next pressure pulse is produced. As a result, the pressure waves due to consecutive pulses interact. This coupling varies as frequency changes, which leads to different DOD drop sizes and velocities [60]. The coupling can lead to a start-stop problem, different from the "first drop" discussed previously. When jetting frequency is sufficiently high and the idle time is sufficiently short that the “first-drop” problem is insignificant, the drop triggered by the first pulse after the nozzle is idle is identical to the drop fired at low frequency because the previous pulse has been fully damped by viscous dissipation before the first pulse is produced.

Wang [60] investigated the effect of frequency DOD drop formation of a Newtonian liquid, which was a mixture (glycerin (43.7 wt%), isopropanol (11.4 wt%) and DI water (44.9 wt%)) with shear viscosity of 6.3 cp and surface tension of 32 mN/m at a driving voltage of 19.5V. When the nozzle went from idle to jetting for frequencies lower than 6.7 kHz, the drop formation triggered by the first pulse was found to be identical to subsequent drops in the sequence and independent of jetting frequency. However, at jetting frequencies higher than 6.7 kHz, DOD drop formation after idle varied over the first four pulses. A modulating pulse was added before the first pulse to simulate the pressure variation inside the nozzle chamber before each pulse when the nozzle is continuously fired. When the modulating pulse was properly

selected, DOD drop formation of the first pulse after idle was identical to DOD drop formation in equilibrium.

A study of the effect of jetting frequency on drop formation of PEO aqueous solution is discussed next. The results for the PEO solutions are compared with those for distilled water. The voltage amplitude for these tests was 44.2V. For jetting frequencies from 0.2 Hz to 800 Hz, the DOD drop formation for distilled water (see Figure 37) was very similar and repeatable; however, as jetting frequency was increased above 800 Hz, apparently the pressure waves due to consecutive pulses apparently interact. The interaction consecutive pulses occurred at a much lower jetting frequency than observed by Wang [60] for a mixture (glycerin (43.7 wt%), isopropanol (11.4 wt%) and DI water (44.9 wt%)) of Newtonian liquids. The ink in Wang's experiments had a much higher shear viscosity (6.3 cP versus 1.06 cP), which dissipates oscillatory energy more rapidly in the chamber. As jetting frequency was increased from 800 to 3000 Hz, the interaction was destructive, resulting in primary drop speed decreasing and satellite formation changing, but ending with two satellites as occurred for lower jetting frequency. Above 4000 Hz, the interaction was apparently constructive. The leading drop speed increased by about 40% at a jetting frequency of 4000 Hz; several satellites were formed; and the location of the drops varied, as shown in Figure 37. As jetting frequency was increased above 4000 Hz, the drop formation process was not reproducible. The ejected liquid broke up into several drops with comparable size with no obvious primary drop. For frequencies at and above 13,000 Hz, no jetting occurred.

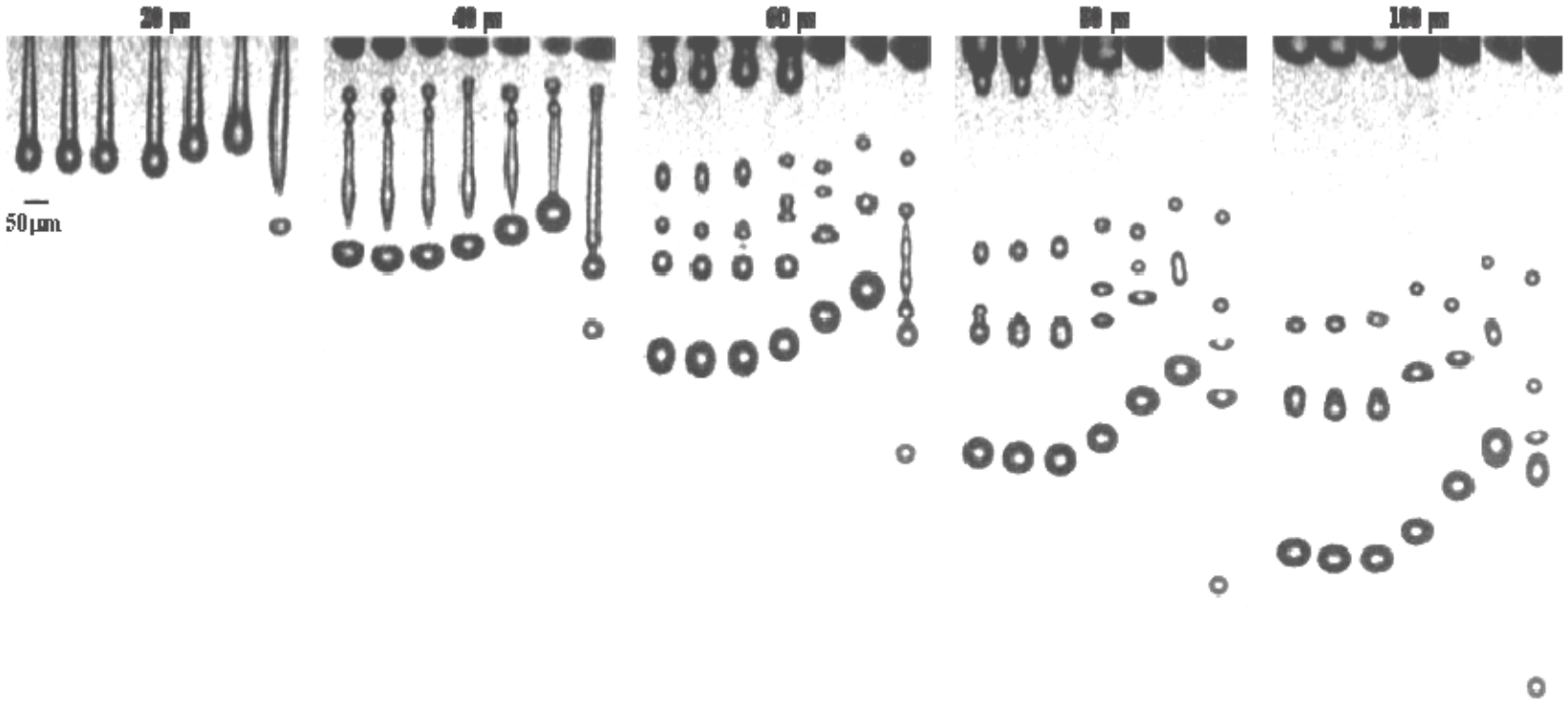

Figure 37 DOD drop formation of distilled water. From left to right on each figure: jetting frequency = 0.2, 20, 800, 1000, 2000, 3000 and 4000 Hz. Images are shown every 20 µs from 0 µs to 100 µs after liquid emerges from the nozzle. Driving voltage = 44.2 V.

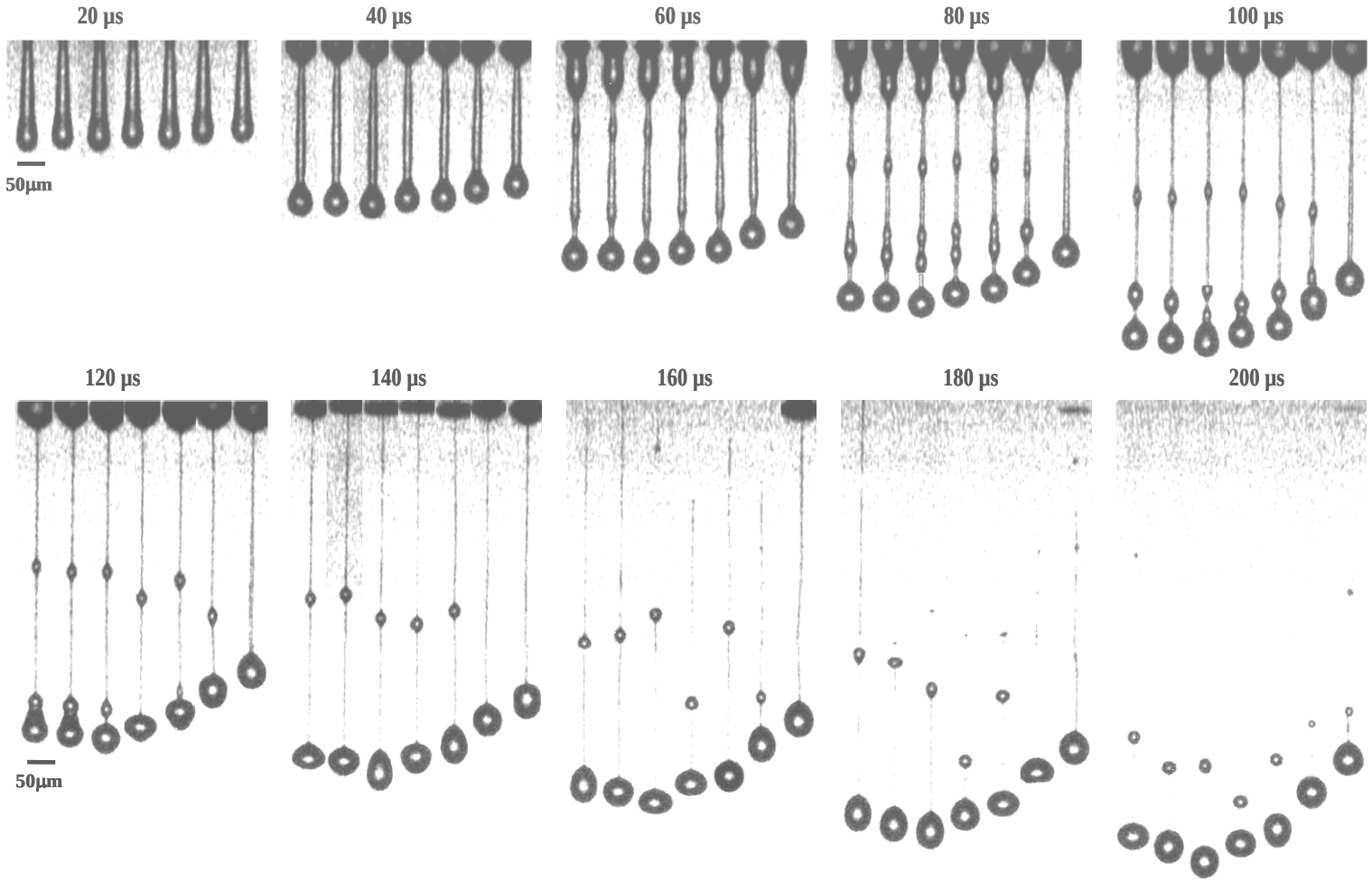

Figure 38 DOD drop formation of PEO aqueous solution containing monodispersed PEO with molecular weight of 700k g/mol and concentration of 0.01wt%. From left to right on each figure: jetting frequency = 5, 10, 20, 50, 200, 400 and 800 Hz. Images are shown every 20 µs from 0 µs to 200 µs after liquid emerges from the nozzle. Driving voltage = 44.2 V.

In Figures 38, images of DOD drop formation of dilute PEO solution at different jetting frequencies are shown. For time less than 40 μs after the liquid emerges from the nozzle, the images are similar, but the speed at which the bulbous head (leading point) moves downward varied slightly with jetting frequency. The speed was slightly higher for a jetting frequency of 20 Hz than for 5 and 10 Hz. The lower speeds at the lower jetting frequencies may be due to solvent evaporation at the nozzle. At the lower frequencies, the time between each ejection may be sufficient for the PEO concentration to increase. This conjecture is a based on the observation that when the jetting frequency was reduced to 2 Hz, the nozzle stopped jetting after about 1 minute, which is believed to be due to solvent evaporation resulting in polymer build up at the nozzle.

As jetting frequency was increased from 20 Hz to 800 Hz, the speed of the leading point decreased. As jetting frequency of 1000 Hz, jetting occurred, but stopped in less than one minute. Attempts were made to operate at higher jetting frequencies, but were unsuccessful.

For jetting frequencies below 800 Hz, during the time interval from about 60 to 140 μs after liquid emerged from the nozzle, the liquid thread became a bead-like structure. The bead nearest to the bulbous head travelled faster than the head, and joined it at about 120 μs. A long tail with one bead on it extended from the primary drop to the nozzle, but broke up during the time interval between 160 μs and 180 μs, resulting in a primary drop and a small satellite.

As jetting frequency was increased from 20 to 800 Hz, primary drop speed decreased. The reason for this is to be associated to the interaction of the pressure waves of consecutive pulses. Notice that at a jetting frequency of 800 Hz, liquid can be seen at the nozzle at times of 160 μs and 180 μs, but not for the lower frequencies.

Also, at a time of 140 μs, the liquid volume is larger at 800 Hz that at the lower frequencies. This suggests that there are polymer effects inside the chamber that increase the time required for the pressure variation inside the nozzle chamber due to the previous pulse to be fully damped by viscous dissipation before the next pressure pulse is produced.

7.3 Effects of Voltage Amplitude on DOD Drop Formation

The effects of voltage amplitude on DOD drop formation of PEO solutions are different from those observed by Wang [55] for Newtonian liquids. Both the first and second breakup times were independent of signal amplitude for the Newtonian liquids. A satellite was formed due to end-pinching at the lower amplitude, but as voltage was increased, thread shape remained the same, the ligament length increased, and multiple breakup occurred, apparently due to wave-like instability.

In Figure 39, images of the DOD drop formation of a PEO aqueous solution driven by voltage amplitudes of 29.6 and 44.2 volts. At a lower voltage of 29.6 V, the liquid thread pinched off from the nozzle at 43 μs, and no satellite was formed. As the voltage increased to 44.2 V, the pinchoff time increased to 63 μs, and the primary drop travelled much faster. In contrast, Wang reported that for Newtonian liquid, both the first and second breakup times were independent of signal amplitude. Since the leading edge travelled faster and the liquid thread pinched off from the nozzle later, a longer tail was formed, which was favorable for capillary breakup causing the tail to break up into small satellites that recombined into one satellite. This was similar to the observations for the Newtonian liquid.

The effects of voltage amplitude on DOD drop formation of PEO solutions are different from those for Newtonian liquids because of the elasticity of the PEO

solutions. As the voltage amplitude is increased, the pressure wave generated by the transducer is stronger and imparts more inertial energy to the liquid ejected from the nozzle. As a result the liquid thread elongates more during the stretching stage and the polymer chains are stretched and oriented more compared to those at a lower voltage. Thus, at the higher voltage, it takes longer for the polymer chains to relax to the coil state, i.e., relaxation time increases. As discussed in the previous chapters, the breakup time in DOD drop formation of PEO solutions can be scaled by the effective relaxation time, so the breakup time in DOD drop formation of PEO solutions at a higher voltage is longer than at a lower voltage.

As voltage amplitude is increased, two opposing factors are important. As mentioned above, the pressure wave generated by the transducer increases with increasing voltage amplitude, and more inertial energy is imparted to the liquid ejected from the nozzle, causing primary drop speed to increase. On the other hand, relaxation time increases as the stretching and orientation of polymer chains increase with increasing voltage amplitude, which tends to decrease primary drop speed. The effects of increasing inertial energy of the ejected liquid are larger, and the primary drop speed increases as voltage amplitude is increased. This is similar to what is observed for ejecting Newtonian liquids. However, in the case of polymer solutions, inertial energy must not only be sufficient to overcome viscous and surface energy effects, but also sufficient to oppose elastic effects. Thus higher voltage amplitude is required to jet polymer solutions.

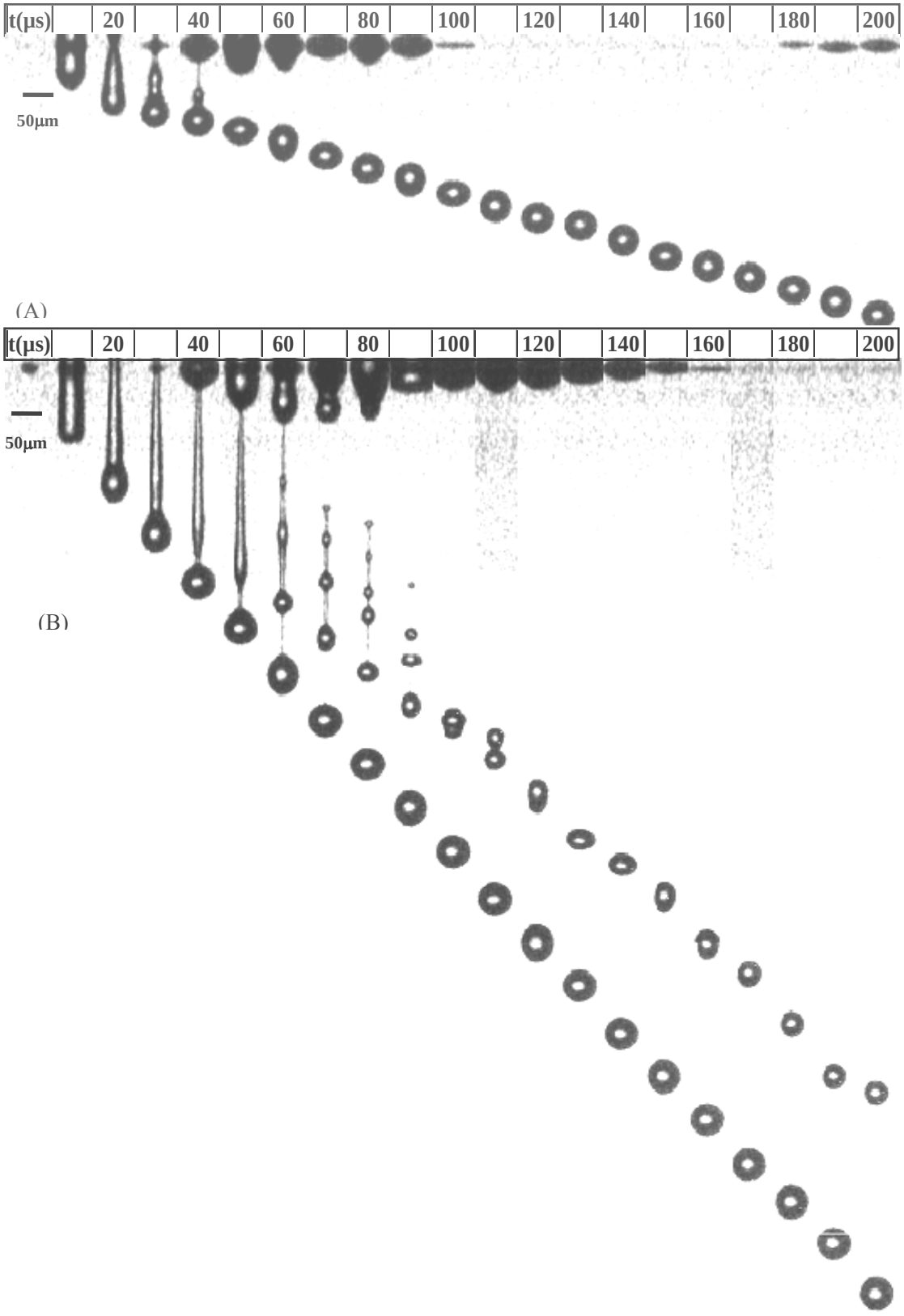

Figure 39 Images of DOD drop formation of aqueous solution containing polydispersed PEO with molecular weight of 300,000 g/mol, concentration of 0.01wt% and c/c* = 0.03. (A) Driving voltage = 29.6 V (B) driving voltage = 44.2 V, frequency = 20 Hz. Images begin at 0 μs when liquid emerges from the nozzle and are shown for every 10 μs through 200 μs.

7.4 Effects of Waveform Shape on DOD Drop Formation

A double peak waveform, suggested by the Trident printhead user's manual and shown in Figure 40, was used in the previous DOD drop formation study. In this section a series of different waveform shapes are applied to the piezo transducer during DOD drop formation of PEO solutions.

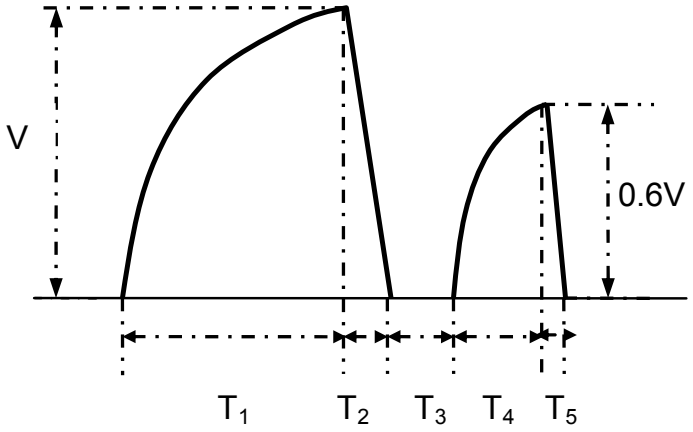

Figure 40 Double Peak waveforms rising time T_1=10.6 μs, falling time T_2=2.6 μs, dead time T_3=5.3 μs, rising time T_4 of minor peak=4.4 μs, falling time T_5 of minor peak=3.0 μs.

During the rising time (T_1), the piezo transducer expands which causes liquid to fill the nozzle chamber. A slow rising time is used to prevent air from being sucked into the channel through the nozzle orifice. During the falling time (T_2), the reduction of voltage causes the transducer to retract to its original length, increasing the pressure on the liquid in the chamber. As a result, liquid is ejected from the nozzle orifice. After the voltage falls to zero, it is held there for a short time (T_3). Then a smaller pulse is applied to the transducer. The shape is similar to the initial pulse, but the voltage maximum amplitude is smaller, and corresponding the rising time (T_4) is shorter. After reaching the voltage reaches its maximum, it falls over a falling time (T_5) in a fashion similar to that of the initial pulse. The smaller pulse is used to

promote separation of liquid from the nozzle orifice by producing a negative pressure in the nozzle. The falling pressure decelerates the liquid causing it to break from the nozzle orifice.

DOD drop formation of aqueous solution using a driving waveform in Figure 40 is shown in Figure 41, which has been discussed in detail in Chapter 5. A bulbous head formed on the ejected liquid at around 20 μs after liquid first appeared at the nozzle exit. A bead-like structure began forming on the liquid thread at about 60 μs. The bead-like structure travelled downward faster than the bulbous head and joined it at about 110 μs. The long tail appears to pinch off from the nozzle at about 180 μs, and then due to capillarity broke up into several small satellites. The amount of liquid at the nozzle decreases from a maximum at about 60 μs until no liquid can be seen at about 160 μs. It reappears in the image taken at 170 μs, but cannot be seen in the following images. The motion of the liquid at the nozzle exit is associated with the pressure variation in the chamber.

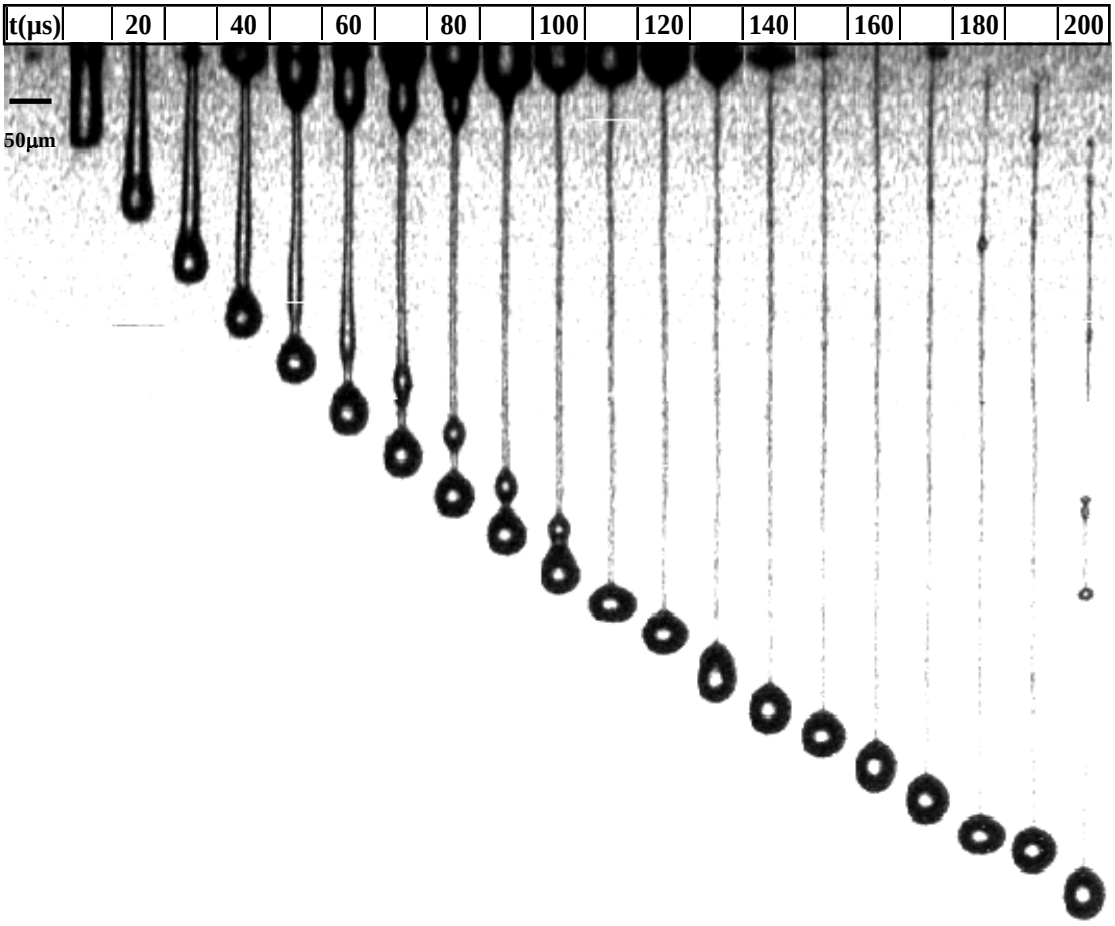

Figure 41 Images of DOD drop formation process for PEO aqueous solution containing polydispersed PEO with molecular weight of 1000k g/mol and concentration of 0.01wt%. Waveform shape of the driving signal is shown in Figure 40. Driving voltage = 44.2 V, frequency = 20 Hz. Images begin at 0 μs when liquid emerges from the nozzle and are shown for every 10 μs through 200

DOD drop formation of aqueous solution using a driving waveform in Figure 42 is shown in Figure 43. Compared to the standard waveform in Figure 40, the smaller pulse used to promote separation of liquid from the nozzle orifice was removed. When jetting Newtonian fluids the purpose of the smaller pulse is to promote separation of liquid from the nozzle orifice by producing a negative pressure in the nozzle. However, when it was removed from the signal waveform, the PEO solution pinched off sooner (160 versus 180 μs). The pinchoff appears to occur in the

liquid thread below the wider mass of liquid at the nozzle exit. No bead-like structure was formed during drop formation. The amount of liquid just below the nozzle was larger and did not disappear until about 200 μs. Apparently, the addition of the small pulse may help in dissipating the energy associated with the pressure oscillations inside the liquid chamber. The effects on drop formation for the waveform in Figure 42 compared with the standard waveform are that it decreased breakup time, increased liquid oscillation at the nozzle, increased primary drop speed, and produced a similar number of small satellites.

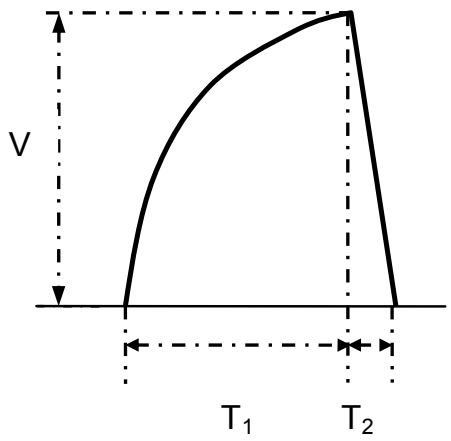

Figure 42 Single peak waveforms rising time T_1=10.6 μs, falling time T_2=2.6 μs.

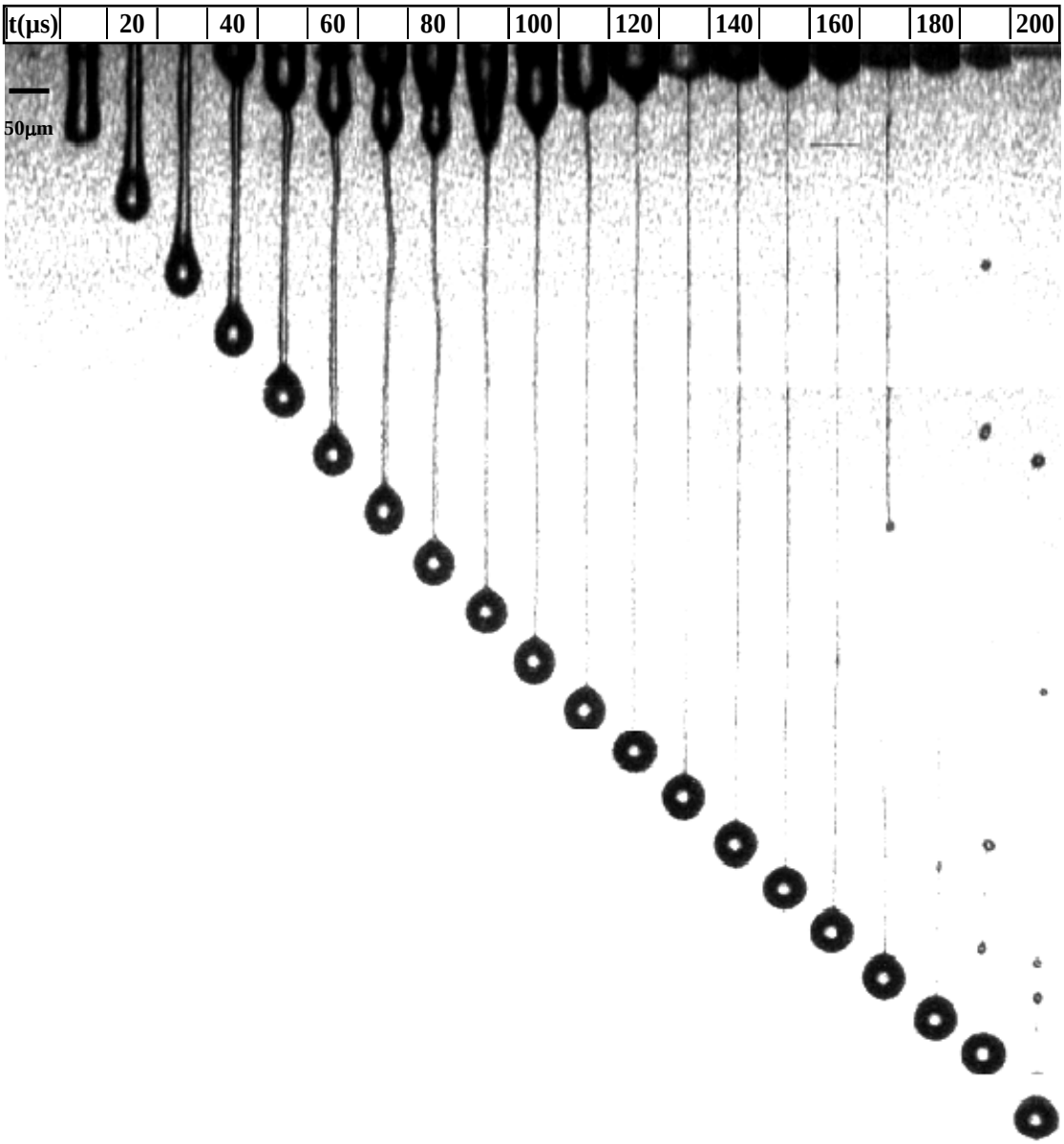

Figure 43 Images of DOD drop formation process of PEO aqueous solution containing polydispersed PEO with molecular weight of 1000k g/mol and concentration of 0.01wt%. Waveform shape of the driving signal is shown in Figure 42. Driving voltage = 44.2 V, frequency = 20 Hz. Images begin at 0 μs when liquid emerges from the nozzle and are shown for every 10 μs through 200

Since the results of the tests suggested that the second pulse may facilitate in dissipating the energy associated with the pressure oscillations inside the liquid chamber, the second pulse in the waveform was modified. For this waveform shown

in Figure 44, the second pulse had a maximum voltage of 44.2 V. Images of the DOD drop formation of aqueous solution using this waveform are shown in Figure 45.

Compared to DOD drop formation of standard waveform, the liquid thread broke up at about 150 μs, and the leading point travelled slower than for the standard waveform. When break up occurred the liquid thread was so small that it was difficult to see, and quickly disappeared, probably due to evaporation of the solvent. Due to the higher voltage of the second pulse, the pressure in the chamber fell faster and sucked liquid back into the chamber more than occurred with the standard waveform. The liquid at the nozzle exit disappeared at about 140 μs, indicating that the pressure in the chamber had decreased. Waves in the liquid thread joining the bulbous head and the wider mass of liquid at the nozzle exit, began to form at about 40 μs, and resulted in a bead-like structure. The beads moved downward faster than the bulbous head, and the two beads recombined with it at about 90 and 160 μs. When the beads caught up with the bulbous head and recombined with it, the bulbous head oscillated. The primary drop size was smaller than that of the standard waveform (47 μm versus 49 μm) and the primary drop speed was smaller than that of the standard waveform (2.8 m/s versus 3.1 m/s). Pinchoff was not occurred along the thread, apparently due to a capillary wave. The position of the pinchoff along the thread was not reproducible. The effects on drop formation for the waveform in Figure 44 compared with the standard waveform are that it decreased breakup time and liquid oscillation at the nozzle, and it eliminated the satellites.

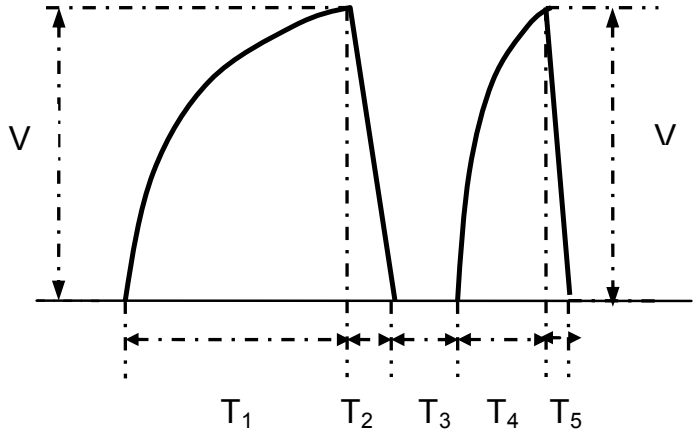

Figure 44 Double Peak waveforms rising time T_1=10.6 μs, falling time T_2=2.6 μs, dead time T_3=5.3 μs, rising time T_4 of minor peak=4.4 μs, falling time T_5 of minor peak=3.0 μs.

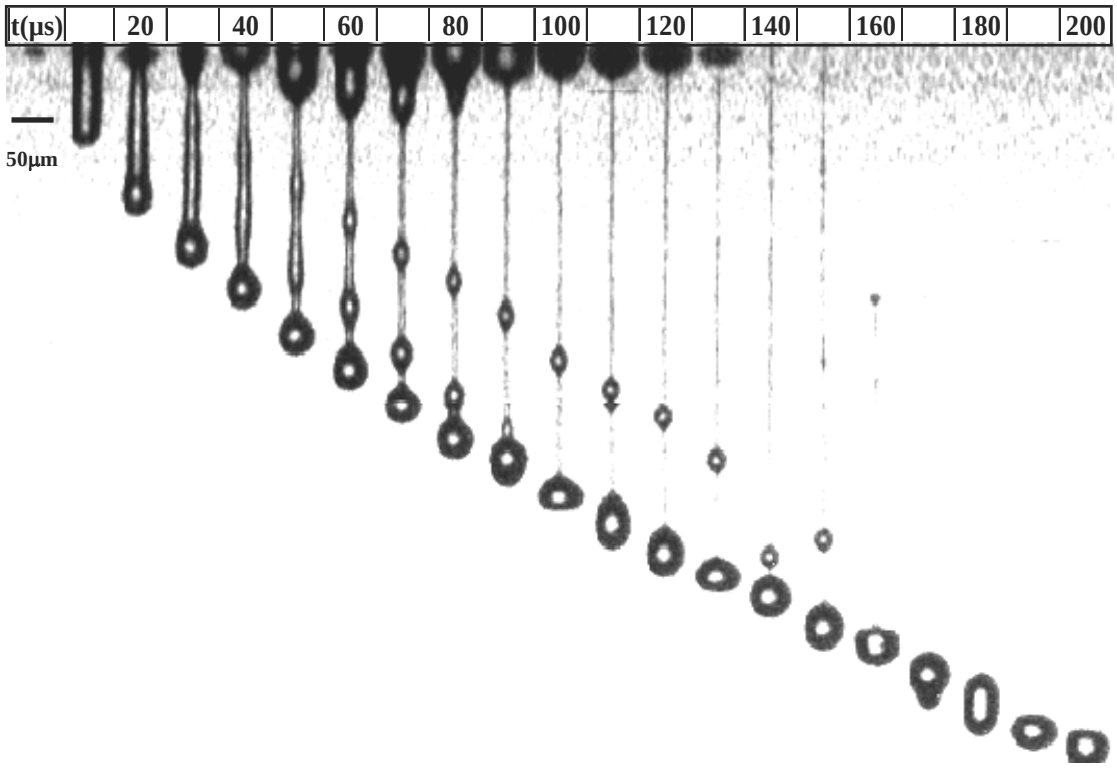

Figure 45 Images of DOD drop formation process of PEO aqueous solution containing polydispersed PEO with molecular weight of 1000k g/mol and concentration of 0.01wt%. Waveform shape of the driving signal is shown in Figure 44. Driving voltage = 44.2 V, frequency = 20 Hz. Images begin at 0 μs when liquid emerges from the nozzle and are shown for every 10 μs through 200 μs.

Compared to the standard waveform, the waveform in Figure 44 decreased breakup time and liquid oscillation at the nozzle, and it eliminated the satellites. Since these effects were considered favorable, the amplitude of the second pulse was increased further to 70.7 V and 79.6 V, see Figures 46 and 48, respectively. Images of the DOD drop formations for these waveforms are shown in Figure 47 and 49, respectively.

For both cases, the amplitude of the second pulse was larger than for the first pulse and apparently destructively interacted with the first pulse since primary drop speed and drop size were reduced. The larger second pulses, briefly caused the pressure in the chamber to fall, resulting in the length of the ligament below the nozzle to be shorter than for the standard pulse. Notice that for the image at 20 μs, that the there is a ligament attached to a much wider ligament emerging from the nozzle. Apparently the second pulse initially reduced the pressure in the chamber that reduced the volume and momentum in the ligament outside of the nozzle. Then when the voltage rapidly fell, the pressure in the chamber rose and pushed liquid out of the nozzle which is seen in the figure as a wider region of the ligament at the nozzle. The two waveforms (Figures 46 and 48) produced shorter breakup times (100 μs and 90 μs), lower leading point speeds (3.1 m/s and 2.4 m/s) and smaller primary drop sizes (43 μm and 39 μm). Bead-like structures were formed, but joined the bulbous heads quicker than occurred with previous waveforms. The larger second pulses increased the liquid oscillation at the nozzle exit which may affect the printing performance during DOD inkjet printing. The amount of liquid just below the nozzle was larger and had not disappeared when the last images were taken at 150 μs.

The voltage amplitude of the second pulse was increased systematically for the cases discussed above. Increasing the amplitude of the second pulse gave shorter breakup time, lower primary drop speed and smaller primary drop size.

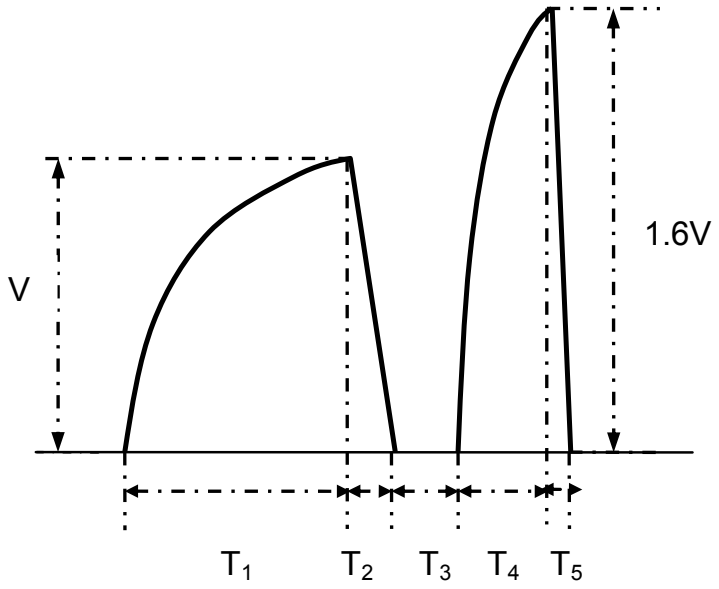

Figure 46 Double Peak waveforms rising time T_1=10.6 μs, falling time T_2=2.6 μs, dead time T_3=5.3 μs, rising time T_4 of minor peak=4.4 μs, falling time T_5 of minor peak=3.0 μs.

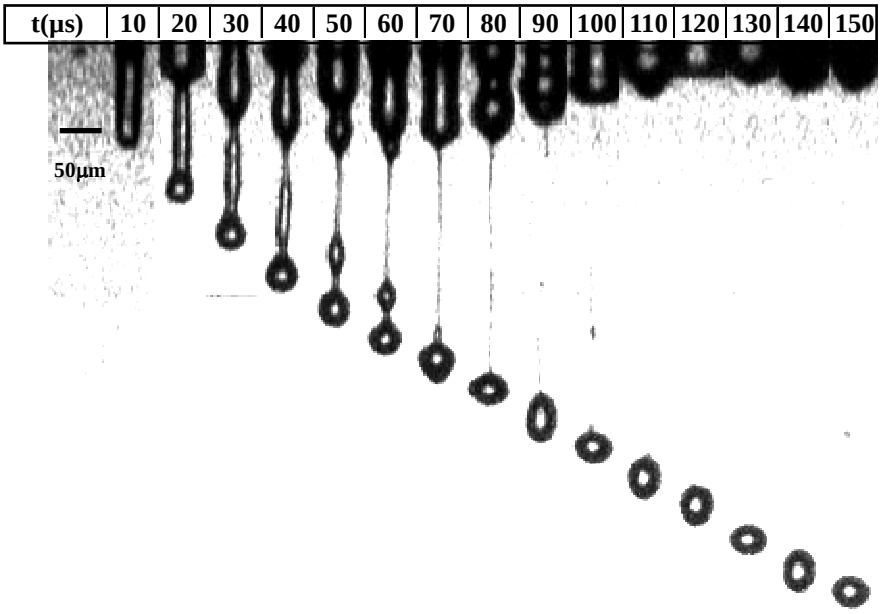

Figure 47 Images of DOD drop formation process of PEO aqueous solution containing polydispersed PEO with molecular weight of 1000k g/mol and concentration of 0.01wt%. Waveform shape of the driving signal is shown in Figure 48. Driving voltage = 44.2 V, frequency = 20 Hz. Images begin at 0 μs when liquid emerges from the nozzle and are shown for every 10 μs through 150 μs.

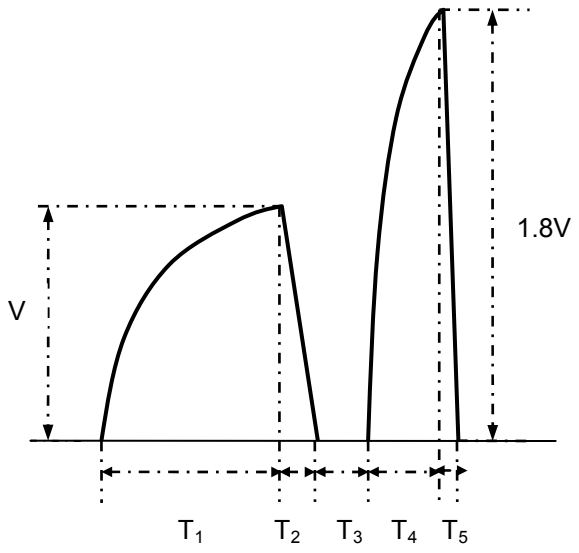

Figure 48 Double Peak waveforms rising time T_1=10.6 μs, falling time T_2=2.6 μs, dead time T_3=5.3 μs, rising time T_4 of minor peak=4.4 μs, falling time T_5 of minor peak=3.0 μs.

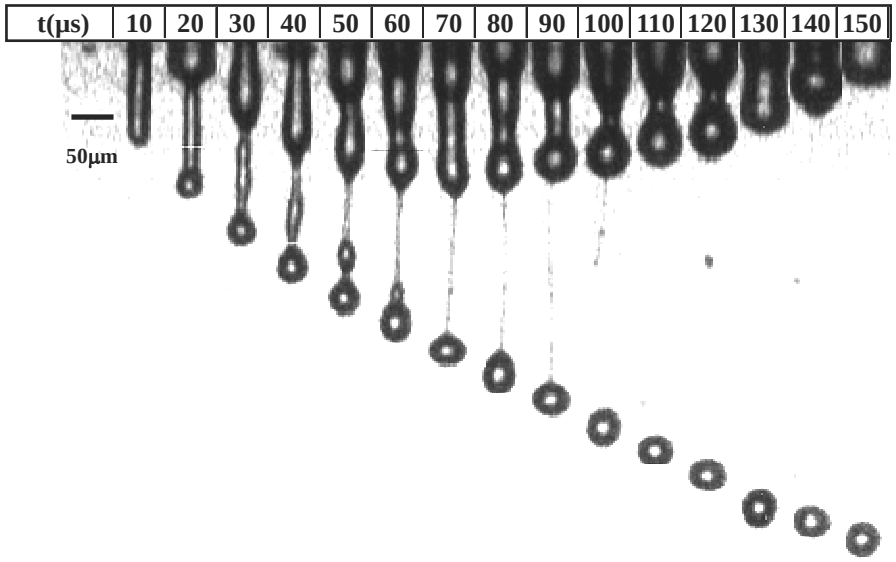

Figure 49 Images of DOD drop formation process of PEO aqueous solution containing polydispersed PEO with molecular weight of 1000k g/mol and concentration of 0.01wt%. Waveform shape of the driving signal is shown in Figure 50. Driving voltage = 44.2 V, frequency = 20 Hz. Images begin at 0 μs when liquid emerges from the nozzle and are shown for every 10 μs through 150

A test was conducted to determine if a longer dead time would decrease time needed for the pressure in the chamber to dissipate and promote quicker pinchoff. The waveform used for this test is shown in Figure 50. The dead time, T_3, has been increased from 5.3 μs to 25 μs. The images of the DOD drop formation process are shown in Figure 51. The test results indicate that the longer dead time did not produce the anticipated effects, but instead a larger amount of liquid was ejected and formed a second drop slightly larger than the first drop.

The effects on drop formation for the waveform in Figure 50 compared with the standard waveform are that it produced two drops with the second drop being larger, significantly increased liquid oscillation at the nozzle, increased primary drop speed, and produced no significant satellite.

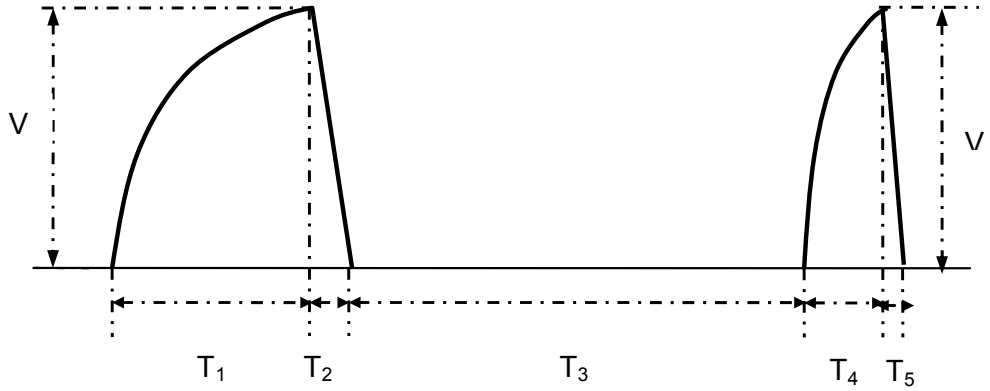

Figure 50 Double Peak waveforms rising time T_1 = 10.6 µs, falling time T_2 = 2.6 µs, dead time T_3 = 25.0 µs, rising time T_4 of minor peak = 4.4 µs, falling time T_5 of minor peak = 3.0 µs.

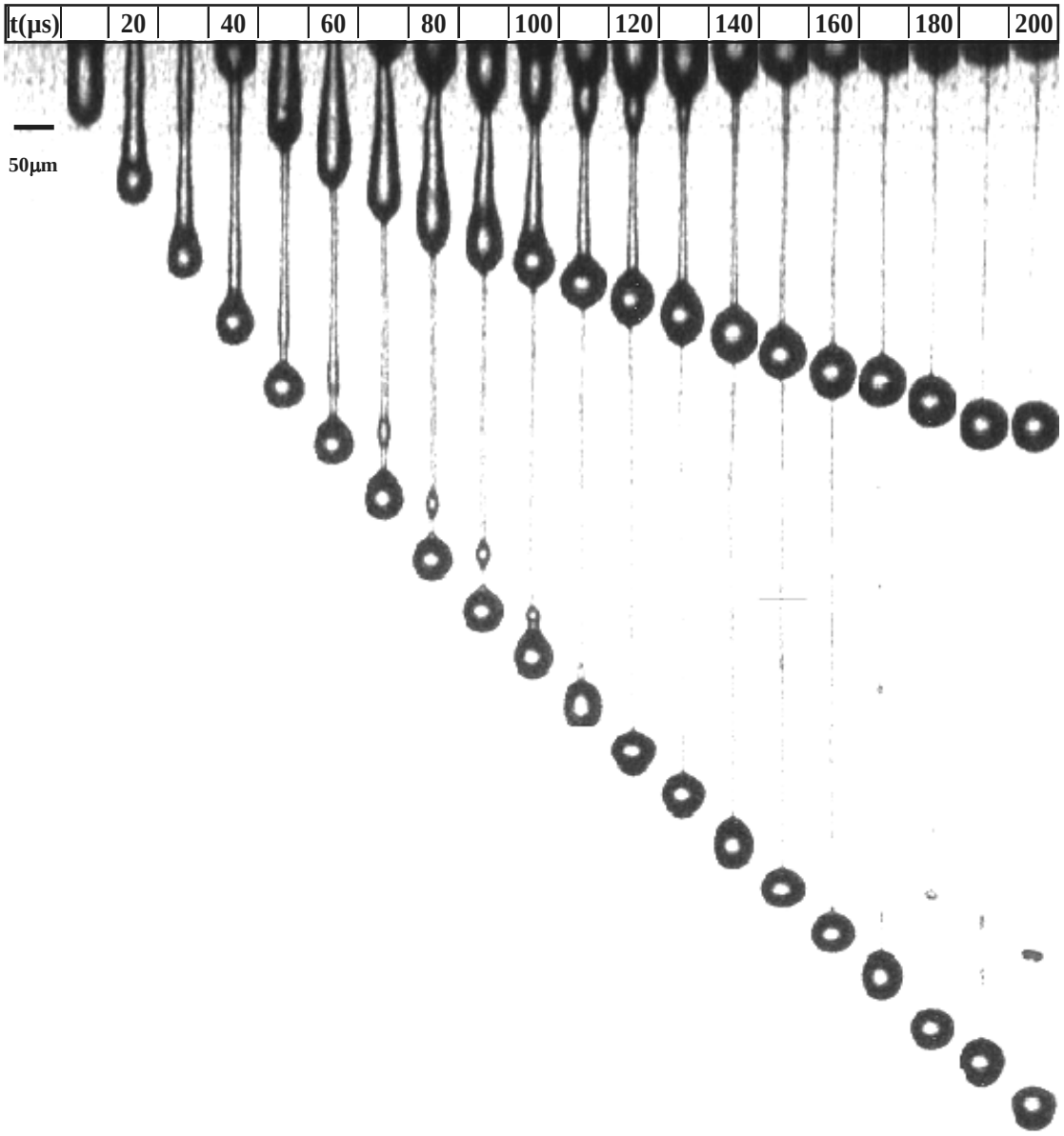

Figure 51 Images of DOD drop formation process of PEO aqueous solution containing polydispersed PEO with molecular weight of 1000k g/mol and concentration of 0.01wt%. Waveform shape of the driving signal is shown in Figure 46. Driving voltage = 44.2 V, frequency = 20 Hz. Images begin at 0 μs when liquid emerges from the nozzle and are shown for every 10 μs through 200

The results of the tests for the six waveforms discussed above are summarized in Table 13.

Table 13 Breakup time, primary drop speed and drop size of aqueous solutions containing PEO with molecular weight of 1000k g/mol and concentration of 0.01wt% during DOD drop formation for different waveform shapes. Driving voltage = 44.2 V and frequency = 20 Hz.

Test	Voltage amplitude of second pulse	Breakup time (μs)	Primary drop speed (m/s)	Primary drop diameter (μm)	Liquid oscillation at nozzle exit	Satellites
Waveform in Figure 42	0	160	4.7	53	Larger oscillation not stop until about 200 μs	Several small satellites
Standard pulse (Figure 40)	0.6V*	180	2.8	49	Stop at about 160 μs	Several small satellites
Waveform in Figure 44	V*	150	2.6	47	Stop at about 150 μs	No obvious satellites
Waveform in Figure 46	1.6V*	100	3.1	43	Larger oscillation not stop until about 200 μs	No obvious satellites
Waveform in Figure 48	1.8V*	90	2.4	39	Larger oscillation not stop until about 200 μs	No obvious satellites
Waveform** in Figure 50	V*					
A. First drop formed		170	5.0	49	Larger oscillation not stop until about 200 μs	Several small satellites
B. Second drop formed		200	1.6	60		

*V = 44.2 Volts

** Note that T3 = 25 μs.

7.5 Conclusions

The effects of waveform and jetting frequency on DOD drop formation were investigated in this chapter. The major conclusions and observations are:

1. *First Drop Problem* - For PEO solutions, if idle time is increased, it takes longer for concentrations at the end of the nozzle to stabilize and for the drop formation process to become reproducible. As molecular weight or concentration is increased, the open time is shortened. In order to get a good repeatability in DOD drop formation of polymer solutions, a series of non-stop signals in a certain frequency were used to trigger the printhead to avoid the first drop problem.
2. *Jetting Frequency Effects* - Over jetting frequencies from 0.2 Hz to 800 Hz, DOD drop formation for distilled water was very similar and repeatable; however, as jetting frequency was increased above 800 Hz, the pressure waves due to consecutive pulses apparently interacted. As jetting frequency was increased from 800 to 3000 Hz, the interaction was destructive, resulting in primary drop speed decreasing and satellite formation changing, but ending with two satellites. Above 4000 Hz, the interaction was apparently constructive. As jetting frequency was increased above 4000 Hz, the drop formation process drop formation process was not reproducible. The ejected liquid broke up into several drops with comparable size with no obvious primary drop. For DOD jetting of PEO solutions, as jetting frequency was increased from 20 Hz to 800 Hz, the speed of the leading point decreased. As jetting frequency of 1000 Hz, jetting stopped in less than one minute.

3. *Voltage Amplitude Effects* - The effects of voltage amplitude on DOD drop formation of PEO solutions were different from those for Newtonian liquids because of the elasticity of the PEO solutions. Due to elastic effects, for the PEO solutions, higher voltage amplitude is required to jet polymer solutions. Also, breakup time increased with increasing voltage amplitude. Primary drop speed increased as voltage amplitude was increased, which is similar to what was observed for Newtonian liquids.
4. *Waveform Shape Effects* - Increasing the amplitude of the second pulse gave shorter breakup time, lower primary drop speed and smaller primary drop size.

CHAPTER 8

CONCLUSIONS AND RECOMMENDATIONS

8.1 Conclusions

In this dissertation, PEO solutions for different molecular weights, concentrations and polydispersities have been used to investigate the effects of PEO on DOD drop formation.

The addition of PEO increased the shear viscosity at all molecular weights, but the change was small for dilute solutions. However, the addition of a small amount of PEO could have a significant effect on the DOD drop formation process, increasing breakup time, decreasing primary drop speed and decreasing the number of satellites in some cases. The effects depend on both molecular weight and concentration. At lower molecular weights (14k and 35k g/mol), the effect of PEO over the dilute solution regime was small when the drop formation process for the dilute solution was compared with that of a Newtonian liquid having similar shear viscosity, and the effect of PEO was small even at concentrations large enough that the solution did not fall in the dilute regime.

As molecular weight was increased, the effects of PEO on DOD drop formation increased significantly, and the effects of concentration became important. These effects are explained by the fluid elasticity which increases with increasing in molecular weight and concentration. When the liquid jets out of the nozzle, the polymer chains are stretched, and thus depart from their ideal coiled state. As a result, an elastic stress

develops in the liquid column and resists capillarity-driven pinch off from the nozzle and is responsible for the decrease in drop speed and longer breakup time.

Breakup time and drop speed were shown to scale with Modified Zimm longest relaxation time, λ_{eff}. However, for polydispersed PEO, when breakup time is plotted versus λ_{eff}, the data for 1000k g/mol PEO did not lie on the same line as that for the 100k and 300k g/mol PEO. This is due to the molecular weight distributions of the polydispersed PEO. When more than one species were present, viscous average molecular weight did not adequately account for the long chain species making up the polymer sample.

DOD drop formation data were shown to correlate closely with effective relaxation time, λ_{eff}, proposed by Tirtaatmadja [1] based on Rouse-Zimm theory. When driving voltage amplitude was 44.2 V, two important parameters (breakup time and primary drop speed) in DOD drop formation for solutions containing monodispersed PEO and aqueous solutions containing mixtures of monodispersed PEO were closely predicted by the following equations:

$$t_b - t_{b0} = 0.6029\lambda_{eff} \quad [6.5]$$

$$v / v_0 = 1 - 0.0026\lambda_{eff} \quad [6.6]$$

When solutions containing monodispersed PEO and aqueous solutions containing mixtures of monodispersed PEO had similar effective relaxation time, the drop formation processes were similar. In calculating relaxation time for mixtures of monodispersed PEO, the concentration and molecular weight of each species was accounted for by using the following mixture rule:

$$\lambda_{eff} \cong 5.38\times10^{-8}\times\left(M_n{}^{3.185}c\right)_{eff}{}^{0.65} = 5.38\times10^{-8}\times\left(\sum_{i=A}^{N} M_{ni}{}^{3.185}c_i\right)^{0.65} \quad [6.12]$$

which indicated that weight average and viscous average molecular weight underestimated the effect of the molecular weight of each of the species in the mixture.

The repeatability of breakup time in DOD drop formation of monodispersed PEO solutions was better than that of solutions containing mixtures of monodispersed PEO. The repeatability of breakup time containing mixtures of monodispersed PEO were similar to those of the polydispersed PEO solutions.

The addition of polydispersed PEO had a greater effect on DOD drop formation compared to that of monodispersed PEO with similar number average molecular weight. This is due to the polydispersed PEO having a fraction of longer chain molecules with corresponding longer relaxation times.

When different structures of monodispersed PEO with similar number average molecular weight were compared, little difference was observed because the molecular weights of the samples were too low.

For PEO solutions, the first drop problem was encountered. As molecular weight or concentration was increased, the first drop problem was more severe. In order to get good repeatability in DOD drop formation of PEO solutions, a series of non-stop signals with jetting frequency of 20 Hz were used to trigger the printhead.

Varying jetting frequency affected DOD drop formation of PEO solutions differently than for distilled water. For DOD jetting of PEO solutions, as jetting frequency was increased from 20 Hz to 800 Hz, the speed of the leading point decreased. As jetting frequency of 1000 Hz, jetting stopped in less than one minute. Over jetting frequencies from 0.2 Hz to 800 Hz, DOD drop formation for distilled water was very

similar and repeatable; however, as jetting frequency was increased above 800 Hz, the pressure waves due to consecutive pulses apparently interacted. As jetting frequency was increased above 4000 Hz, the drop formation process drop formation process was not reproducible.

The effects of voltage amplitude on DOD drop formation of PEO solutions are different from those for Newtonian liquids because of the elasticity of the PEO solutions. Due to elastic effects, for the PEO solutions, higher voltage amplitude is required to jet polymer solutions. Also, breakup time increased with increasing voltage amplitude. Primary drop speed increased as voltage amplitude is increased, which is similar to Newtonian liquids.

Six waveforms, including the standard waveform were applied to DOD drop formation process of aqueous PEO solution. Increasing the amplitude of the second pulse gives shorter breakup time, lower primary drop speed and smaller primary drop size.

8.2 Recommendations

The effect of adding PEO to distilled water on DOD drop formation was investigated in the research discussed in this dissertation, and predictive equations were developed to correlate important parameters in drop formation for solutions containing monodispersed PEO and mixtures of monodispersed PEO. It is recommended that the molecular weight distribution of polydispersed PEO could be obtained so that the mixture rule can be used to calculate the effective relaxation times for polydispersed PEO. It is also recommended that the effects of adding other polymers (for example, sodium polystyrene sulfonate (SPS)) with different hydrophilicities be investigated. The

polymers are expected to have different chain orientations in the water and different relaxation times. The research could lead to more general equations for predicting the effects of polymers on DOD drop formation.

Water soluble polymers might be studied in other solvents since most polymers are not soluble in water. It would be good to select polymers and solvent systems that have potential applications. For example, solutions of sodium polystyrene sulfonate (SPS) dissolved in tetrahydrofuran (THF) could be investigated. SPS is frequently used in scientific research. Tetrahydrofuran is suggested because it is a colorless, water-miscible organic liquid with low viscosity and is an effective solvent for a lot of polymers.

The jetting frequency, voltage amplitude and the shape of waveform were adjusted to investigate the effects of the printing system on DOD drop formation. The upper jetting frequency limit for PEO solution was much lower than that for distilled water. The low upper limit for polymer solution may be a barrier for industrial applications of inkjet printing for polymer solutions. Further study of the effect of waveform on DOD inkjet printing of polymer solutions might be useful for the inkjet industry. For example, viscosity of the base solution could be varied since higher viscosities might damp out more quickly the pressure effects of the ejection of the previous drop.

During the post drop formation stage, which includes the drop impaction, oscillation, evaporation and film deposition, another media, the substrate are important in the DOD jetting process. It would be interesting to investigate the post drop formation stage on different substrates for different inks and different parameters of the printing system, so that optimal conditions for film deposition on different substrates of different

polymers could be found. This should aid in improving polymer film deposition and pattern control on the micro scale.

APPENDIX

PROPERTIES OF MONODISPERSED PEO

The properties of the monodispersed PEO used in this thesis are listed in this appendix, which are provided and permitted to publish by PolymerSource.

Sample Name:
Poly(ethylene glycol) methyle ether or Poly ethylene oxide

Sample #: **P2798-EO**

Structure:

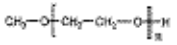

Composition:

Mn x 10^3	PDI
59.0	1.02

Synthesis Procedure:
Synthesis Procedure:
Poly (ethylene glycol) is obtained by living anionic polymerization and the reaction. Scheme of the polymerization is illustrated below:

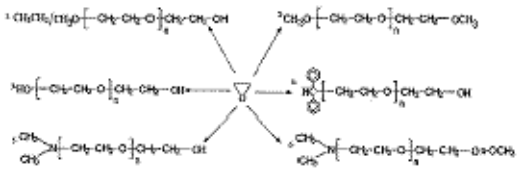

	Initiator System	Resulting Polymer
1)	$CH_3OCH_2CH(CH_3)OK$	polyethylene glycol methyl ether
2)	$CH_3OCH_2CH(CH_3)OK$	α, ω-term. methyl ether polyethylene glycol
3)	$KOCH_2CH_2OK$	polyethylene glycol
4)	$CH(C_6H_5)_2CK$	polyethylene glycol diphenyl ether
5)	$(CH_3)_2$ N-CH_2CH_2 OK	methyl amino terminated PEG
6)	$(CH_3)_2$ N-CH_2CH_2 OK	ω-methyl amino α-methyl ether term. PEG

Characterization:
By Size exclusion chromatography (SEC): Varian liquid chromatograph equipped with UV and refractive detector. SEC columns from Supelco were used with THF containing 2 vol% $(Et)_3N$ as the eluent. The molecular weights were determined using light scattering detector and viscosity detector. The molecular weights and the polydispersity indice were calculated. An aqueous GPC column from Supelco(G5000 PWXL) was also used with 0.5 M acetic acid and 0.8 M NaNO3 as the eluent. It was kept at a constant temperature of 50°C. The flow rate was 1.0 ml/min. The column was calibrated with monodisperse poly(ethylene oxide) standards. The molecular weights and the polydispersity index of polyethylene oxide were calculated by using a Visual Basic GPC software.

Purification of the obtained polymer:

Purification of the obtained polymer was carried out rigorously as follows to ensure the removal of the catalyst side product:

1. Dissolved the polymer in de-ionized distilled water to remove the any insoluble organic catalyst side product.
2. Polymer extracted from water with dichloromethane.
3. Polymer solution in dichloromethane was dried over anhydrous sodium sulfate.
4. Solution filtered and than passed through a column packed with basic Al_2O_3 .
5. Solution concentrated on rota-evaporator
6. Solution precipitated in cold diethyl ether.
7. Dried under vacuum for 48h at 38 oC.

Solubility:
Poly(ethyl glycol) is soluble in toluene, THF, water and $CHCl_3$. The polymer is insoluble in hexane, ether, cold isopropanol and ethanol.

SEC of Sample of the polymer
P2798-EO

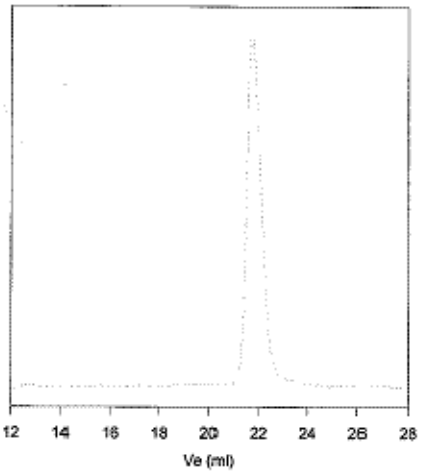

Size Exclusion Chromatography of Polyethylene oxide (SEC in THF at 35 oC):
M_n=59000, M_w =60200 PI=1.02 with on line Viscotech light scattering detector.
Intrinsic viscosity: 0.78 dl/g Radius of gyration: 12.1 nm

Sample Name:

Four arm Poly ethylene oxide

Sample #: **P8846-4EOOH**

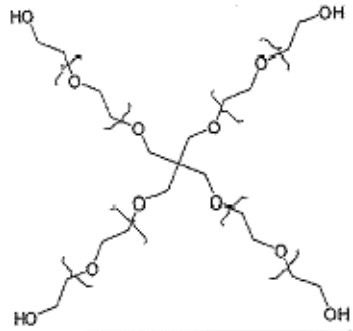

Mn x 10³ (total)	PDI
60.0	1.15

Synthesis Procedure:

The polymer was prepared by anionic living polymerization of ethylene oxide using pentaerythritol potasium salt as the initiator. The scheme of the reaction is illustrated below:

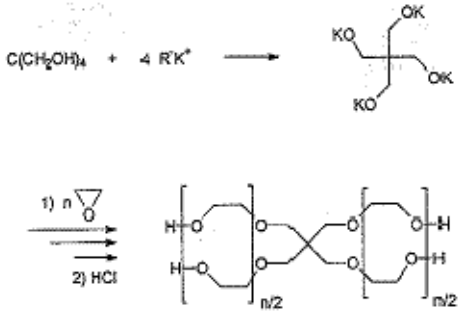

Characterization.

By Size exclusion chromatography (SEC): Varian liquid chromatograph equipped with UV and refractive detector. SEC columns from Supelco were used with THF containing 2 vol% $(Et)_3N$ as the eluent. The molecular weights were determined using light scattering detector and viscosity detector. The molecular weights and the polydispersity indice were calculated.

An aqueous GPC column from Supelco(G5000 PWXL) was also used with 0.5 M acetic acid and 0.8 M NaNO3 as the eluent. It was kept at a constant temperature of 50°C. The flow rate was 1.0 ml/min. The column was calibrated with monodisperse poly(ethylene oxide) standards. The molecular weights and the polydispersity index of polyethylene oxide were calculated by using a Visual Basic GPC software.

Purification of the obtained polymer:

Purification of the obtained polymer was carried out rigorously as follows to ensure the removal of the catalyst side product:

1. Dissolved the polymer in de-ionized distilled water to remove the any insoluble organic catalyst side product.
2. Polymer extracted from water with dichloromethane.
3. Polymer solution in dichloromethane was dried over anhydrous sodium sulfate.
4. Solution filtered and than passed through a column packed with basic Al_2O_3 .
5. Solution concentrated on rota-evaporator
6. Solution precipitated in cold diethyl ether.
7. Dried under vacuum for 48h at 38 oC.

Solubility:

Polymer is soluble in toluene, THF, water and $CHCl_3$. The polymer is insoluble in hexane, ether, cold isopropanol and ethanol.

SEC of the product

P8846-4EOOH

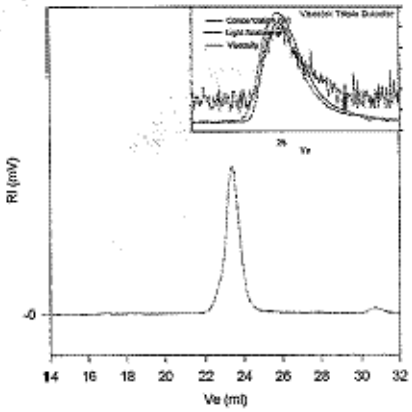

Size Exclusion Chromatography of four-arm Poly(ethylene oxide)

—— M_n = 60,000, M_w = 69,000, M_w/M_n = 1.15

Light Scattering data: dn/dc in THF at 35°C: 0.067ml/g

Solution Viscosity in THF at 35°C: 0.581dl/g

Radius of Gyration: Rg= 12.55 nm

Sample Name:
Poly ethylene oxide Poly(ethylene glycol) or

Sample #: P5656-EG2OH
Structure:

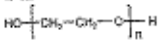

Composition:

Mn x 10^3	PDI
90.0	2.5

Synthesis Procedure:
Poly (ethylene glycol) is obtained by living anionic polymerization and the reaction. Scheme of the polymerization is illustrated below:

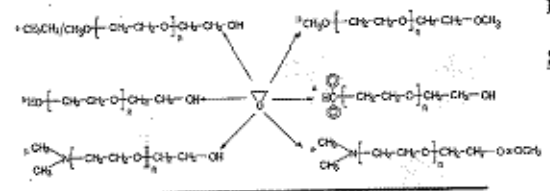

	Initiator System	Resulting Polymer
1)	$CH_3OCH_2CH(CH_3)OK$	polyethylene glycol methyl ether
2)	$CH_3OCH_2CH(CH_2)OK$	α, α-term. methyl ether polyethylene glycol
3)	$KOCH_2CH_2OK$	polyethylene glycol
4)	$CH(C_6H_5)_2CK$	polyethylene glycol diphenyl ether
5)	$(CH_3)_2$ N-CH_2CH_2 OK	methyl amino terminated PEG
6)	$(CH_3)_2$ N-CH_2CH_2 OK	α-methyl amino α-methyl ether term. PEG

Characterization:
By Size exclusion chromatography (SEC): Varian liquid chromatograph equipped with UV and refractive detector. SEC columns from Supelco were used with THF containing 2 vol% $(Et)_3N$ as the eluent. The molecular weights were determined using light scattering detector and viscosity detector. The molecular weights and the polydispersity indice were calculated.
An aqueous GPC column from Supelco(G5000 PWXL) was also used with 0.5 M acetic acid and 0.8 M NaNO3 as the eluent. It was kept at a constant temperature of 50°C. The flow rate was 1.0 ml/min. The column was calibrated with monodisperse poly(ethylene oxide) standards. The molecular weights and the polydispersity index of polyethylene oxide were calculated by using GPC software.

Purification of the obtained polymer:

Purification of the obtained polymer was carried out rigorously as follows to ensure the removal of the catalyst side product:

1. Dissolved the polymer in de-ionized distilled water to remove the any insoluble organic catalyst side product.
2. Polymer extracted from water with dichloromethane.
3. Polymer solution in dichloromethane was dried over anhydrous sodium sulfate.
4. Solution filtered and than passed through a column packed with basic Al_2O_3.
5. Solution concentrated on rota-evaporator
6. Solution precipitated in cold diethyl ether.
7. Dried under vacuum for 48h at 38 oC.

Solubility:
Poly(ethyl glycol) is soluble in toluene, THF, water and $CHCl_3$. The polymer is insoluble in hexane, ether, cold isopropanol and ethanol.

SEC of Sample of the polymer

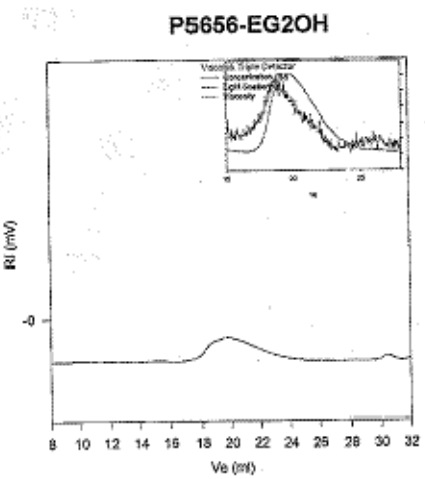

Size Exclusion Chromatography of poly(ethylene glycol): Poly (ethylene Oxide);
—— M_n = 90,000, M_w = 225,000, M_w/M_n = 2.5
dn/dc in THF at 35 oC: 0.067ml/g
Solution Viscosity in THF at 35 oC: 1.795dl/g
Rgw: 20.70 nm

Sample Name:

Poly Ethylene oxide or Poly(ethylene glycol)

Sample #: **P5377-EG2OH**

Structure:

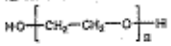

Composition:

Mn x 10^3	PDI
95.0	1.08

Synthesis Procedure:

Poly (ethylene oxide) is obtained by living anionic polymerization and the reaction. Scheme of the polymerization is illustrated below:

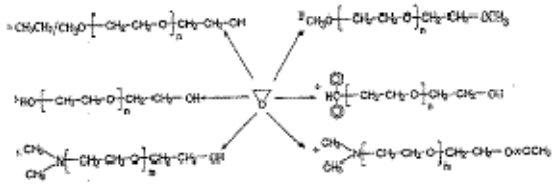

	Initiator System	Resulting Polymer
1)	$CH_3OCH_2CH(CH_3)OK$	polyethylene glycol methyl ether
2)	$CH_3OCH_2CH(CH_3)OK$	α, ω-term. methyl ether polyethylene glycol
3)	$KOCH_2CH_2OK$	polyethylene glycol
4)	$CH(C_6H_6)_2CK$	polyethylene glycol diphenyl ether
5)	$(CH_3)_2$ N-CH_2CH_2 OK	methyl amino terminated PEG
6)	$(CH_3)_2$ N-CH_2CH_2 OK	α-methyl amino ω-methyl ether term. PEG

Characterization:

By Size exclusion chromatography (SEC): Varian liquid chromatograph equipped with UV and refractive detector. SEC columns from Supelco were used with THF containing 2 vol% $(Et)_3N$ as the eluent. The molecular weights were determined using light scattering detector and viscosity detector. The molecular weights and the polydispersity indice were calculated.

An aqueous GPC column from Supelco(G5000 PWXL) was also used with 0.5 M acetic acid and 0.8 M NaNO3 as the eluent. It was kept at a constant temperature of 50°C. The flow rate was 1.0 ml/min. The column was calibrated with monodisperse poly(ethylene oxide) standards. The molecular weights and the polydispersity index of polyethylene oxide were calculated by using a Visual Basic GPC software.

Purification of the obtained polymer:

Purification of the obtained polymer was carried out rigorously as follows to ensure the removal of the catalyst side product:

1. Dissolved the polymer in de-ionized distilled water to remove the any insoluble organic catalyst side product.
2. Polymer extracted from water with dichloromethane.
3. Polymer solution in dichloromethane was dried over anhydrous sodium sulfate.
4. Solution filtered and than passed through a column packed with basic Al_2O_3 .
5. Solution concentrated on rota-evaporator
6. Solution precipitated in cold diethyl ether.
7. Dried under vacuum for 48h at 38 oC.

Solubility:

Polymer is soluble in toluene, THF, water and $CHCl_3$. The polymer is insoluble in hexane, ether, cold isopropanol

SEC of Sample of the polymer

P5377-EG2OH

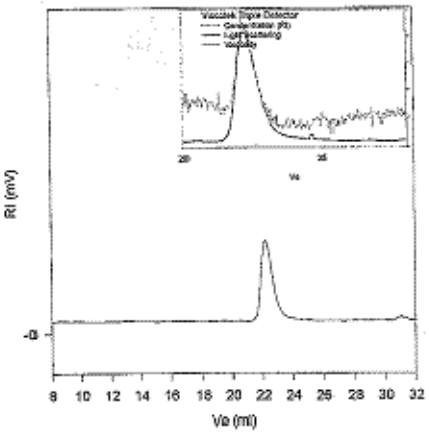

Size Exclusion Chromatography of poly(ethylene glycol): Poly (ethylene Oxide);

—— M_n = 95,000, M_w = 102,000, M_w/M_n = 1.08
dn/dc in THF at 35 oC: 0.087ml/g
Solution Viscosity in THF at 35 oC: 1.240dl/g
Rgw: 15.98 nm

Sample Name:
Poly(ethylene glycol)

Sample #: **P4214-EG2OH**
Structure:

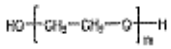

Composition:

Mn x 10^3	PDI
203.0	1.14

Synthesis Procedure:
Synthesis Procedure:
Poly (ethylene glycol) is obtained by living anionic polymerization and the reaction.
Scheme of the polymerization is illustrated below:

	Initiator System	Resulting Polymer
1)	$CH_3OCH_2CH(CH_3)OK$	polyethylene glycol methyl ether
2)	$CH_3OCH_2CH(CH_3)OK$	α, ω-term. methyl ether polyethylene glycol
3)	$KOCH_2CH_2OK$	polyethylene glycol
4)	$CH(C_3H_6)_2CK$	polyethylene glycol diphenyl ether
5)	$(CH_3)_2$ N-CH_2CH_2 OK	methyl amino terminated PEG
6)	$(CH_3)_2$ N-CH_2CH_2 OK	α-methyl amino ω-methyl ether term. PEG

Characterization:
By Size exclusion chromatography (SEC): Varian liquid chromatograph equipped with UV and refractive detector. SEC columns from Supelco were used with THF containing 2 vol% $(Et)_3N$ as the eluent. The molecular weights were determined using light scattering detector and viscosity detector. The molecular weights and the polydispersity indice were calculated.
An aqueous GPC column from Supelco(G5000 PWXL) was also used with 0.5 M acetic acid and 0.8 M NaNO3 as the eluent. It was kept at a constant temperature of 50°C. The flow rate was 1.0 ml/min. The column was calibrated with monodisperse poly(ethylene oxide) standards. The molecular weights and the polydispersity index of polyethylene oxide were calculated by using a Visual Basic GPC software.

Purification of the obtained polymer:

Purification of the obtained polymer was carried out rigorously as follows to ensure the removal of the catalyst side product:

1. Dissolved the polymer in de-ionized distilled water to remove the any insoluble organic catalyst side product.
2. Polymer extracted from water with dichloromethane.
3. Polymer solution in dichloromethane was dried over anhydrous sodium sulfate.
4. Solution filtered and than passed through a column packed with basic Al_2O_3 .
5. Solution concentrated on rota-evaporator
6. Solution precipitated in cold diethyl ether.
7. Dried under vacuum for 48h at 38 oC.

Solubility:
Poly(ethyl glycol) is soluble in toluene, THF, water and $CHCl_3$. The polymer is insoluble in hexane, ether, cold isopropanol and ethanol.

SEC of Sample of the polymer

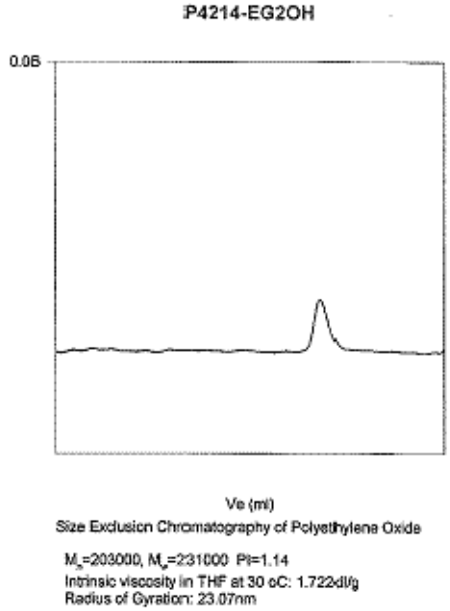

Size Exclusion Chromatography of Polyethylene Oxide

M_n=203000, M_w=231000 PI=1.14
Intrinsic viscosity in THF at 30 oC: 1.722dl/g
Radius of Gyration: 23.07nm

Sample Name: Poly(ethylene glycol) or Poly ethylene oxide
Sample #: P5617-EG2OH or P5617-EO
Structure:

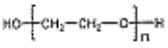

Composition:

Mn × 10^3	PDI
420.0	1.12

Synthesis Procedure:
Poly (ethylene glycol) is obtained by living anionic polymerization and the reaction. Scheme of the polymerization is illustrated below:

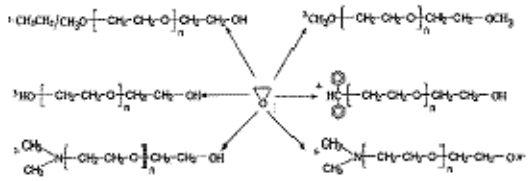

	Initiator System	Resulting Polymer
1)	$CH_3OCH_2CH(CH_3)OK$	polyethylene glycol methyl ether
2)	$CH_3OCH_2CH(CH_3)OK$	α, ω-term. methyl ether polyethylene glycol
3)	$KOCH_2CH_2OK$	polyethylene glycol
4)	$CH(C_6H_5)_2CK$	polyethylene glycol diphenyl ether
5)	$(CH_3)_2$ N-CH_2CH_2 OK	methyl amino terminated PEG
6)	$(CH_3)_2$ N-CH_2CH_2 OK	α-methyl amino ω-methyl ether term. PEG

Characterization:
By Size exclusion chromatography (SEC): Varian liquid chromatograph equipped with UV and refractive detector. SEC columns from Supelco were used with THF containing 2 vol% $(Et)_3N$ as the eluent. The molecular weights were determined using light scattering detector and viscosity detector. The molecular weights and the polydispersity indice were calculated.
An aqueous GPC column from Supelco(G5000 PWXL) was also used with 0.5 M acetic acid and 0.8 M NaNO3 as the eluent. It was kept at a constant temperature of 50°C. The flow rate was 1.0 ml/min. The column was calibrated with monodisperse poly(ethylene oxide) standards. The molecular weights and the polydispersity index of polyethylene oxide were calculated by using GPC software.
Solubility:
Poly(ethyl glycol) is soluble in toluene, THF, water and $CHCl_3$. The polymer is insoluble in hexane, ether, isopropanol and cold ethanol.

Purification of the obtained polymer:
Purification of the obtained polymer was carried out rigorously as follows to ensure the removal of the catalyst side product:

1. Dissolved the polymer in de-ionized distilled water to remove the any insoluble organic catalyst side product.
2. Polymer extracted from water with dichloromethane.
3. Polymer solution in dichloromethane was dried over anhydrous sodium sulfate.
4. Solution filtered and than passed through a column packed with basic Al_2O_3 .
5. Solution concentrated on rota-evaporator
6. Solution precipitated in cold diethyl ether.
7. Dried under vacuum for 48h at 38 oC.

SEC of Sample

P5617-EG2OH (PEO)

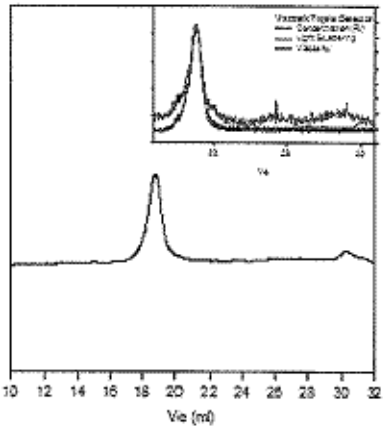

Size exclusion chromatography of polymer
Mn=420,000; Mw/Mn=1.12
dn/dc in THF, 0.067 ml/g; Rgw 34.62 nm

Sample Name:
Poly(ethylene glycol) or Poly ethylene oxide

Sample #: **P5614-EG2OH**
Structure:

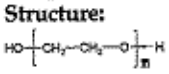

Composition:

Mn x 10^3	PDI
700.00	1.20

Synthesis Procedure:

Poly (ethylene glycol) is obtained by living anionic polymerization and the reaction. Scheme of the polymerization is illustrated below:

	Initiator System	Resulting Polymer
1)	$CH_3OCH_2CH(CH_3)OK$	polyethylene glycol methyl ether
2)	$CH_3OCH_2CH(CH_3)OK$	α, ω-term. methyl ether polyethylene glycol
3)	$KOCH_2CH_2OK$	polyethylene glycol
4)	$CH(C_6H_5)_2CK$	polyethylene glycol diphenyl ether
5)	$(CH_3)_2$ N-CH_2CH_2 OK	methyl amino terminated PEG
6)	$(CH_3)_2$ N-CH_2CH_2 OK	α-methyl amino ω-methyl ether term. PEG

Characterization:
By Size exclusion chromatography (SEC): Varian liquid chromatograph equipped with UV and refractive detector. SEC columns from Supelco were used with THF containing 2 vol% $(Et)_3N$ as the eluent. The molecular weights were determined using light scattering detector and viscosity detector. The molecular weights and the polydispersity indice were calculated.
An aqueous GPC column from Supelco(G5000 PWXL) was also used with 0.5 M acetic acid and 0.8 M NaNO3 as the eluent. It was kept at a constant temperature of 50°C. The flow rate was 1.0 ml/min. The column was calibrated with monodisperse poly(ethylene oxide) standards. The molecular weights and the polydispersity index of polyethylene oxide were calculated by using Visual Basic GPC software.

Purification of the obtained polymer

Purification of the obtained polymer was carried out rigorously as follows to ensure the removal of the catalyst side product:

1. Dissolved the polymer in de-ionized distilled water to remove the any insoluble organic catalyst side product.
2. Polymer extracted from water with dichloromethane.
3. Polymer solution in dichloromethane was dried over anhydrous sodium sulfate.
4. Solution filtered and than passed through a column packed with basic Al_2O_3.
5. Solution concentrated on rota-evaporator
6. Solution precipitated in cold diethyl ether.
7. Dried under vacuum for 48h at 38 oC.

Solubility:
Poly(ethyl glycol) is soluble in toluene, THF, water and $CHCl_3$. The polymer is insoluble in hexane, ether, cold isopropanol and ethanol.

SEC of Sample of the polymer
P5614-EO2OH or EG2OH

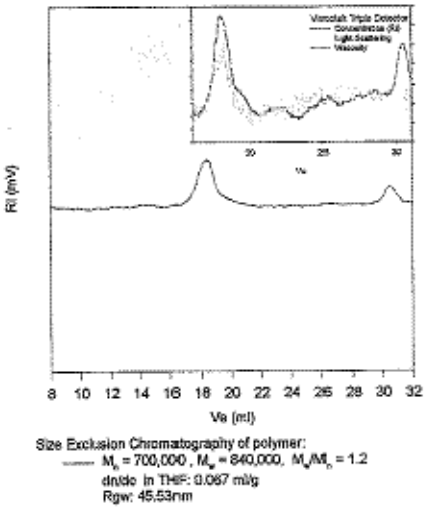

Size Exclusion Chromatography of polymer:
M_n = 700,000 , M_w = 840,000, M_w/M_n = 1.2
dn/dc in THF: 0.067 ml/g
Rgw: 45.53nm

REFERENCES

1. Tirtaatmadja, V., G.H. McKinley, and J.J. Cooper-White, *Drop formation and breakup of low viscosity elastic fluids: Effects of molecular weight and concentration.* Physics of Fluids, 2006. **18**(4): p. 18.

2. Dong, H.M., *Doctoral Thesis.* 2006.

3. Geissler, M. and Y.N. Xia, *Patterning: Principles and some new developments.* Advanced Materials, 2004. **16**(15): p. 1249-1269.

4. Hartmann, U., *Magnetic force microscopy.* Annual Review of Materials Science, 1999. **29**: p. 53-87.

5. Park, S., et al., *Self-assembly of mesoscopic metal-polymer amphiphiles.* Science, 2004. **303**(5656): p. 348-351.

6. Liu, B., et al., *Fabricating super-hydrophobic lotus-leaf-like surfaces through soft-lithographic imprinting.* Macromolecular Rapid Communications, 2006. **27**(21): p. 1859-1864.

7. de Gans, B.J., P.C. Duineveld, and U.S. Schubert, *Inkjet printing of polymers: State of the art and future developments.* Advanced Materials, 2004. **16**(3): p. 203-213.

8. Clift`, R.`, Grace`, J. R. and Weber M. E.`, Bubbles`, drops and particles`, Academic`, New York`, 1978

9. Hoth, C.N., et al., *Printing highly efficient organic solar cells.* Nano Letters, 2008. **8**(9): p. 2806-2813.

10. Bidoki, S.M., et al., *Inkjet printing of conductive patterns on textile fabrics.* Aatcc Review, 2005. **5**(6): p. 11-14.

11. Sawhney, A., et al., *Soft-structured sensors and connectors by inkjet printing.* Aatcc Review, 2007. **7**(6): p. 42-46.

12. de Gans, B.J., S. Hoeppener, and U.S. Schubert, *Polymer-relief microstructures by inkjet etching.* Advanced Materials, 2006. **18**(7): p. 910-+.

13. Calvert, P., *Inkjet printing for materials and devices.* Chemistry of Materials, 2001. **13**(10): p. 3299-3305.

14. Sirringhaus, H., et al., *High-resolution inkjet printing of all-polymer transistor circuits.* Science, 2000. **290**(5499): p. 2123-2126.

15. Zhang, X.G. and O.A. Basaran, *An Experimental-Study of Dynamics of Drop Formation.* Physics of Fluids, 1995. **7**(6): p. 1184-1203.

16. Dong, H.M., W.W. Carr, and J.F. Morris, *An experimental study of drop-on-demand drop formation.* Physics of Fluids, 2006. **18**(7).

17. Eggers, J., *Nonlinear dynamics and breakup of free-surface flows.* Reviews of Modern Physics, 1997. **69**(3): p. 865-929.

18. Tekin, E., B.J. de Gans, and U.S. Schubert, *Ink-jet printing of polymers - from single dots to thin film libraries.* Journal of Materials Chemistry, 2004. **14**(17): p. 2627-2632.

19. Haverinen, H.M., R.A. Myllyla, and G.E. Jabbour, *Inkjet printing of light emitting quantum dots.* Applied Physics Letters, 2009. **94**(7): p. -.

20. Choi, J., et al., *Drop-on-demand printing of conductive ink by electrostatic field induced inkjet head.* Applied Physics Letters, 2008. **93**(19): p. -.

21. Kim, J., et al., *The spontaneous metal-sitting structure on carbon nanotube arrays positioned by inkjet printing for wafer-scale production of high sensitive gas sensor units.* Sensors and Actuators B-Chemical, 2009. **135**(2): p. 587-591.

22. Batchelor, J.C., et al., *Inkjet printing of frequency selective surfaces.* Electronics Letters, 2009. **45**(1): p. 7-8.

23. Barret, M., S. Sanaur, and P. Collot, *Inkjet-printed polymer thin-film transistors: Enhancing performances by contact resistances engineering.* Organic Electronics, 2008. **9**(6): p. 1093-1100.

24. Chou, W.Y., et al., *Polymer light-emitting diodes with thermal inkjet printed poly(3,4-ethylenedioxythiophene): polystyrenesulfonate as transparent anode.* Thin Solid Films, 2007. **515**(7-8): p. 3718-3723.

25. Liu, Y., K. Varahramyan, and T.H. Cui, *Low-voltage all-polymer field-effect transistor fabricated using an inkjet printing technique.* Macromolecular Rapid Communications, 2005. **26**(24): p. 1955-1959.

26. Chang, S.C., et al., *Dual-color polymer light-emitting pixels processed by hybrid inkjet printing.* Applied Physics Letters, 1998. **73**(18): p. 2561-2563.

27. Mustonen, T., et al., *Inkjet printing of transparent and conductive patterns of single-walled carbon nanotubes and PEDOT-PSS composites.* Physica Status Solidi B-Basic Solid State Physics, 2007. **244**(11): p. 4336-4340.

28. Chang, S.C., et al., *Multicolor organic light-emitting diodes processed by hybrid inkjet printing.* Advanced Materials, 1999. **11**(9): p. 734-737.

29. Kobayashi, H., et al., *A novel RGB multicolor light-emitting polymer display.* Synthetic Metals, 2000. **111**: p. 125-128.

30. Yoshioka, Y. and G.E. Jabbour, *Inkjet printing of oxidants for patterning of nanometer-thick conducting polymer electrodes.* Advanced Materials, 2006. **18**(10): p. 1307-1312.

31. Mabrook, M.F., et al., *The morphology, electrical conductivity and vapour sensing ability of inkjet-printed thin films of single-wall carbon nanotubes.* Carbon, 2009. **47**(3): p. 752-757.

32. Kelly, P.F., R.S.P. King, and R.J. Mortimer, *Fingerprint and inkjet-trace imaging using disulfur dinitride.* Chemical Communications, 2008(46): p. 6111-6113.

33. Xu, T., et al., *Inkjet-Mediated Gene Transfection into Living Cells Combined with Targeted Delivery.* Tissue Engineering Part A, 2009. **15**(1): p. 95-101.

34. Xu, T., et al., *Inkjet gene printing: A novel approach to achieve gene modified cells for tissue engineering.* Tissue Engineering Part A, 2008. **14**(5): p. 869-870.

35. Saunders, R.E., J.E. Gough, and B. Derby, *Delivery of human fibroblast cells by piezoelectric drop-on-demand inkjet printing.* Biomaterials, 2008. **29**(2): p. 193-203.

36. Derby, B., *Bioprinting: inkjet printing proteins and hybrid cell-containing materials and structures.* Journal of Materials Chemistry, 2008. **18**(47): p. 5717-5721.

37. Li, Y.C., et al., *Inkjet Printed Electrode Arrays for Potential Modulation of DNA Self-Assembled Monolayers on Gold.* Analytical Chemistry, 2008. **80**(22): p. 8814-8821.

38. Bharathan, J. and Y. Yang, *Polymer electroluminescent devices processed by inkjet printing: I. Polymer light-emitting logo.* Applied Physics Letters, 1998. **72**(21): p. 2660-2662.

39. Hoth, C.N., et al., *High photovoltaic performance of inkjet printed polymer: Fullerene blends.* Advanced Materials, 2007. **19**(22): p. 3973-+.

40. Chen, A.U. and O.A. Basaran, *A new method for significantly reducing drop radius without reducing nozzle radius in drop-on-demand drop production.* Physics of Fluids, 2002. **14**(1): p. L1-L4.

41. Evans`, C. M.`, Fox`, J. E.`, Hall`, K. P.`, and Goodwin`, P. D.`, "Optimisation of ink jet droplet formation through polymer selection`," IS&T NIP 15`, pp. 78-81`, 1999.

42. Lopez`, B.`, Vadillo`, D.`, Pierron`, P.`, and Sourcemarianadin`, A.`, "Transient phenomena during drop formation in DOD printing`," IS&T NIP`, vol. 18`, pp.170-175`, 2002.

43. Dong, H.M., W.W. Carr, and J.F. Morris, *Visualization of drop-on-demand inkjet: Drop formation and deposition.* Review of Scientific Instruments, 2006. **77**(8).

44. Park, H., et al., *Single drop impaction on a solid surface.* Aiche Journal, 2003. **49**(10): p. 2461-2471.

45. Adams, R.L. and J. Roy, *A one-dimensional numerical-model of a drop-on-demand ink jet.* Journal of Applied Mechanics-Transactions of the Asme, 1986. **53**(1): p. 193-197.

46. Shield, T.W., D.B. Bogy, and F.E. Talke, *A numerical comparison of one-dimensional fluid jet models applied to drop-on-demand printing.* Journal of Computational Physics, 1986. **67**(2): p. 327-347.

47. Fromm, J.E., *Numerical-calculation of the fluid-dynamics of drop-on-demand jets.* Ibm Journal of Research and Development, 1984. **28**(3): p. 322-333.

48. Feng, J.Q., *A general fluid dynamic analysis of drop ejection in drop-on-demand ink jet devices.* Journal of Imaging Science and Technology, 2002. **46**(5): p. 398-408.

49. Xu, Q. and O.A. Basaran, *Computational analysis of drop-on-demand drop formation.* Physics of Fluids, 2007. **19**(10): p. 12.

50. Hoyt, J.W. and J.J. Taylor, *Turbulence structure in a water jet discharging in air.* Physics of Fluids, 1977. **20**(10): p. S253-S257.

51. Rouse, P.E., *A theory of the linear viscoelastic properties of dilute solutions of coiling polymers.* Journal of Chemical Physics, 1953. **21**(7): p. 1272-1280.

52. Zimm, B.H., *Dynamics of polymer molecules in dilute solution - viscoelasticity, flow birefringence and dielectric loss.* Journal of Chemical Physics, 1956. **24**(2): p. 269-278.

53. Hsieh, C.C., L. Li, and R.G. Larson, *Modeling hydrodynamic interaction in Brownian dynamics: simulations of extensional flows of dilute solutions of DNA and polystyrene.* Journal of Non-Newtonian Fluid Mechanics, 2003. **113**(2-3): p. 147-191.

54. Liu, Y.G., Y.G. Jun, and V. Steinberg, *Concentration dependence of the longest relaxation times of dilute and semi-dilute polymer solutions.* Journal of Rheology, 2009. **53**(5): p. 1069-1085.

55. Christanti, Y. and L.M. Walker, *Effect of fluid relaxation time of dilute polymer solutions on jet breakup due to a forced disturbance.* Journal of Rheology, 2002. **46**(3): p. 733-748.

56. Christanti, Y. and L.M. Walker, *Surface tension driven jet break up of strain-hardening polymer solutions.* Journal of Non-Newtonian Fluid Mechanics, 2001. **100**(1-3): p. 9-26.

57. Shore, H.J. and G.M. Harrison, *The effect of added polymers on the formation of drops ejected from a nozzle.* Physics of Fluids, 2005. **17**(3): p. 7.

58. Xu, D., et al., *Inkjet printing of polymer solutions and the role of chain entanglement.* Journal of Materials Chemistry, 2007. **17**(46): p. 4902-4907.

59. Vadillo, D.C., et al., *Evaluation of the inkjet fluid's performance using the "Cambridge Trimaster" filament stretch and break-up device.* Journal of Rheology, 2009. **54**(2): p. 261-282.

60. Wang, X., *Doctoral Thesis.* 2008.

61. Rubinstein M, C.R., *Polymer Physics.* 2003.

62. Rodd, L.E., et al., *Capillary break-up rheometry of low-viscosity elastic fluids.* Applied Rheology, 2005. **15**(1): p. 12-27.

63. R. B. Bird Dynamic of Polymeric Liquids 1987

64. Kohler, D., et al., *Speckle Reduction in Pulsed-Laser Photographs.* Optics Communications, 1974. **12**(1): p. 24-28.

65. *Comments from Xi Wang.* May 2010.

66. Cooper-White, J.J., et al., *Drop formation dynamics of constant low-viscosity, elastic fluids.* Journal of Non-Newtonian Fluid Mechanics, 2002. **106**(1): p. 29-59.

67. Stokes, J.R., *Swirling flow of viscoelastic fluids.* Ph. D thesis, 1998.